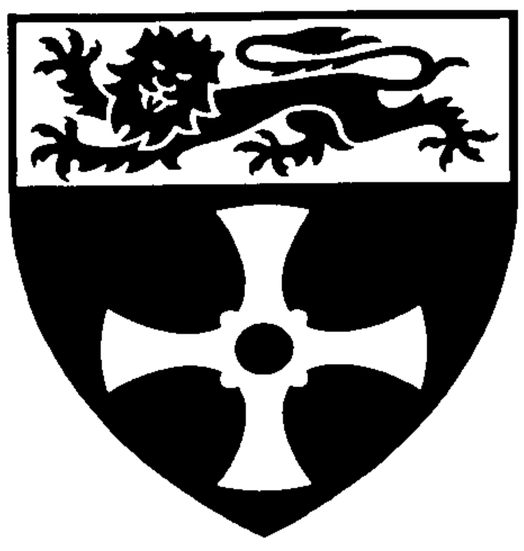

Newcastle University

Long-Term Behaviour of Aramid Fibre

This thesis is submitted in accordance with the requirements of Newcastle University for the degree of Doctor of Philosophy

By

Gasem M. Fallatah

Centre for Composite Materials Engineering,

School of Mechanical and Systems Engineering,

Newcastle University

October 2006

Table of Content

Dedication

To the soul of my father, who always dreamed that one of his sons or daughters would get a PhD,

My mother, who I'll never be able to compensate for being my mother,

My wife and children, who have supported me and sustained the hardship and pain of being with me,

My brothers and sisters, who have supported me and made me their role model.

Acknowledgements

I acknowledge the guidance and support of Professor Gibson who acted as my PhD supervisor. I acknowledge the support of my sponsor company Saudi Aramco for giving me the opportunity of doing this programme. I also acknowledge the financial support offered by the members of the JIP "*Implementation of Reinforced Thermoplastic Pipes in the Oil and Gas Industry*".

I would like to thank all the technical and administrative staff at Newcastle University and the School of Mechanical and Systems Engineering who have helped me with my work. In particular, I would like to thank Dr. Nievell Dodds and Mr. Ron Jensen and all other members of the Centre for Composite Materials Engineering for their help and friendship throughout my research programme.

Finally, I would like to thank my family, Aishah, Salma, Abdulelah, and Sumayah for their patience and overwhelming encouragement and support.

Abstract

An investigation of the creep rupture of Kevlar® 29, Twaron® 1000, and Technora T200® aramid fibre yarns was carried out in the temperature range 25-120°C in air and three other environments (Saudi/Iranian crude oil, pure water, and low pH water) at 65°C with the objective of characterising the long term failure behaviour of these fibres and determine if they can be used to replace the stress rupture test conducted on RTP for qualification purposes.

The standard $\log_{10}$-$\log_{10}$ ISO 9080 extrapolation procedure, the modified lin-$\log_{10}$ ISO 9080 extrapolation procedure and the time temperature superposition method were used to model and interpret the results.

When tested in air, the different yarns showed similar but not identical regression parameters. The results of the standard $\log_{10}$-$\log_{10}$ ISO 9080 and the modified lin-$\log_{10}$ methods correlated well. The standard $\log_{10}$-$\log_{10}$ form, however, gave slightly higher values for the 20 year mean stress and LPL. Its use is recommended because it is consistent with the model assumed in the regression of RTP. There was no evidence of any 'knee' in the relationships after long periods or at high temperatures. This suggests that there is no change in failure mechanism, and lends confidence to both the long term use of aramid fibre in air and the recommended qualification procedures. RTP regression curve constants and those of tested aramid fibre were similar indicating the validity of aramid fibre stress rupture tests as a replacement for RTP tests.

Crude oil immersion produced a small but significant reduction in behaviour. At 65°C a suitable crude oil reduction factor applied to the long term LPL would be 0.9. Pure water produces a marked reduction in strength after short periods, at 65°C. Finally, water of low pH resulted in a large reduction in performance and considerable scatter with one fibre type. With the other, the effect appeared to be similar to that of pure water.

Based on the understanding of the failure mechanism and the creep process in aramid fibres, a creep strain model is proposed for estimating the strain to failure based on the material's properties.

List of Figures

List of Tables

Nomenclature and Abbreviations

Terms	Abbreviation
American Petroleum Institute	API
American Society of Testing Materials	ASTM
Carbon dioxide	CO_2
Cross sectional area [mm^2]	A
Curve intercept	F
Denier = g/9,000m	Den
Density [g/cm^3]	ρ
Deutsches Institut für Normung	DIN
Differential Scanning Calorimetry	DSC
High density polyethylene	HDPE
Hydrogen Sulphate	H_2SO_4
Hydrogen sulphide	H_2S
International Standardization Orgnization	ISO
ISO 9080 statistical model parameters	c_1, c_2, c_3, c_4
Joint Industry Project	JIP
Limiting Oxygen Index	LOI
Linear density [dtex]	LD
Linear variable differential transformer	LVDT
Liquid crystalline	LC
Lower Confidence Limit	LCL
Lower Prediction Limit	LPL
Mass [g] of a yarn with a length of 10,000m	dtex
Mass [g] of a yarn with a length of 1000m	tex
Mega Pascal	MPa
Poly (p-phenylene terephthalamide)	PPTA
Polytetrafluoroethylene	PTFE
Polyvinylidene fluoride	PVDF
Regression line slope	G
Reinforced Thermoplastic Pipe	RTP
Scanning Electron Microscope	SEM
Sodium sulphate	Na_2SO_4
Strain	ε
Stress level in megapascals	σ
Test temperature in °Kelvin	T
Thermogravimetric Analysis	TGA
Thermomechanical Analysis	TMA
Time temperature superposition	TTS
Time to failure in hours	t_f
TTS shift factor	a_T
Ultra violet	UV

List of Publications

1. Fallatah, G. M., Gibson, A. G. and Dodds, N.
   Behaviour of Highly Loaded Aramid Fibre as used in Reinforced Thermoplastic Pipes;
   Proceedings of NACE 11th Middle East Corrosion Conference, Kingdom of Bahrain, March 2006.

2. Fallatah, G. M., Gibson, A. G. and Dodds, N.
   Long Term Creep and Stress Rupture of Aramid Fibre;
   Proceedings of 7th International Conference on Durability of Composite Systems, Blacksburg, Virginia, USA, Septembers 2006.

Chapter 1 Introduction and Objectives

1.1 Introduction

The use of aramid fibres is becoming more acceptable in many different applications and in the manufacturing of Reinforced Thermoplastic Pipe (RTP) in particular. Indeed, RTP currently represents one of the most highly loaded applications of aramid fibres. Therefore an understanding of the mechanical behaviour of these fibres when they are subjected to loading for long periods of time becomes crucial. Moreover, it is important to gain a detailed understanding of the physical structure of the fibre and how this is related to deformation and failure processes. This understanding is necessary in order to be able to predict the fibre's durability with some degree of confidence.

A Joint Industry Project (JIP) was set up with the aim of promoting RTP applications in the transport of onshore oilfield fluids, crude oil, natural gas and in subsea flowlines. The project, titled "*Implementation of Reinforced Thermoplastic Pipes in the Oil and Gas Industry*", was funded by the principal RTP manufacturers, the suppliers of its key raw materials and end users. The JIP was managed jointly by the Centre of Composite Materials Engineering of Newcastle University and the Advance Research Partnership of Manchester University. The aim of the JIP was to remove barriers restricting the use of RTP in different application areas.

One of the main hurdles facing the promotion of RTP is the financial burden of the long term stress rupture testing needed for the qualification of all non-metallic piping products. These tests require the application of constant pressure and measuring failure times up to and exceeding 10,000 hours. The JIP investigated a number of ways in which this testing burden might be reduced in the future. One of these was to characterise the long term failure behaviour of aramid fibre yarn, representative of the reinforcement used in RTP. Surprisingly, such work had not been carried out before.

More specifically, the industry has identified the need for data on the long term stress rupture or regression behaviour of aramid fibre yarns. Data on the long term effects of temperature, water, low pH water and crude oil were deemed desirable for periods between 100 hours and 10,000 hours. Having such data available at the most useful design temperature for RTP, which is 65°C, will assist with the prediction of RTP behaviour and will reduce the need for expensive long term tests on pipe samples. Additional information at high temperatures is also required to confirm whether or not there are any changes in behaviour over long periods of time or in high temperature conditions. Such information can also be used to confirm the behaviour of predictive models.

Questions have also been raised concerning the precise effects of certain environmental factors on the regression behaviour and failure mechanisms of aramid fibres, and particularly the effects of humidity and crude oil.

Answering the above questions will assist considerably in the deployment of aramid fibres in RTP and other highly loaded applications. This will eventually help in overcoming the financial burden of the long-term RTP stress rupture testing needed for its qualification, hence leading to a wider utilization of RTP in the industry.

Based on the understanding of the failure mechanism of aramid fibre, it is deemed necessary to model the creep behaviour of these fibres. This model can be utilized for estimating the strain to failure based on the material's properties.

1.2 Objectives

The objectives of this thesis are as follows:

- To provide general technical information about aramid fibres and their most highly loaded application, the RTP, through a concise literature survey on their long term behaviour and factors that influence it.
- To evaluate the long term behaviour of aramid fibres when subjected to constant rupture stress under different temperatures and in various environments.

Long-Term Behaviour of Aramid Fibre

- To model the long term stress response of aramid fibres under a range temperatures and environments using different modelling techniques.
- To investigate the failure mechanism of aramid fibres physically and microscopically when subjected to constant load.
- To model the failure mechanism of aramid fibres when subjected to constant load and to estimate the failure strain based on the material's properties and the stress applied.

1.3 Thesis Structure

This thesis consists of eight chapters. The first chapter provides an introduction to the project and lists its main objectives.

The second chapter is devoted to the literature review conducted on the subject area.

The third chapter provides an explanation of the experimental procedures utilized in the experiments related to this project.

Chapters four and five contain the analysis and discussion of the experimental results. In chapter four the results of the tests in air are discussed, while chapter five discusses the results of the tests conducted in water, low pH water and crude oil environments.

Chapter six provides a theoretical explanation of the creep behaviour of aramid fibres and the constituent laws that governs their behaviour.

In chapter seven, a fractography analysis is presented to support the theoretical explanation of the failure behaviour of the fibres.

Finally, chapter eight summarizes the research, draws the final conclusions and makes recommendations for future work.

Chapter 2 Literature Review

2.1 Reinforced Thermoplastic Pipe

Reinforced Thermoplastic Pipe is a fluid-tight liner composite construction that consists of the following essential components (ISO/TS 18226, 2004) and Kruijer (2004):

- A thermoplastic liner, usually polyethylene, the main function of which is to contain the fluid being transmitted.
- An even number of balanced helical windings of continuous reinforcement, which will entirely take the pressure and other loads.
- An outer protective thermoplastic cover which will protect the reinforcement and the pipe in general from external effects.

Figure 2.1 gives a schematic illustration of RTP construction (Fallatah et al, 2006).

RTP is manufactured by a continuous helical winding process, using non-impregnated aramid (currently du Pont Kevlar 29, or the similar product, Teijin/Twaron 1000) fibre yarn as reinforcement, which will take the entire pressure load.

Glass and Carbon fibres are regarded as unsuitable for RTP as they need to be impregnated in a polymeric resin to prevent them from being damaged by abrasion when the RTP is flexed or coiled. Furthermore, impregnating these fibres (i.e. glass and carbon) will add extra cost and complications to the manufacturing process and reduce the pipe's flexibility.

The fibre may be helically wound directly onto the liner or encapsulated in a thermoplastic to form a tape which can be more easily handled. The tape is subsequently wrapped and welded to the liner and cover. Again, the encapsulation of non-impregnated carbon or glass fibres into a tape is undesirable because of excessive damage caused by abrasion between fibres; therefore aramid fibres are generally used. Recently, metallic wires have been used as the load bearing component. Figure 2.2 shows the construction of the reinforcement tape. The reinforcement is wrapped at an angle of ±55°, the optimum angle to resist

internal hydrostatic pressure. Helical tape wrapping is the preferred manufacturing process because it offers a continuous manufacturing process.

RTP can be manufactured with liner materials to suit particular fluid and temperature requirements. Currently, RTP is manufactured with polyethylene liners and covers for use at temperatures up to 65°C. For higher temperatures and more aggressive corrosion environments, polyamide 11 and polyvinylidene fluoride (PVDF) liners are recommended. It is important to note that these liners have not yet been used in any RTP application. The outer cover, on the other hand, needs to be resistant to external environmental effects such as moisture, abrasion and Ultraviolet (UV) degradation.

The reinforcement fibre in RTP is completely insulated from the fluids transported and the outer environment by the inner and outer liners as illustrated in Figures 2.1 and 2.2. However, when joining RTP pipes to fittings or other pipes, the possibility of damaging the fibre insulation exists especially if the joining process is not conducted with care. Figure 2.3 shows the commonly used RTP joining techniques.

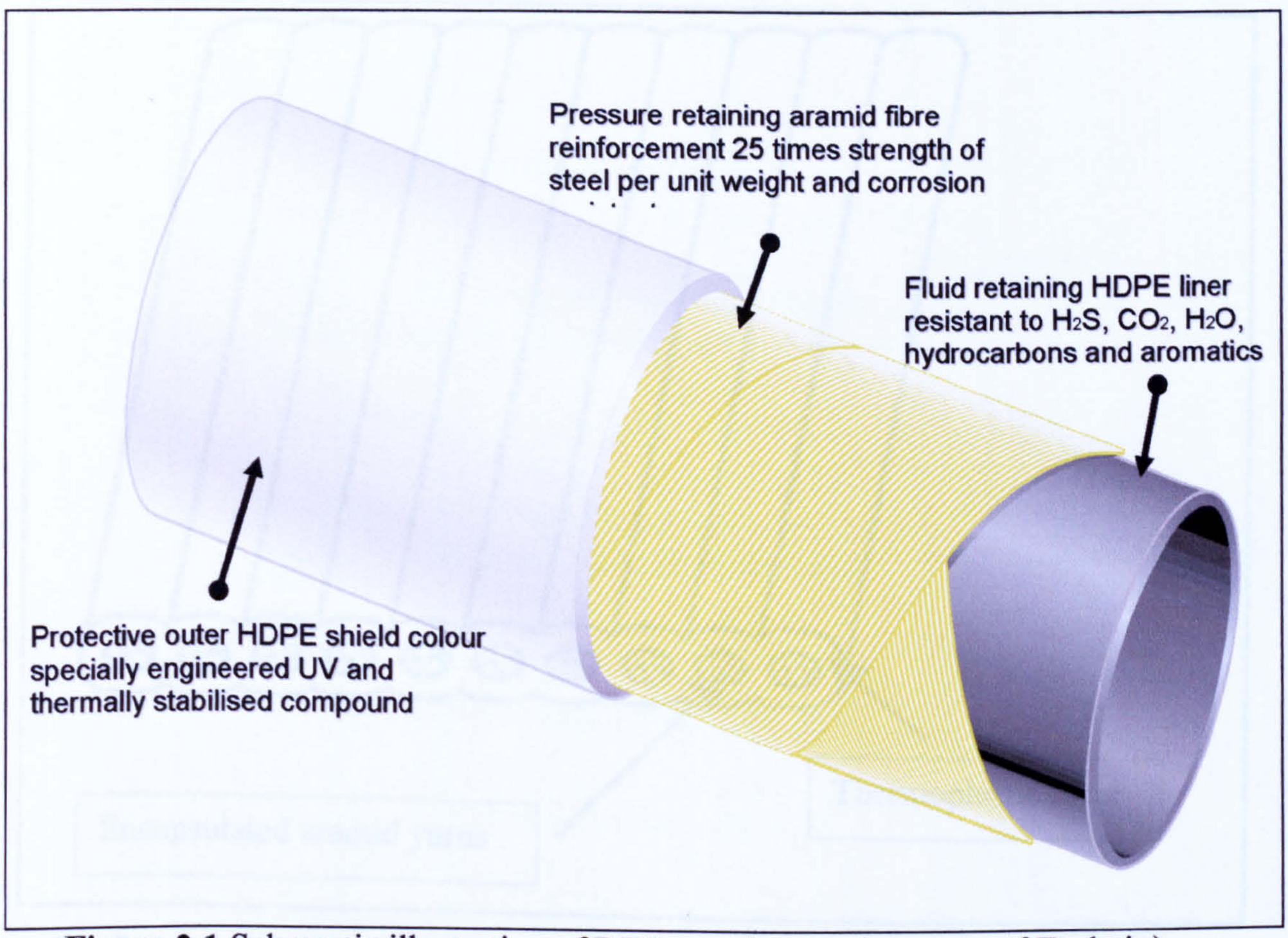

Figure 2.1 Schematic illustration of RTP constituents (courtesy of Technip)

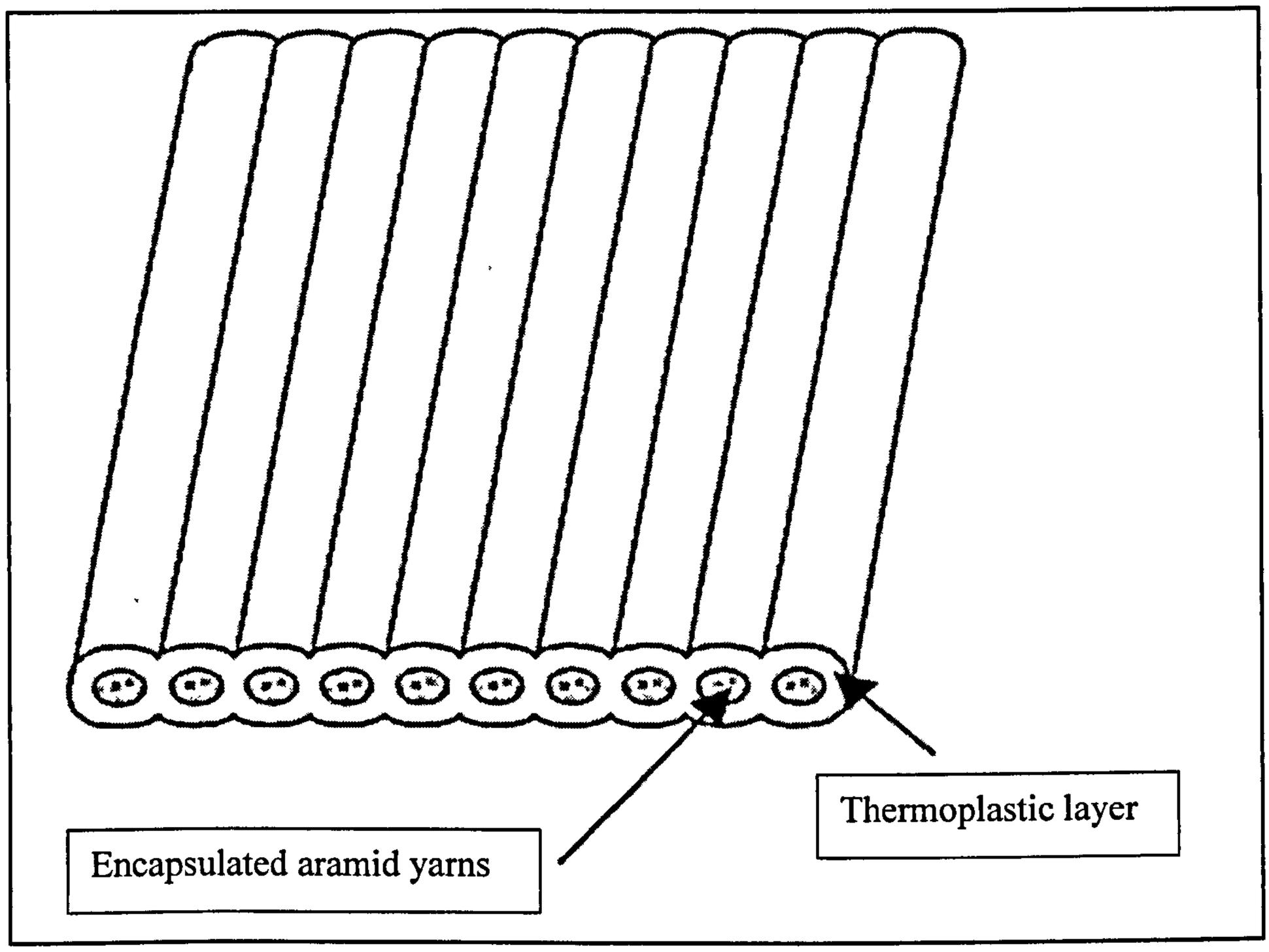

Figure 2.2 Construction of the reinforcement tape for helical RTP winding (Cantrill, 2002)

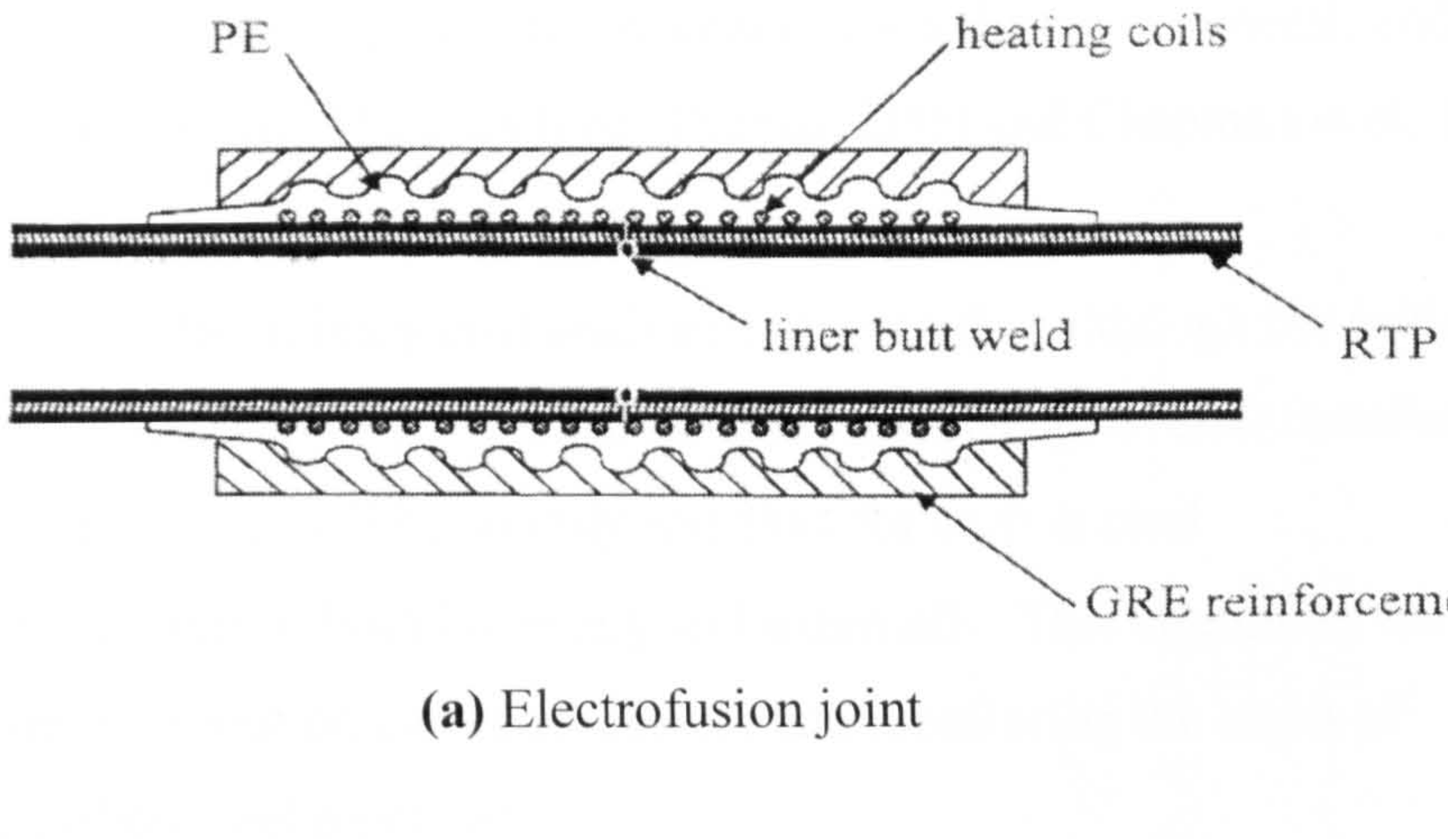

(a) Electrofusion joint

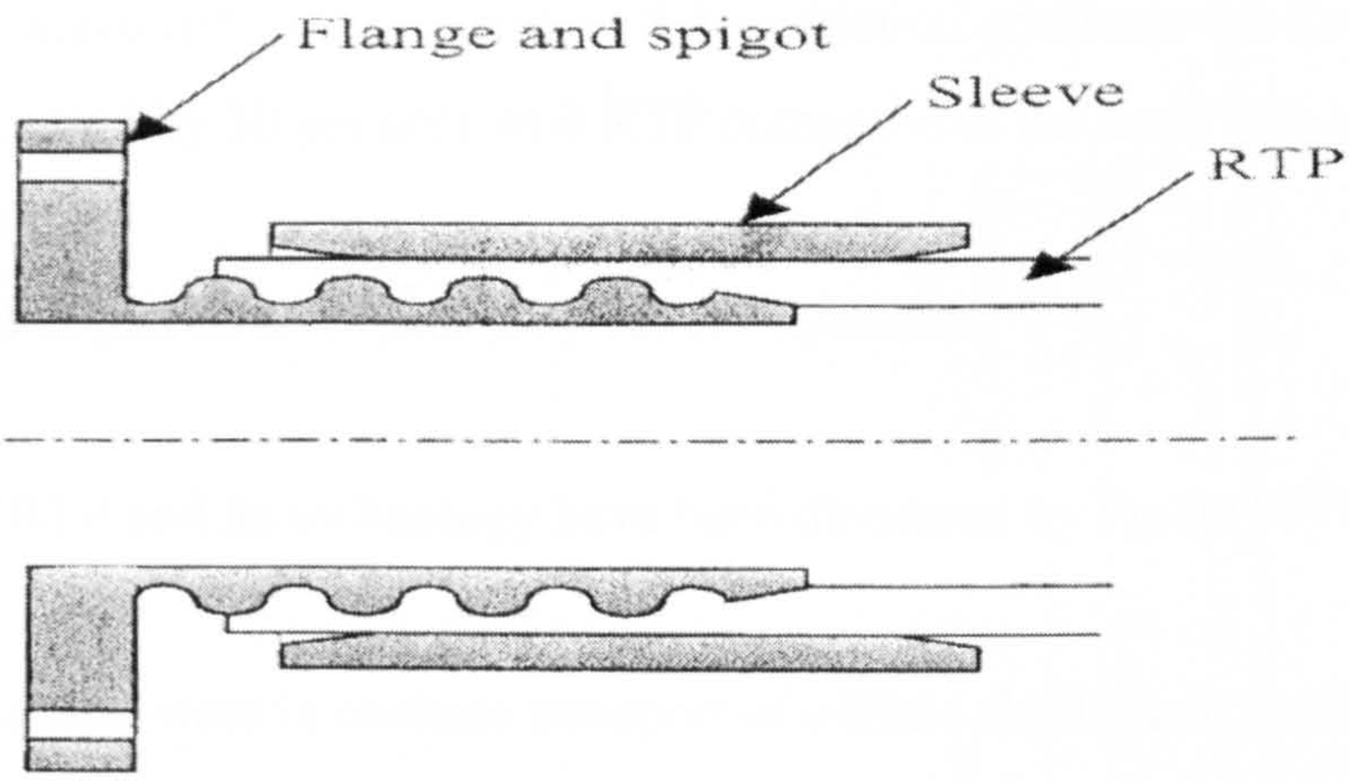

(b) PECAT compression type joint

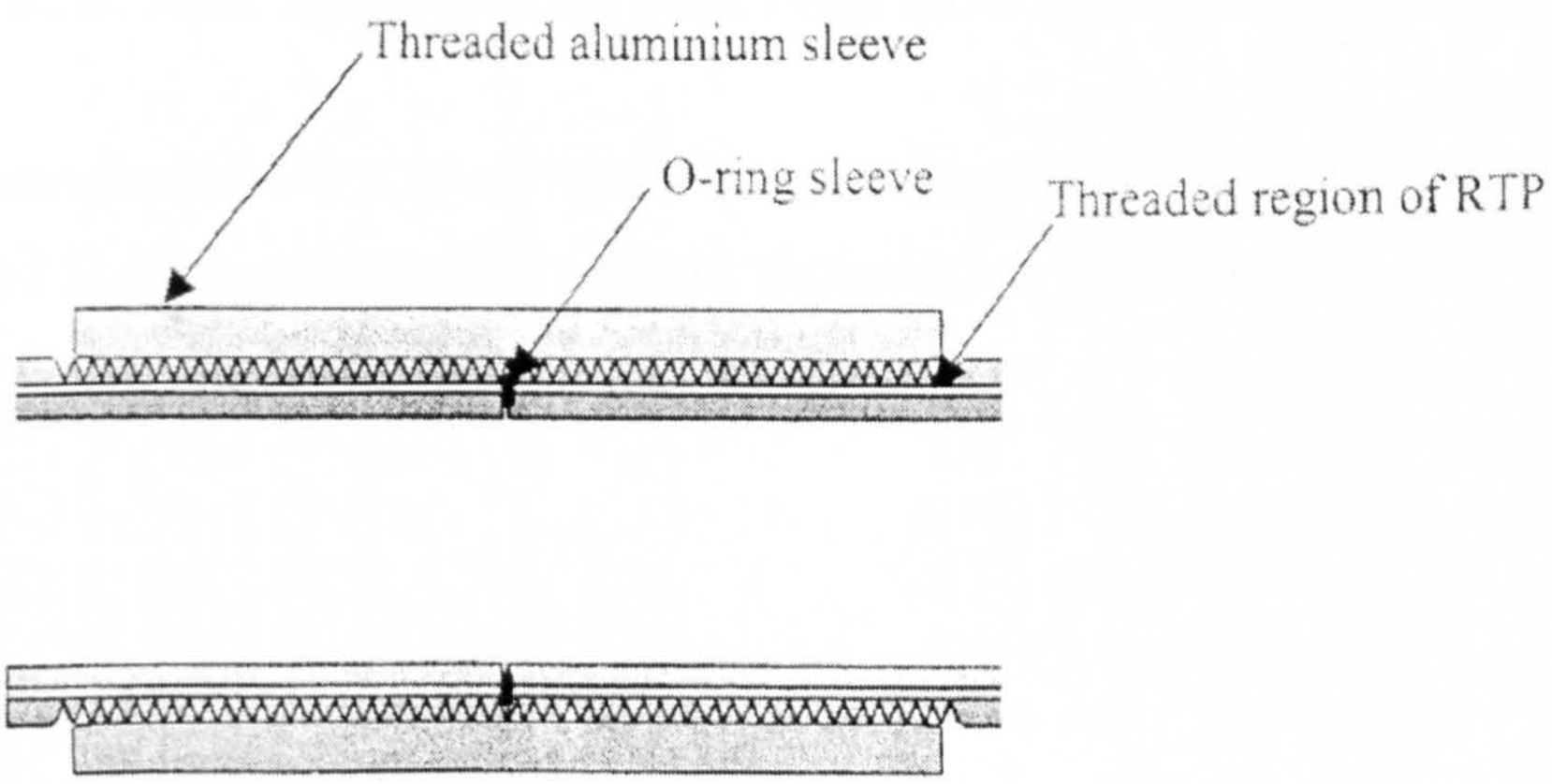

(c) Threaded RTP connector

Figure 2.3 RTP joining techniques (Cantrill, 2002)

Long-Term Behaviour of Aramid Fibre

The use of RTP pipes has many potential advantages for industry in general, and for the oil and gas industry in particular. These include (Olabisi, 2000 and Chapman et al, 1997):

- Ease of installation and speedy completion of projects.
- Cost effectiveness. Preliminary cost analysis indicates that although the initial cost of RTP is higher compared to conventional carbon-steel piping, overall installation costs (including material cost) will be slightly less than for carbon steel.
- Corrosion-free properties, both internally and externally. This eliminates the use of resources normally spent on corrosion control and monitoring the status of conventional carbon steel pipelines.
- Enhanced flow characteristics. In general, with low-friction gradients the fluid flow rate could be increased by 50 per cent with RTP compared to the same size of regular carbon-steel piping.
- The re-usability and potential recyclability of RTP systems.

The development of RTP and its technology have been discussed by Frost (1999).

The first RTP applications were in onshore transport of oilfield fluids such as oil, injection water and production fluids (Figures 2.4 and 2.5) and in gas transmission. More recently, sub-sea applications (e.g. flowlines, jumpers and flexible risers) have arisen, as shown in Figure 2.6. These figures illustrate some of the above mentioned advantages.

The principal manufacturers of RTP are Piplife bv and Technip, and it is available in diameters up to 152.4mm, with working pressure, depending on the application, of up to 12 MPa.

Figure 2.4 RTP in use for the transport of oilfield fluids (courtesy of Pipelife Bv)

Figure 2.5 600m long 4" ID coiled RTP installed on winch towed by A 4WD for one of PDO's Oman applications (courtesy of PDO)

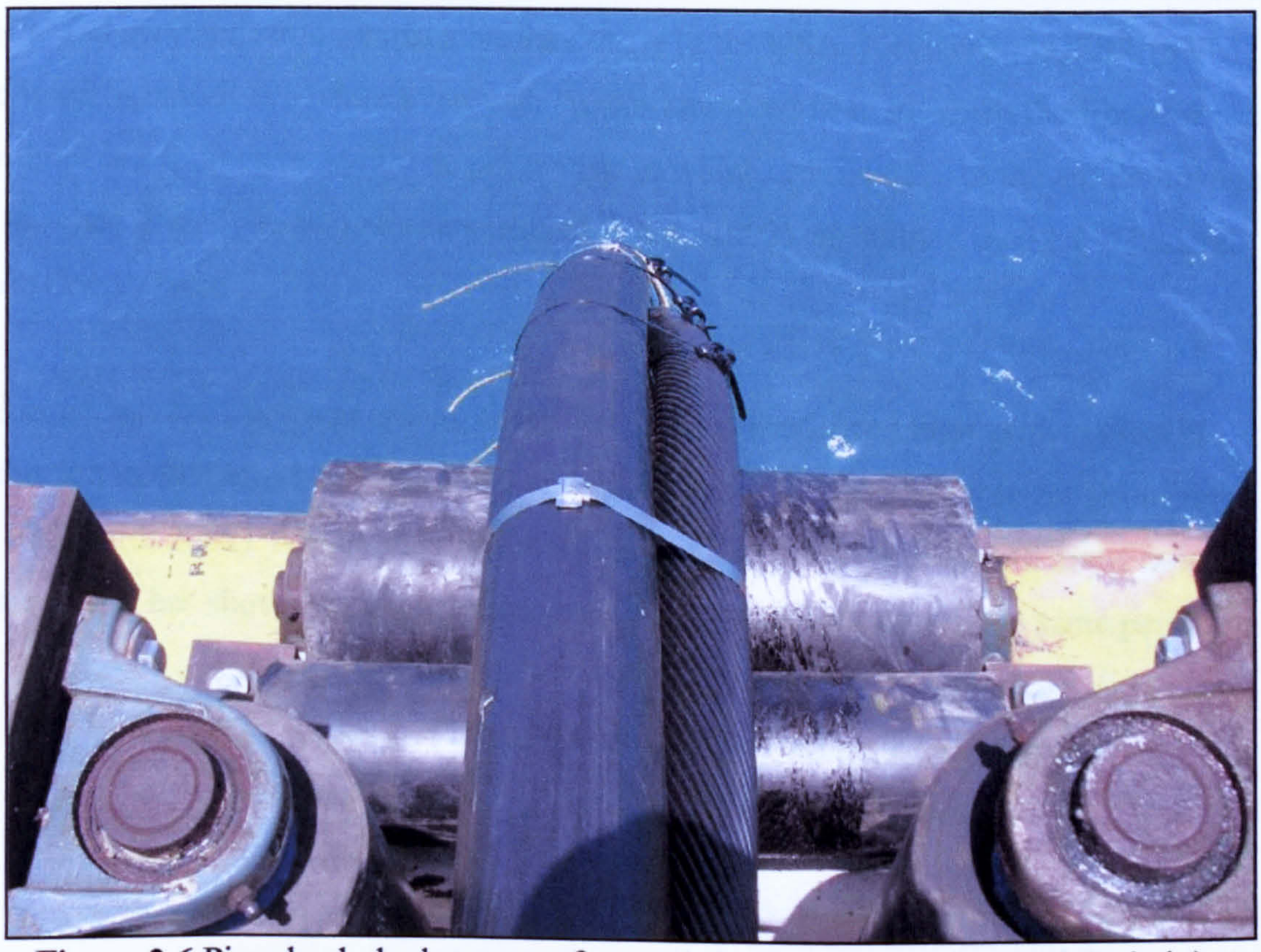

Figure 2.6 Piggyback deployment of an underwater RTP (courtesy of Technip)

2.2 Aramid Fibres

2.2.1 Background History and Applications

High performance fibres are driven by special technical functions that require specific physical properties unique to these fibres. They usually have high levels of at least one of the following properties: tensile strength, operating temperature, heat resistance, flame retardancy and chemical resistance. Aromatic polyamides or aramid fibres are one type of the important high-strength high-modulus fibres that have been known since the end of the 1960s, and they appeared almost simultaneously in the USA (Kevlar) and USSR (SVM). The word 'Aramid' is a generic term for "a manufactured fibre in which the fibre-forming substance is a long chain synthetic polyamide in which at least 85% of the amide linkages are attached directly to two aromatic rings" (Yang, 1992), as defined by the US Federal Trade Commission.

In Europe, aramid fibre was among those fibres that experienced high growth rates in production in the period between 1990 and 2000, as can be seen in Table 2.1 (Bourbigot and Flambard, 2002). Although it was marginal in tonnage compared with many other fibre types, it has shown the highest increase in manufacturing during the same period.

Table 2.1 Types and quantities of technical fibres used in Europe

Fibre Type	1990	2000	Change
	X1000 tonnes		
Polypropylene	325	1145	+252%
Polyethylene	10.5	55	+424%
Polyamide	97	142	+46%
Polyester	235	415	+77%
Polyacrylonitrile	2	26	+1200%
Glass	67	115	+72%
Carbon	0.5	3	+500%
Meta-aramid	1	3.5	+250%
Para-aramid	1	15	+1400%

Long-Term Behaviour of Aramid Fibre

Kevlar (a registered trademark of du Pont, USA), Twaron (a registered trademark of Teijin Ltd, Japan, formerly developed by Akzo BV, the Netherlands), and Technora (a registered trademark of Teijin Ltd, Japan) are the main aramid fibres in commercial production at the present.

Table 2.2 lists some of the applications of aramid fibres, while Table 2.3 gives estimates of the annual production levels of the three commercially available aramid fibre types (Buschow, 2001). Figure 2.7 includes photographs of some of these applications.

Table 2.2 Some aramid fibre applications

Application	Property Used
Brake linings	Modulus, temperature resistance
Ballistics protection	Tenacity, modulus
Protective clothing (heat etc)	Temperature resistance
Mechanical rubber goods (e.g. conveyor belts)	Tenacity, modulus
Tires, pipes, and hoses	Tenacity, modulus
Concrete reinforcement	Modulus
Optical cables, fibre reinforced composites	Tenacity, modulus, temperature resistance

Table 2.3 Approximate annual production

Brand	Polymer	Producer	Production tons/year
Twaron	PPTA	Teijin Twaron	12000
Kevlar	PPTA	du Pont	18000
Technora	p-aramid	Teijin	2000

As will be shown, the preference for using aramid fibre as a reinforcement material is due to its resistance to attack from many fluids. Moreover, it can be used without excessive damage in its non-impregnated state. Aramid fibre also shows very well defined, reproducible long term behaviour under load, which is important for establishing a long-term design basis.

Long-Term Behaviour of Aramid Fibre

Although aramid fibres are known for their high chemical resistance, they are still relatively weak in resistance to strong acids and bases. However, with the introduction of the copolymer aramid fibre Technora by Teijin in 1985 into the high performance fibre market, it became possible to use these fibres in much harsher chemical environments.

Figure 2.7 Photographs of some of the current aramid fibre applications (courtesy of Twaron)

2.2.2 Chemical Structure

Aramid fibres are made from the condensation reaction of para-phenylene diamine and terephthaloyl chloride shown in Figure 2.8 (Pigliacampi, 1995). They are based on poly (p-phenylene terephthalamide) (PPTA) macromolecules that are essentially aromatic (benzene) nuclei linked by amide bonds, and the linear rod-like molecules are cross-linked by hydrogen bonds and arranged along the axis with a high degree of regularity (see Figure 2.9). Dobb et al (1977) suggested that these fibres consist of a system of H-bonded sheets regularly pleated along their axes and arranged radially. The angle between adjacent components of the pleat is approximately 170°. Many studies have claimed that this supermolecular structure leads to a periodic banding along the fibre axis, some of which may be associated with defect layers (Morgan et al, 1983).

Another more chemically resistant para-aramid fibre, introduced by Teijin in 1985, is Technora fibre. Technora is a copolymer para-aramid fibre with a fine surface structure making it much more chemically resistant than PPTA (Bourbigot and Flambard, 2002). Figure 2.10 shows the chemical structure of the Technora fibre.

Aramid polymer, in solution, possesses a liquid crystallite structure of the nematic type (Wang et al, 1992). Liquid crystals are substances that exhibit a phase of matter that has properties between those of a conventional liquid and those of a solid crystal. For instance, a liquid crystal may flow like a liquid, but have the molecules in the liquid arranged and/or oriented in a crystal-like way. Liquid crystals can be divided into thermotropic and lyotropic LCs. Thermotropic LCs exhibit a phase transition into the LC phase as temperature is changed, whereas lyotropic LCs exhibit phase transitions as a function of concentration of the mesogen in a solvent (typically water) as well as temperature.

In both PPTA and the copolymer-PPTA, the carbon backbone bond is of the very strong covalent type, while the hydrogen bonding is of the relatively weak van der Waal type (Greenwood and Rose, 1974). So, the high strength and stiffness in the chain direction can be attributed to the aromatic groups and the covalent bonds, whereas the hydrogen bonds link the planar array formed by the chains in the transverse direction.

Long-Term Behaviour of Aramid Fibre

More in-depth investigations on the structure and properties of aramid fibre have been conducted by Dobb et al (1977), Wilfong and Zimmerman (1977), Northolt (1980), Lafitte and Bunsell (1982), Rogozinsky and Bazhenov (1992), Yang (1992)., Young et al (1992), and Kostikov (1995).

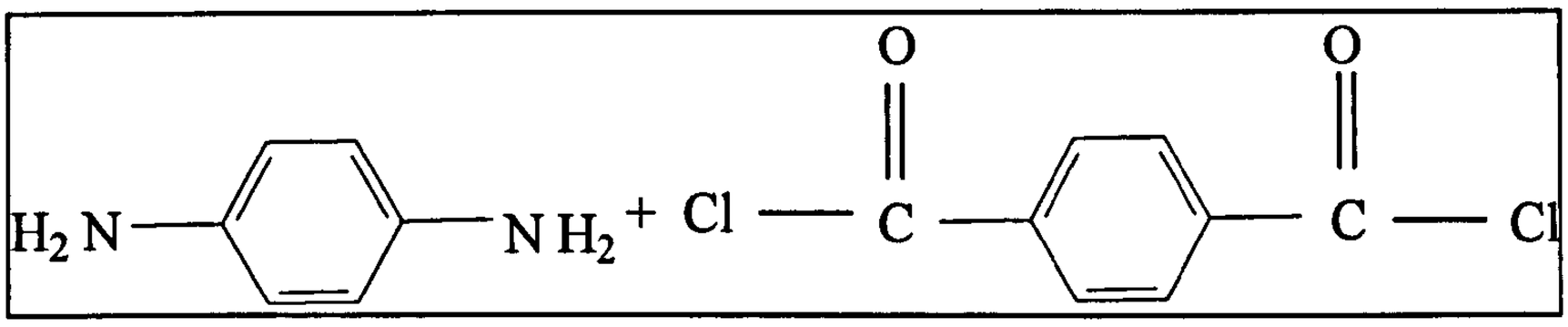

Figure 2.8 Constituents of aramid fibre: **(a)** Para-phenylene diamine, **(b)** Terephthaloyl chloride

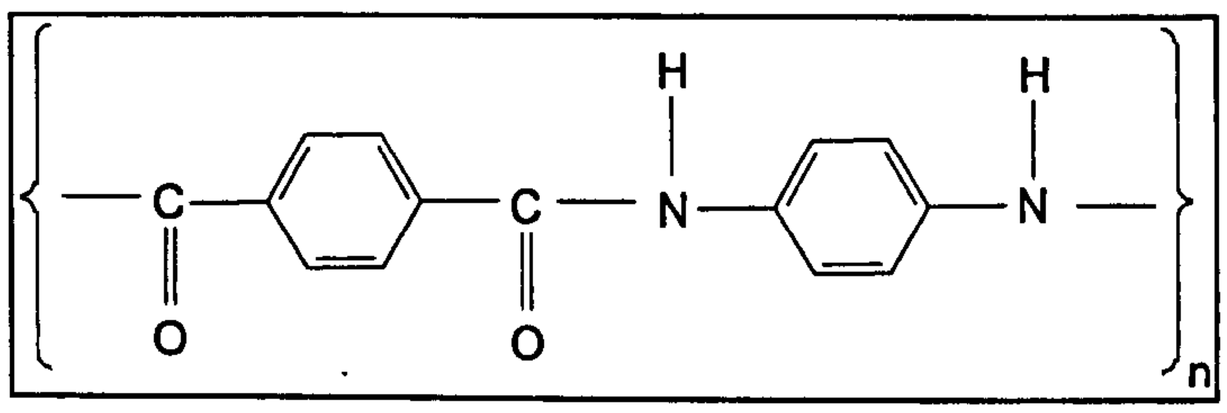

(a)

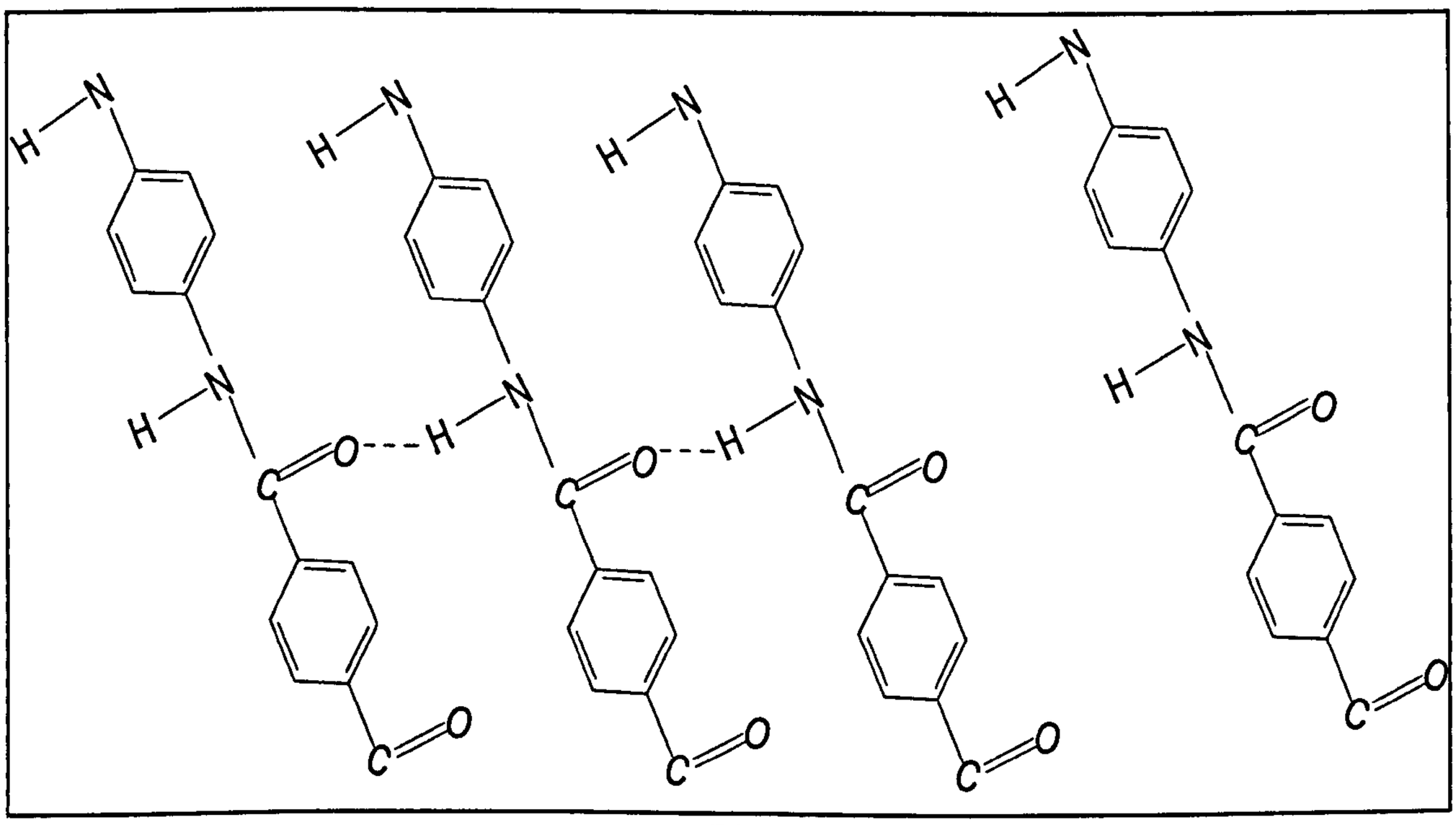

(b)

Figure 2.9 (a) Chemical structure of the PPTA polymer, **(b)** Planar representation of a unit crystal cell

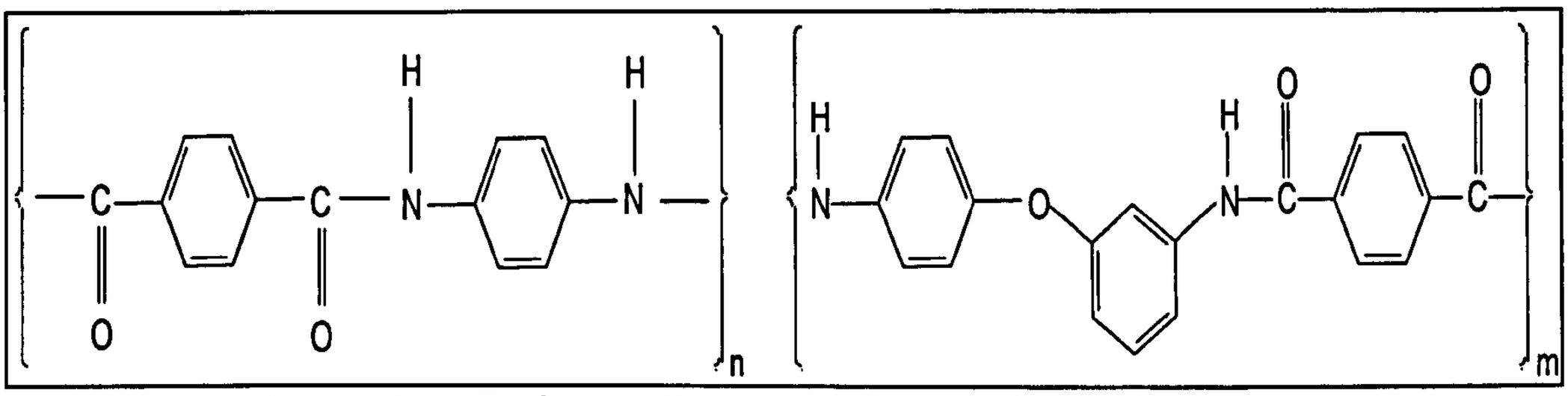

Figure 2.10 Technora (Copolymer-PPTA) chemical structure

2.2.3 Physical Properties

In addition to their favourable high strength-to-weight and modulus-to-weight ratios, aramid fibres have many outstanding properties that make them the best choice for many industrial and civilian applications. They possess a unique combination of physical, mechanical, damping, electrical and thermal properties. These remarkable properties are due to their molecular structure, which consists of highly ordered rigid chains aligned parallel to the axis leading to a high degree of crystallinity and high longitudinal modulus of elasticity (Dobb, 1979) and (Penn, 1979). Additional strength is also provided by the presence of the conjugated benzene rings that prevent bond rotation in the main chain in addition to giving the material chemical stability and mechanical stiffness. Heat treatment while under tension increases the crystalline orientation of aramid fibre and hence increases it modulus (Pigliacampi, 1995).

The hydrogen bonds in the transverse direction lend stability to the amide groups; however, they are much weaker than the covalent bonds in the fibre direction. The different kind of bonding in each direction leads to a high longitudinal strength and a low transverse strength.

ISO 2060 defines the linear density 'tex' as the mass [g] of a yarn with a length of 1000m and dtex as the mass [g] of a yarn with a length of 10,000m; hence for aramid fibres tex = g/1000m and dtex = g/10,000m alternatively, denier, which is the mass in grams of 9000m of fibre is Den = denier = g/9,000m.

Long-Term Behaviour of Aramid Fibre

In order to calculate the cross sectional area A of a yarn, the following equation can be used:

$$A = \frac{LD}{\rho} \times 10^{-4}, \qquad [2.1]$$

where, A is in mm^2;

ρ is density in g/cm^3;

LD is linear density in dtex.

The breaking force of aramid fibre is commonly expressed as tenacity, which is obtained by dividing the breaking force [N] by the linear density [dtex]. Aramid fibres' tensile modulus is expressed by means of a chord or secant modulus according to either an ASTM or DIN standard. The ASTM takes the tensile modulus between tenacity values of 300 and 400mN/tex, compared to 400 and 800mN/tex for the DIN standard (Figure 2.11).

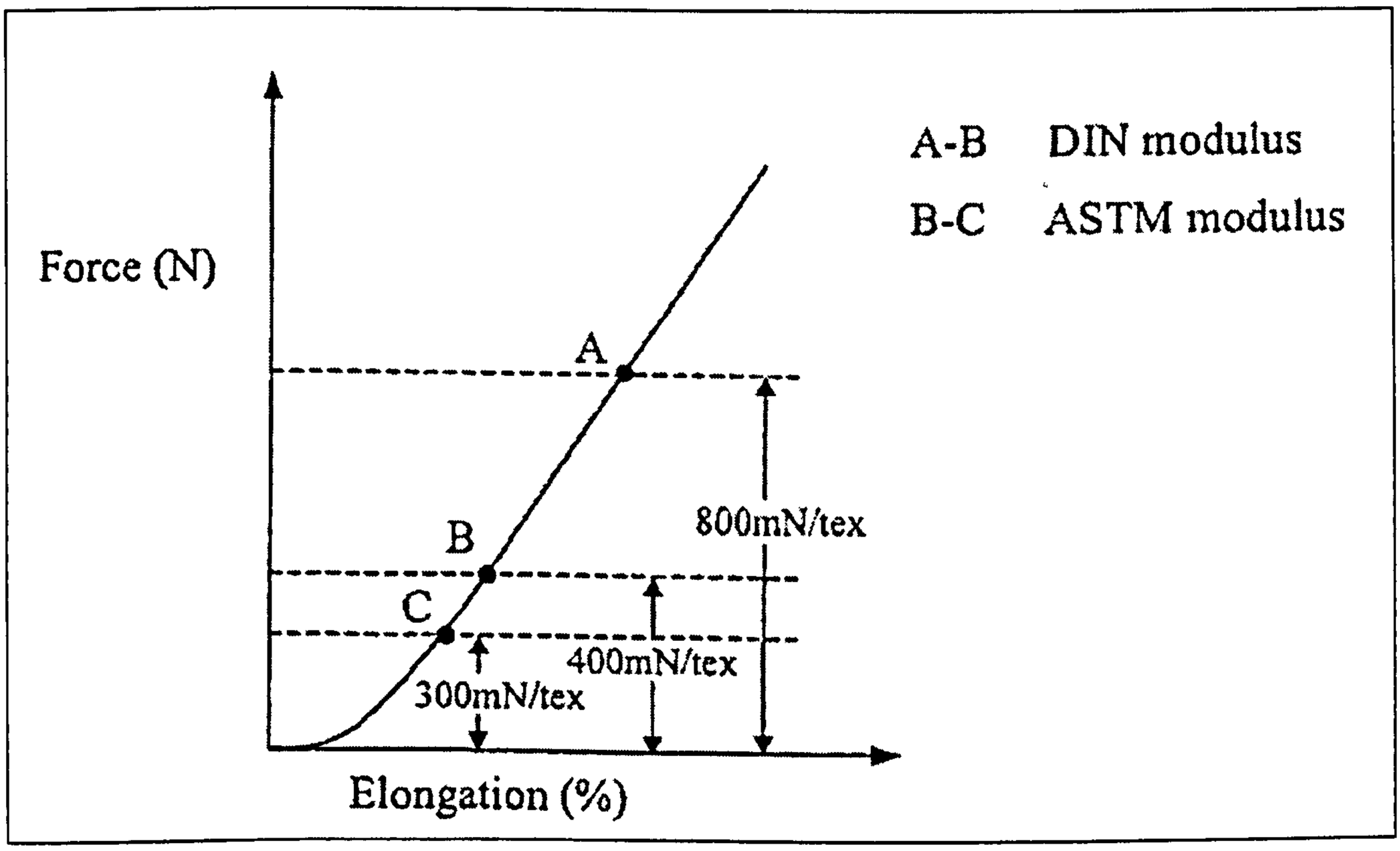

Figure 2.11 Methods used for determining the chord modulus from the force elongation curve, according to ASTM D885 and DIN 65356 Pt2

Long-Term Behaviour of Aramid Fibre

Aramid fibres have high breaking tenacity, high tensile modulus, low elongation at break, and low density. Also they are inherently stable with very small shrinkage at relatively high temperatures, and have low creep and a rather high glass transition temperature. In addition, they are corrosion resistant, non-conductive, and resistant to most chemicals except strong acids and bases. Table 2.4 and Figure 2.12 show some physical properties of different types of aramid fibres compared to those of other types of fibres (Lafitte and Bunsell, 1982; Yeh and Young, 1999).

Table 2.4 Comparison of the properties of different filaments

Sample	Strength (GN/m^2)	Modulus (GN/m^2)	Breaking Strain (%)	Density (g/cm^3)
Kevlar 29	2.60	62.0	4.2	1.44
Kevlar 49	2.70	130.0	2.0	1.45
Technora	3.4	73	4.6	1.39
Nomex	0.65	20.0	23.0	1.38
Nylon T728	1.00	5.6	18.5	1.14
Steel	2.80	200.0	2.0	7.83
Boron	3.00	370.0	1.0	2.70
Glass	3.50	70.0	4.8	2.54
Carbon HS	2.70	270.0	0.8	1.80
Carbon HM	2.00	400.0	0.5	1.95

As shown in Table 2.4, aramid fibres have a tensile strength and modulus comparable to that of glass fibre, yet their density is almost half that of glass. In the case of these properties of aramid fibres, the table also shows that different preferred properties can be attained, at the expense of others, to meet specific application requirements. For example, Kevlar 49, although exhibiting similar strength to that of Kevlar 29, has double the tensile modulus but with reduced breaking extension (Dobb and Robson, 1990).

Dobb and Robson (1990) illustrated the effect of high molecular orientation on the tensile properties of different types of aramid fibres. According to their study, high orientation

promotes efficient load-sharing between molecular chains, and hence increases the tensile modulus of the fibre.

The commercially available yarns consist of many fibres usually twisted together. Yarn twisting usually results in more consistency in measurements of the breaking strength and elongation at break because of the distribution of tensile forces between the yarn's filaments. It has been noted that the level of twist in an aramid fibre yarn or cord will affect its physical properties such as tenacity, modulus, and elongation as well as its fatigue performance. Figure 2.13 shows the influence of twist on the yarn tensile properties of Kevlar aramid fibre. As can be noticed from the figure, yarn tenacity is maximized at a twist multiplier of about 1.1. Modulus declines with increasing twist level; slowly at low twist levels, and more rapidly at higher twist levels. Elongation increases slightly with increasing twist. The twist multiplier is related to the added twist (in turns per unit of yarn length) and yarn denier (or dtex), as defined below:

$$Twist\ Multiplier = \frac{Turns\ per\ meter \times \sqrt{dtex}}{3000}, \qquad [2.2], \text{ or}$$

$$Twist\ Multiplier = \frac{Turns\ per\ meter \times \sqrt{Denier}}{2874}, \qquad [2.3]$$

When impregnated, aramid strand with zero twist produced similar positive effects on strength to those of twisted filaments without the adverse consequences of twisting, although this effect is dependant on the fibre volume content and the impregnation resin type (Wilfong and Zimmerman, 1977).

The compressive properties of aramid fibres are significantly different from the tensile properties, mainly because of the highly crystalline structure and high modulus. Table 2.5 presents a comparison of tensile, compressive and shear properties of Kevlar 49 fibre (Deteresa et al, 1984).

Table 2.5 Typical properties of Kevlar aramid 49 yarn

	Tensile	Compressive	Shear	Tensile / Compressive	Tensile / Shear
Strength [GPa]	3.4	0.7	0.18	5	17
Modulus [GPa]	130	130	1.8	1	70
Strain to break or yield %	2.5	0.5	10	5	0.25

It has been noted that aramid fibres have very poor abrasion resistance and tend to fibrillate easily when rubbed against another fibre or metal surface, indicating weak cohesion between fibrils (Konopasek and Hearle, 1977). This could be because of its weak lateral bond forces or the anisotropic nature of its structure.

Dobb et al (1979) indicated that considerable loss in aramid fibre mechanical performance could be encountered due the presence of a system of voids on the fibres. Voids, within the fibre's structure as it will be explained in Section 2.2.4, will tend to reduce both the potential lateral and tensile strengths of the fibre. Moreover, if these voids have length to width ratios greater than unity then the effect will be greater on lateral than on tensile properties, hence contributing to low compression strength. These voids are formed during the solidification of the polymer in the coagulation of the extrusion process. More voids could also be produced during subsequent heat treatment, particularly as a result of some localized shrinkage associated with the improvement in molecular packing.

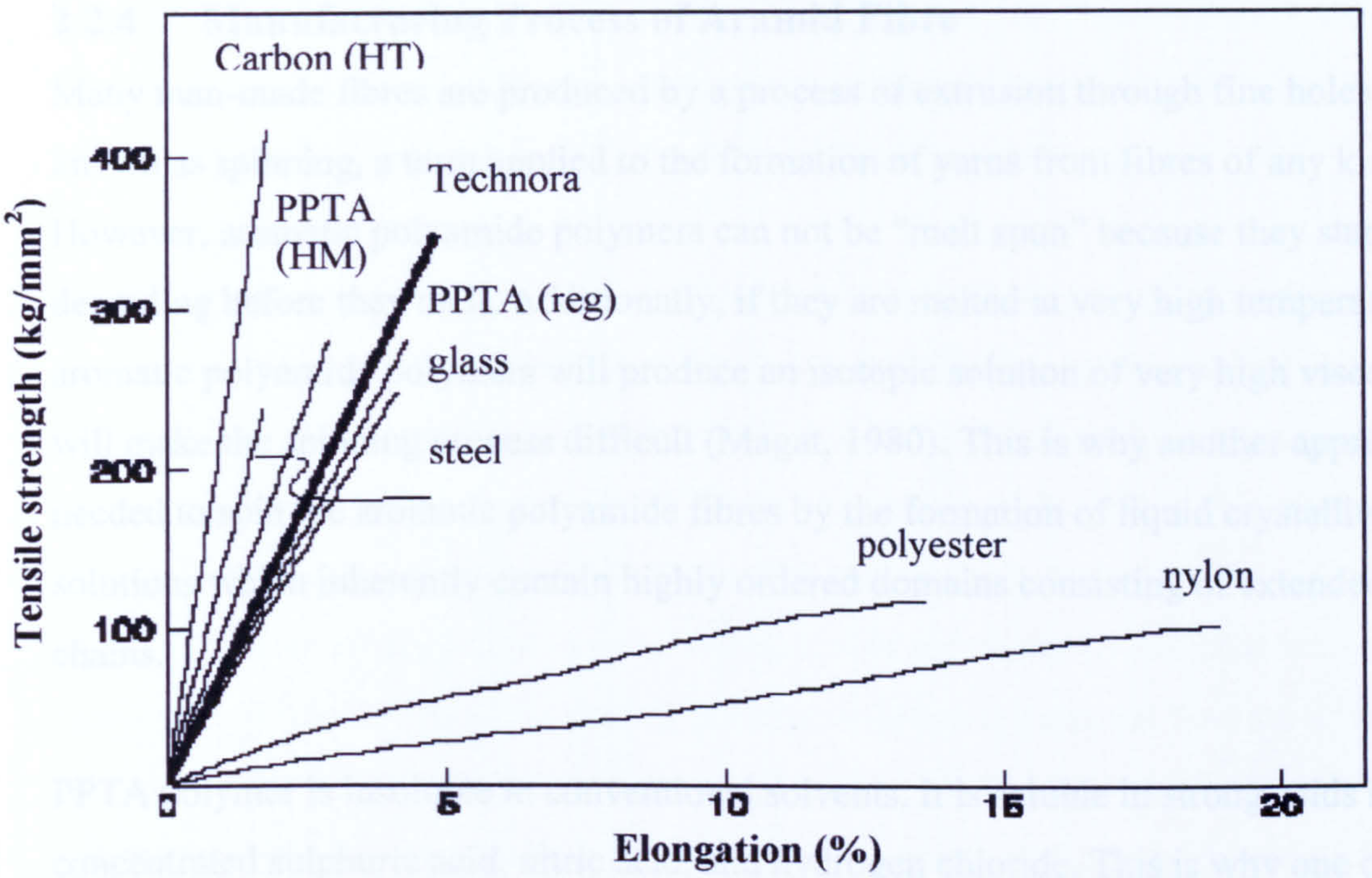

Figure 2.12 Stress-strain curve comparison of different fibre materials (Technora Brochure)

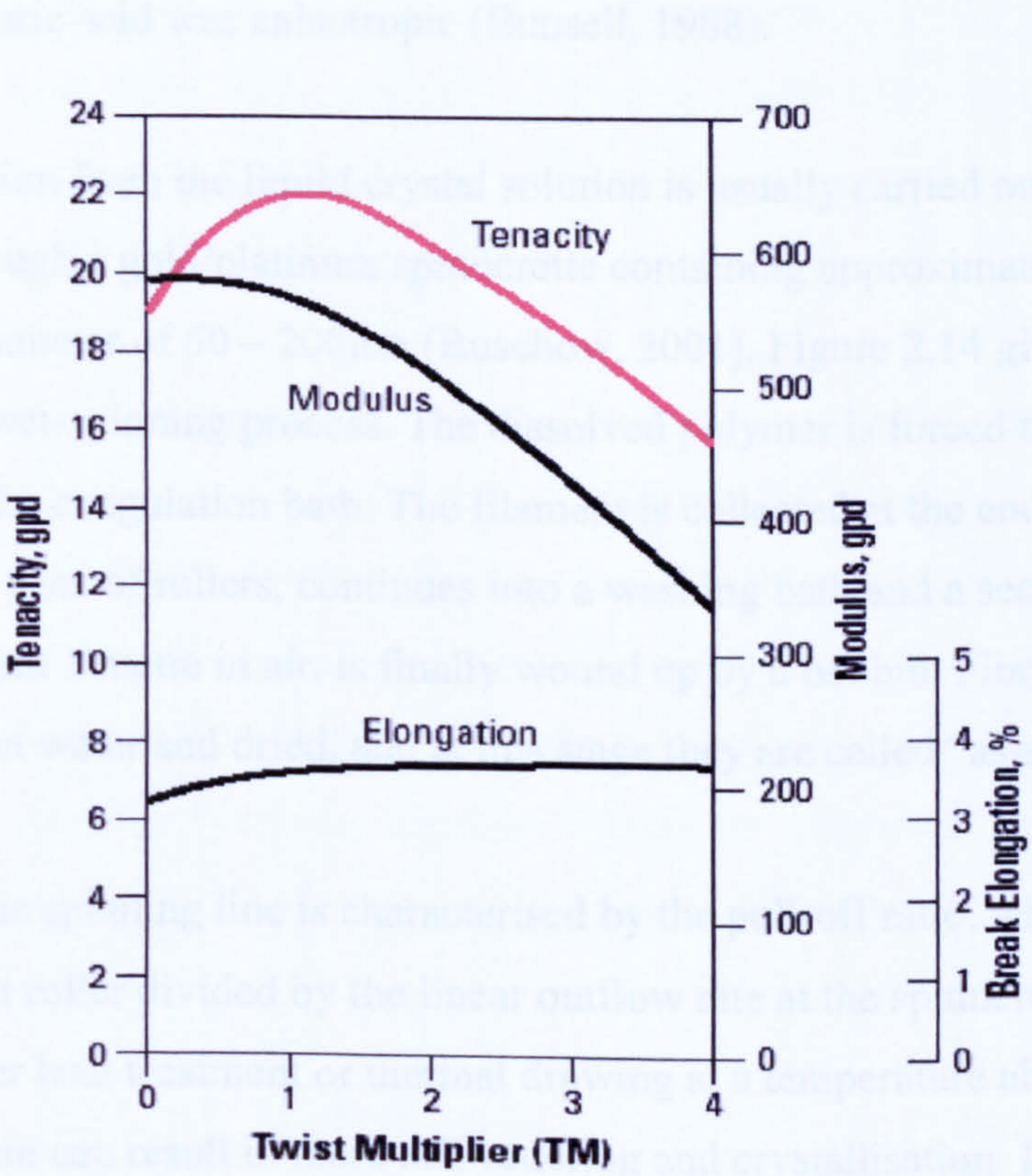

Figure 2.13 Effect of twisting on the properties of Kevlar aramid fibre (du Pont, 2001)

2.2.4 Manufacturing Process of Aramid Fibre

Many man-made fibres are produced by a process of extrusion through fine holes that is known as spinning, a term applied to the formation of yarns from fibres of any kind. However, aromatic polyamide polymers can not be "melt spun" because they start degrading before they melt. Additionally, if they are melted at very high temperatures, aromatic polyamide polymers will produce an isotopic solution of very high viscosity that will make the spinning process difficult (Magat, 1980). This is why another approach was needed to spin the aromatic polyamide fibres by the formation of liquid crystallite spinning solutions which inherently contain highly ordered domains consisting of extended polymer chains.

PPTA polymer is insoluble in conventional solvents. It is soluble in strong acids such as concentrated sulphuric acid, nitric acid, and hydrogen chloride. This is why one of these acids is used to dissolve the polymer so that it can be extruded through the spinnerette holes to form a fibre. In the 1960s Kwolek discovered that a 10% solution of PPTA in at least 98 wt.% sulphuric acid was anisotropic (Bunsell, 1988).

The spinning operation from the liquid crystal solution is usually carried out by extruding the LC solution through a gold/platinum spinnerette containing approximately 1000 capillaries with a diameter of 50 – 200μm (Buschow, 2001). Figure 2.14 gives a schematic view of the dry-jet wet-spinning process. The dissolved polymer is forced through the spinnerette hole to the coagulation bath. The filament is collected at the end of the coagulation bath by a set of rollers, continues into a washing bath and a second set of rollers and, after about 1 metre in air, is finally wound up by a bobbin. Fibres on the bobbin are washed in water and dried, and at this stage they are called "as-spun" fibres.

The tension along the spinning line is characterised by the pull-off ratio, which is the take-up rate by the fastest roller divided by the linear outflow rate at the spinnerette (Ciferri and Ward, 1979). Further heat treatment or thermal drawing at a temperature above the glass transition temperature can result in more self-ordering and crystallisation. In the work conducted by Picken et al (1992), the optimum processing conditions with respect to

coagulation bath temperature, polymer concentration and draw ratio were all determined. The semi-empirical model developed gives values for the degree of molecular orientation and the resultant fibre modulus as a function of the above parameters.

The PPTA molecule contains rigid covalent bonds in its main polymer chain and its chain conformation is almost rod-like. However, when in a dilute solution, the rod-like PPTA molecules are randomly oriented as in Figure 2.15. This solution is isotropic, but when the polymer concentration is increased, PPTA molecules are packed closer together, and when the concentration is increased beyond a certain critical limit, the molecules will begin to adopt an ordered arrangement in small domains that are randomly oriented with respect to each other. When the liquid crystalline polymer solution is extruded through a small spinneret hole, the extensional flow causes rotation and alignment of the domains, ultimately leading to an excellent orientation of the polymer chains with very little shear. When cooled to below the transition temperature, the molecules start forming a two-dimensional solution with a highly ordered anisotropic layered structure which by further cooling will solidify. These phase transformations are characteristic of liquid crystalline polymer solutions (Yang, 1992). The structure of the anisotropic fibres confirms their high degree of crystallinity of up to 75.5%, with an apparent size of crystallites of 5.0 to 10.0 nm stretched along the axis (Dobb, 1977).

When arranged in a certain orientation distribution with respect to the fibre axis, the solidified crystallites form what is called a fibril. Filaments, the next building unit up, consist of many identical fibrils. Finally, yarns contain hundreds of filaments. Figure 2.16 illustrates the structural sequence of a single aramid yarn. This structural description is supported by Panar et al's (1983) study in which the authors were trying to answer the question of whether the intact fibres are bundles of fibrils, or whether fibrils are simply the result of cleavage along the axis of the crystalline polymer on fracture.

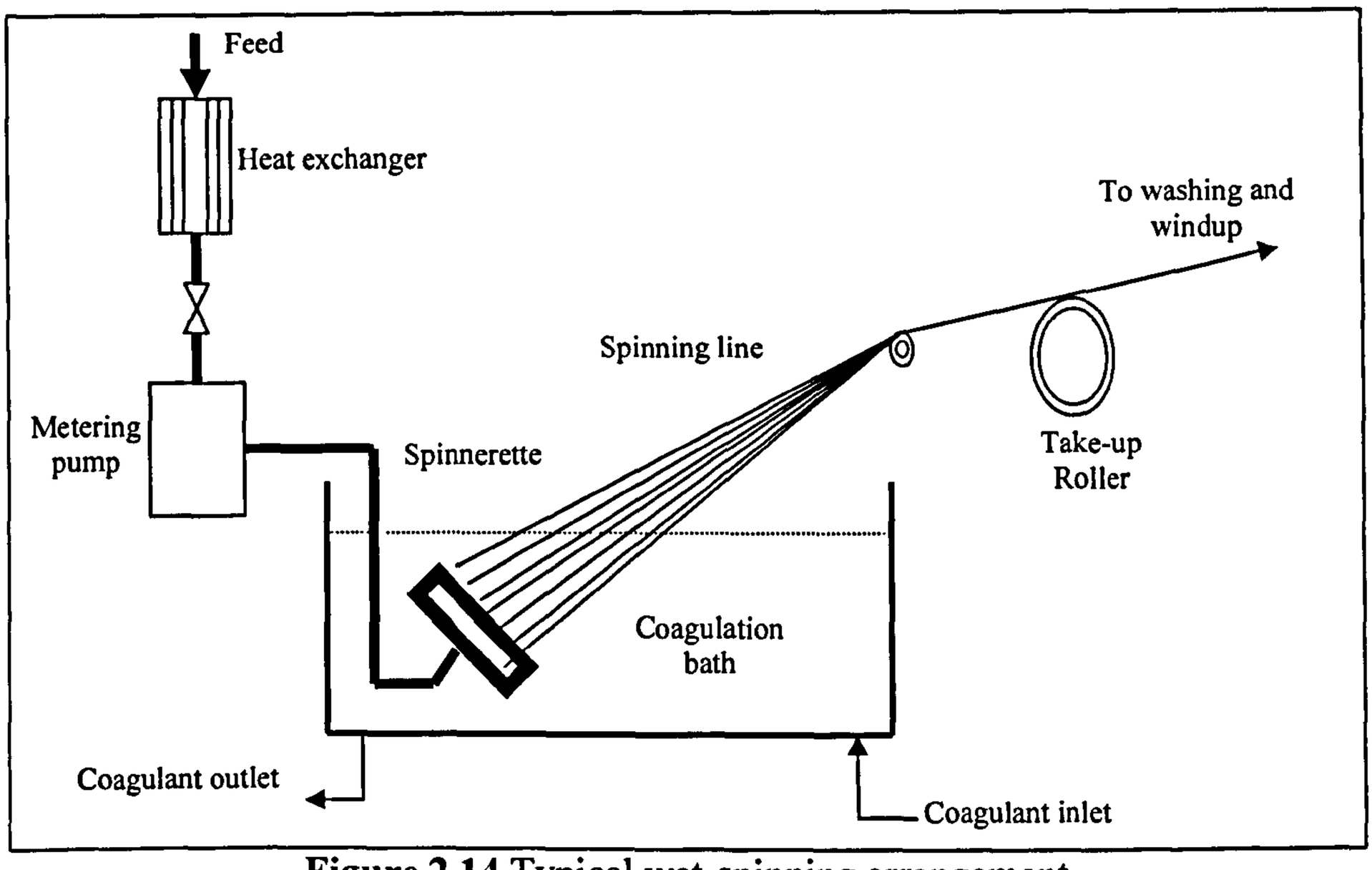

Figure 2.14 Typical wet-spinning arrangement

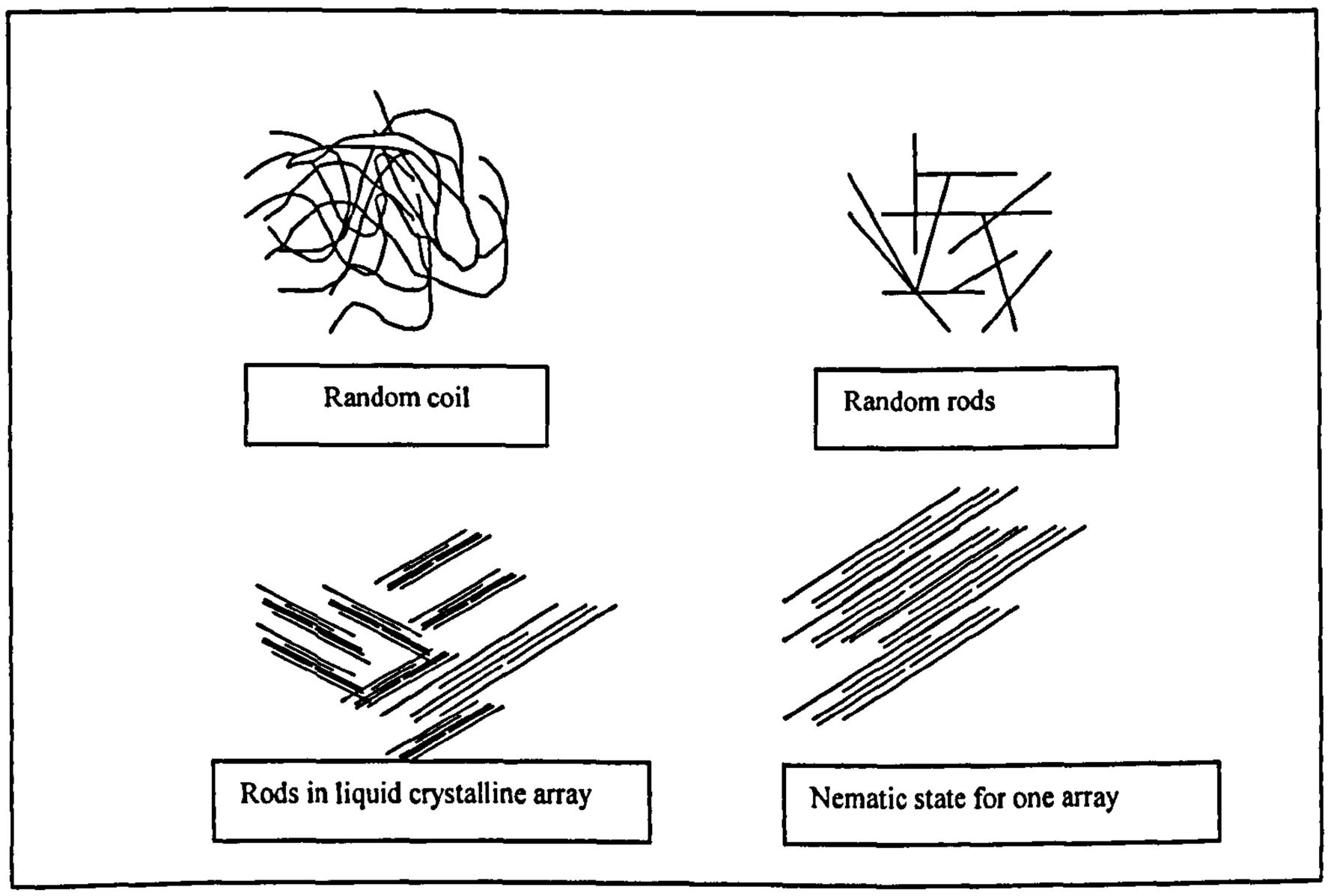

Figure 2.15 Liquid crystalline structures of PPD-T/H_2SO_4 solution

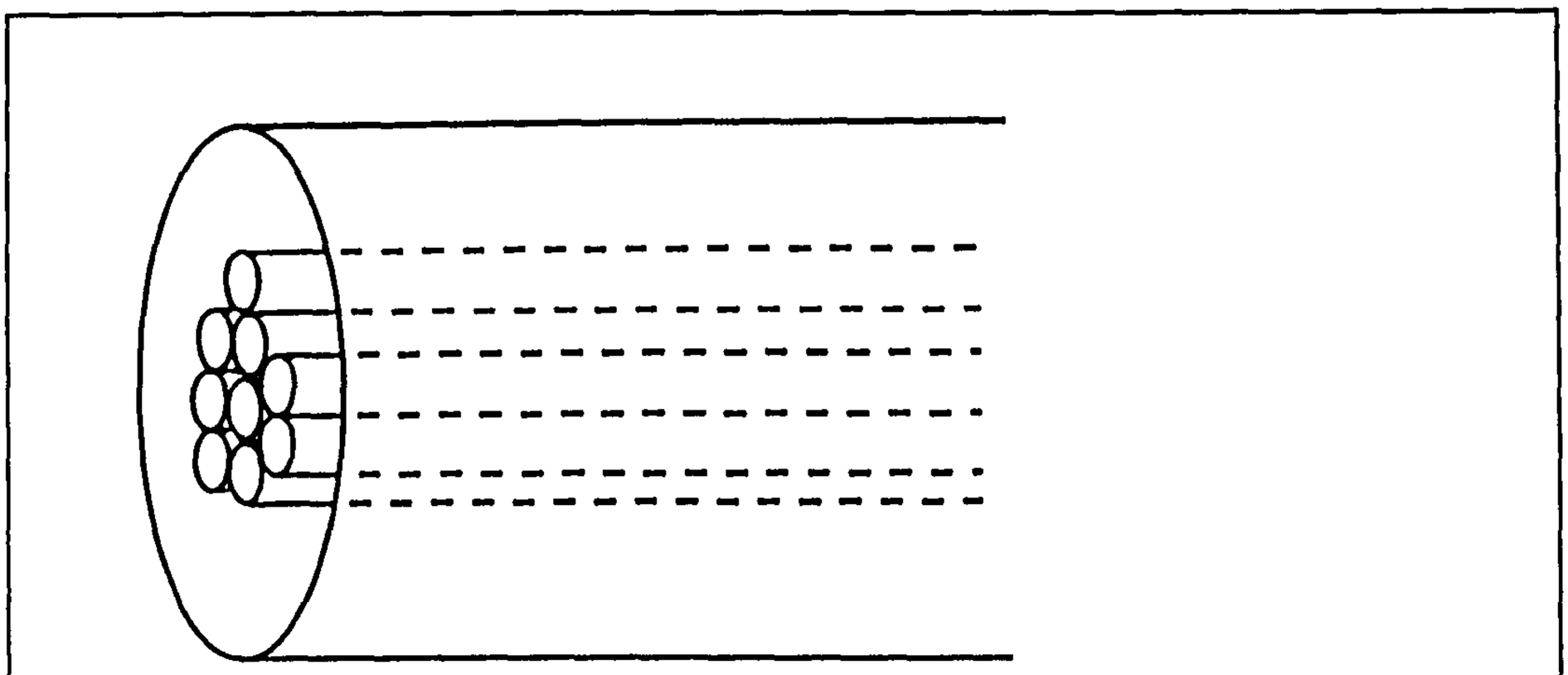

Twaron 1000 **yarn** contains 1000 filaments

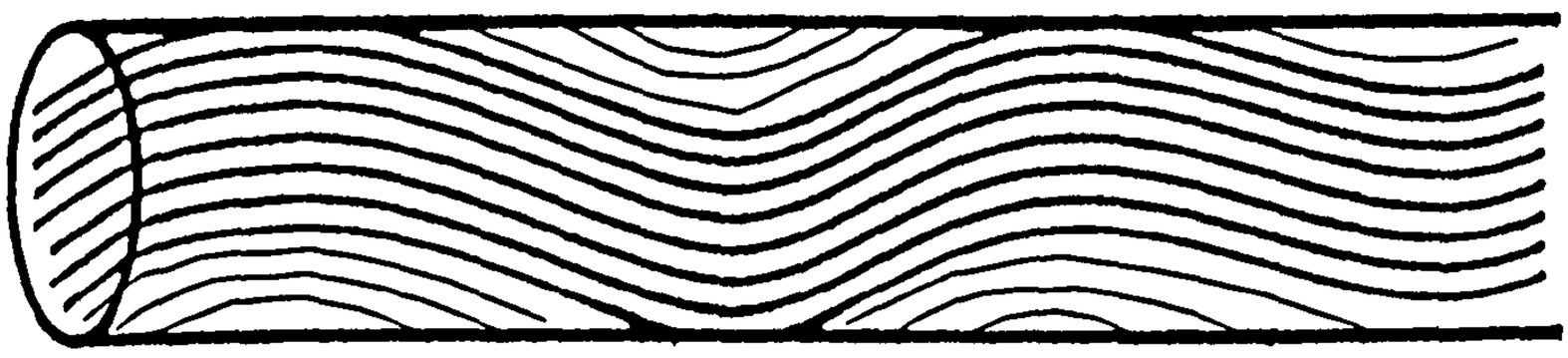

Filament composed of identical fibrils.

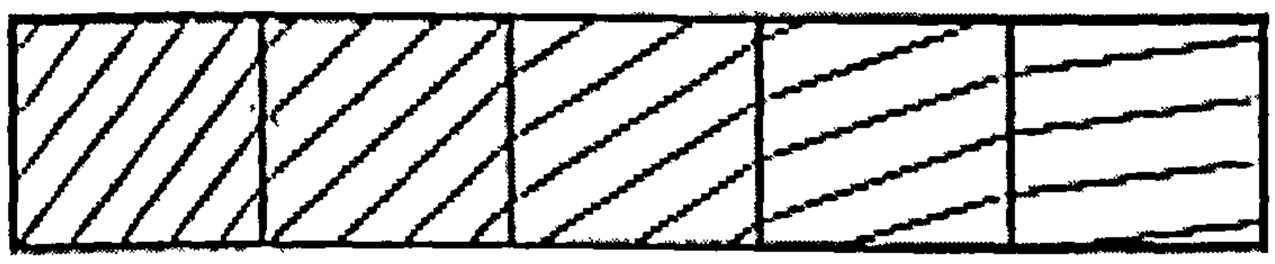

Schematic serial arrangement of **crystalline domains.**

Figure 2.16 Illustration of the structural sequence of a single aramid yarn

2.3 Environmental Effects on Aramid Fibres

Due to the wide range of applications for aramid fibres, it is important to study their interaction with different environments. This is because, with chemical ageing for instance, polymers in general experience a loss in performance due to the gradual breakdown of their molecules into smaller units. On the other hand, polymeric materials are generally known not to be susceptible to corrosion problems caused by electrochemical effects, because they are non-conductors. The sub-sections below explain the effects of various environments relevant to this project on aramid fibres.

2.3.1 Temperature Effects

Many applications involve operation at elevated temperatures; therefore, the effect of temperature on the material's properties is of interest.

Aramid fibres do not have an exactly defined glass transition temperature as would normally be the case with other synthetic polymers. The continuous operating temperature of these fibres in air is up to 190°C, and they will degrade in air above 400°C but do not melt below this temperature. They glow during ignition, and no after-burning is observed after removal from the flame, but char is produced above 450°C. The Limiting Oxygen Index (LOI) for PPTA fibres lies between 28 and 30 vol.% (Bourbigot and Flambard, 2002).

Figure 2.17 shows the effect of temperature on the breaking tenacity of Kevlar aramid fibre. Figure 2.18 shows the effect of temperature on the initial modulus of Kevlar fibre compared to other reinforcement materials. Figure 2.19 shows the time-dependent tenacity of Kevlar aramid fibres at different temperatures.

It is clear from these properties that, for the maximum operating temperature currently specified for RTP (65°C), the temperature dependence of aramid should not be a concern because of the very limited effect of temperature on its strength properties in the 65°C temperature range. However, tests are required at higher temperatures to accelerate undesirable failure modes, if any, into the qualification test period.

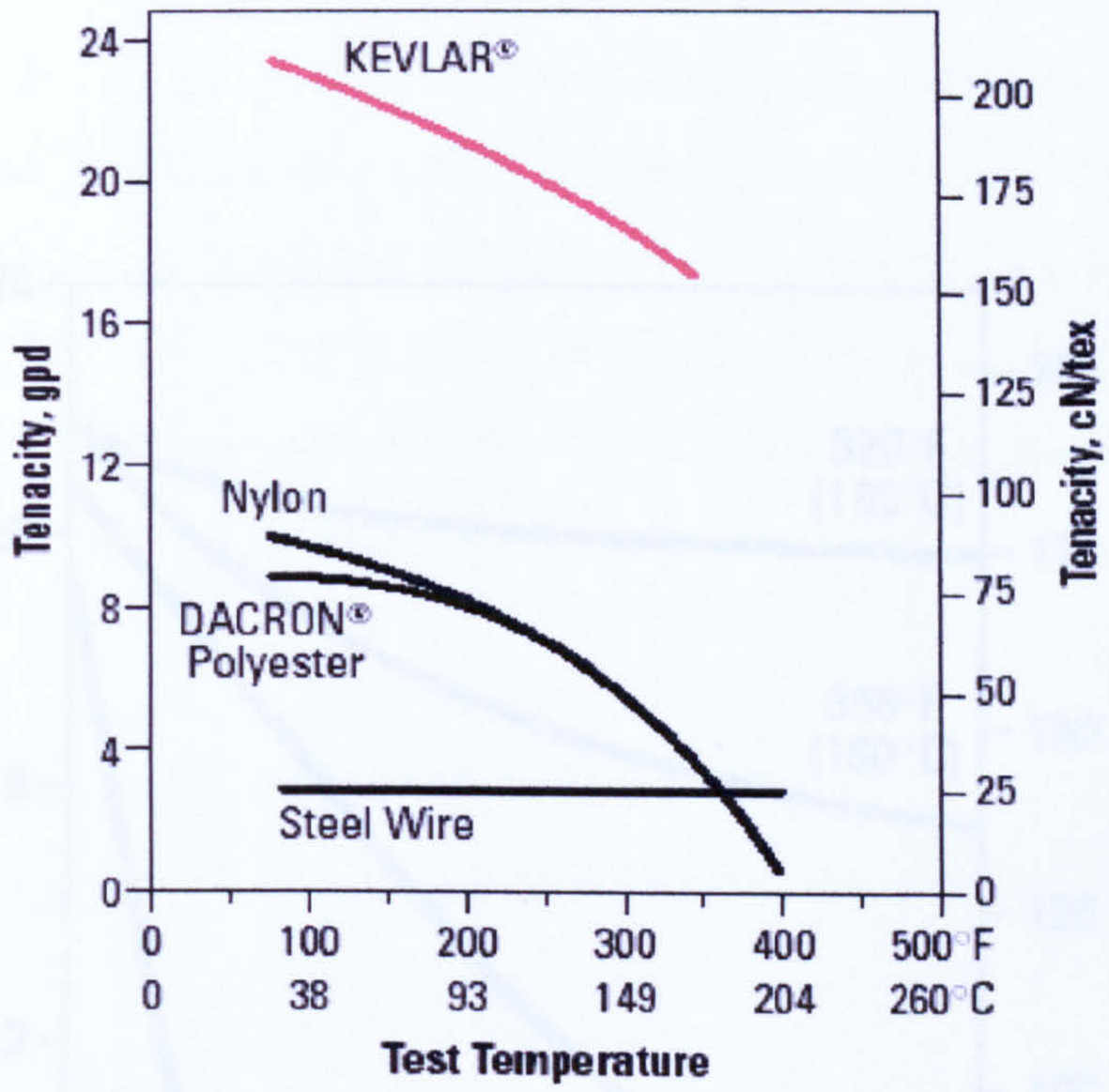

Figure 2.17 Temperature effect on breaking tenacity of Kevlar compared to other industrial filament yarns (du Pont, 2001)

Figure 2.18 Temperature effect on initial modulus of Kevlar compared to other industrial filament yarns (du Pont, 2001)

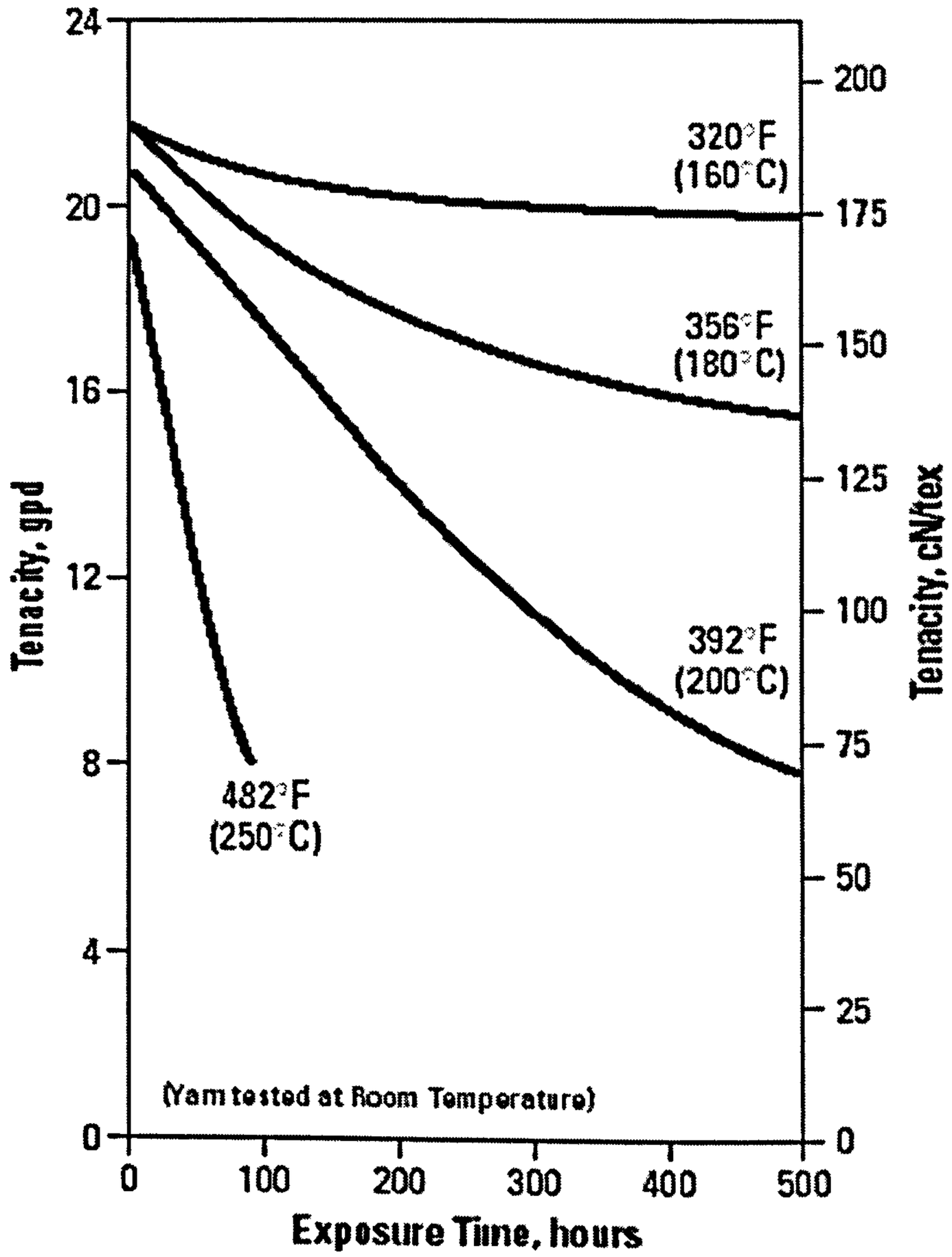

Figure 2.19 Reduction in Kevlar tenacity after prolonged heating in air (du Pont, 2001)

2.3.2 Hydrolysis and Plasticization Effects

It is believed that aramid fibres are susceptible to hydrolysis effects under certain conditions. Bernstein et al (2003) compared between Kevlar and Nylon in terms of hydrolysis effect, and concluded that both polymers are susceptible to hydrolysis. Actually, because water molecules are small and polar, they can approach the hydrogen bonding sites and disrupt the original hydrogen bonds of the fibre (Wang et al, 1992). Morgan et al (1984) suggested that the amide group in the PPD-T molecule may be hydrolyzed and undergo chain scission according to the following reaction:

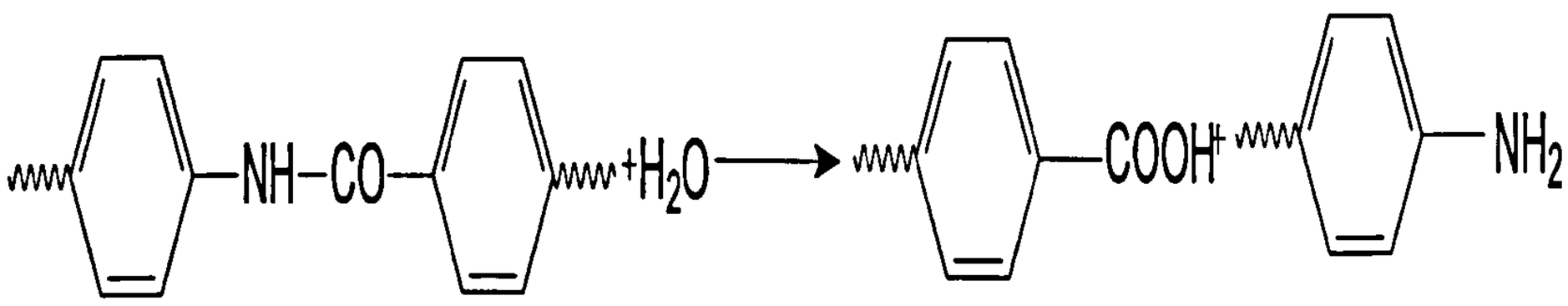

Of course, such hydrolytic degradation will lead to loss of strength. However, and as indicated by Morgan et al, the strength loss in typical environmental conditions is not a serious problem. Cook et al (1982) reported Gourdin's study on Kevlar 49 which concluded that the fibre's tensile strength was only slightly influenced by water immersion. On the other hand, Cantrill (2002) reported that Kevlar lost 16% of its original strength when exposed to saturated steam at 138°C for 80 hours, as a result of hydrolysis. Figure 2.20 shows the effect of 100 hrs exposure to saturated steam on different types of fibres, including aramid fibres.

Three different kinds of water were detected in aramid fibres by Chatzi et al (1986): free unbounded water, weakly hydrogen-bonded water, and strongly hydrogen-bonded water. It is believed that the free unbounded water exists in microvoids and interstices, while both types of hydrogen-bonded water molecules reside between the crystallites of the aramid fibres. It is believed that sites for water sorption and diffusion paths are created where residual amounts of Sodium sulphate (Na_2SO_4) impurities (introduced through the manufacturing process of the fibre) remain trapped in the fibre (Morgan et al, 1983). Na_2SO_4 is a known desiccant and when present in the fibre will definitely contribute to

water absorption. Penn and Larsen (1979) conducted a series of Thermogravimetric Analysis (TGA), Differential Scanning Calorimetry (DSC) and Thermomechanical Analysis (TMA) experiments in which they confirmed the presence of water in different Kevlar fibres. Water accumulation at these sites distorts the molecular packing in the transverse fibre direction and enhances the ease of fibrillation. It is also reported that water content of aramid fibres increases with a decrease in the degree of crystallinity of the fibre (Minsoshima, 2000). Hence, water could also reside in the amorphous regions of the fibre.

Another possible form of water (or moisture) effect is plasticization. This is a reversible reaction, particularly in high temperature environments, that causes reduction in strength and stiffness. Piigliacampi (1995) reported that, at room temperature, the effect of moisture on tensile properties is <5%, while at elevated temperatures the effect of moisture appeared to be reversible.

2.3.3 Chemical Solutions Effects

Aramid has excellent chemical resistance when exposed to most aqueous salt solutions and organic solvents. However, strong acids and alkalis at elevated temperatures and strong concentrations attack aramid. Figure 2.21 shows the effect of pH on the residual strength of Twaron fibres after 3 months exposure at room temperature.

In addition to their observations on the effect of water, Morgan et al (1983) also reported that Na_2SO_4 impurities significantly affect the packing of the PPTA macromolecules in the transverse fibre direction and further enhance fibrillation. The presence of these impurities in the fibre's ash was proven by Penn and Larsen (1979) in their elemental analysis for different Kevlar fibres. Additionally, incomplete neutralization of H_2SO_4 will result in the presence of residual acid in the fibre and subsequently cause fibre degradation as a result of acid-induced chain hydrolysis. Fibres containing residual H_2SO_4 darken and lose their strength.

Extensive data are available from the manufacturers of aramid fibres on the performance of their fibres in different chemicals, but it should be noted that these data relate to exposure

in the unstressed state. There is almost nothing available in the public domain on the performance of aramid fibres in different environmental conditions while under stressed conditions.

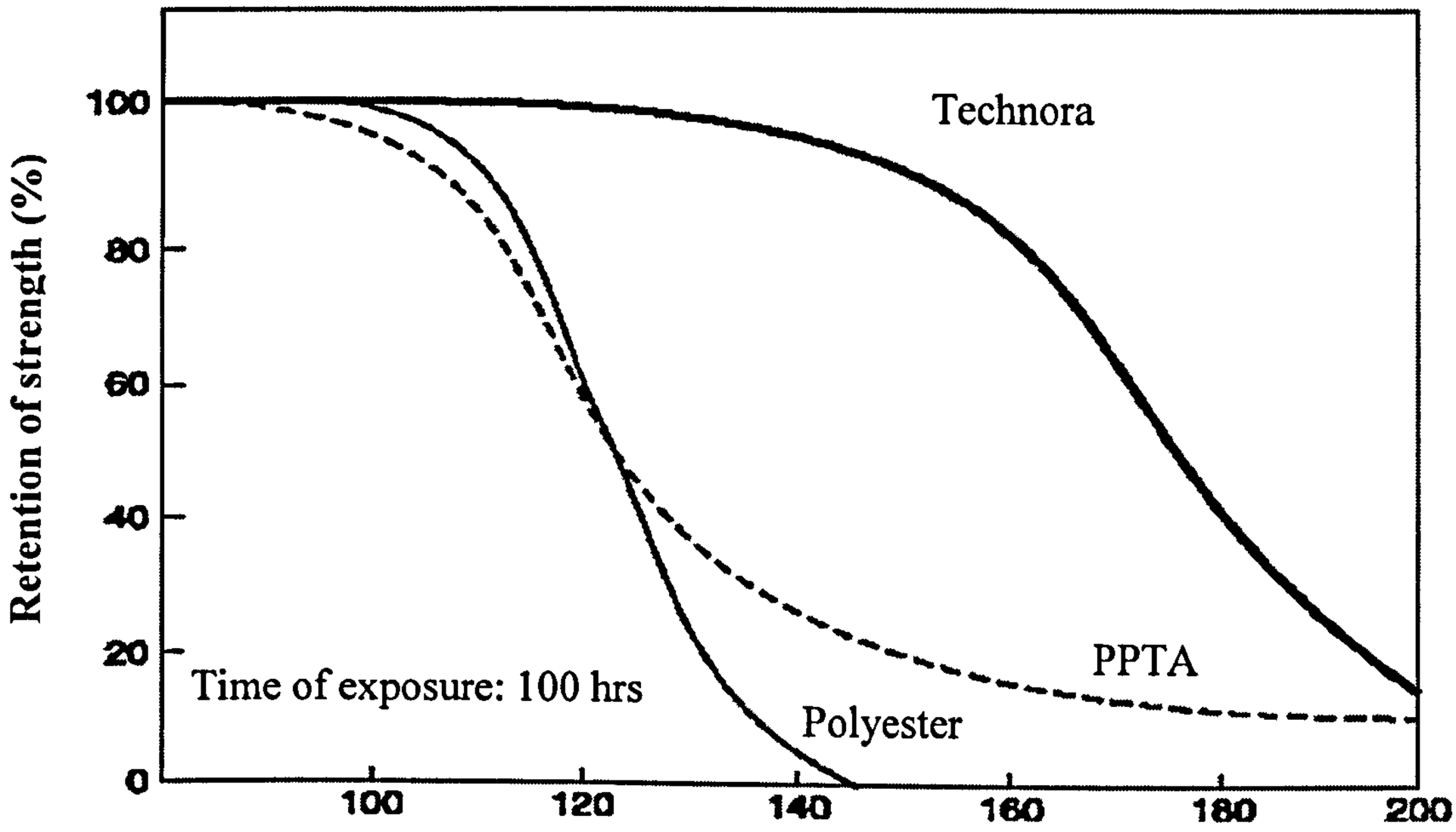

Figure 2.20 Effect of exposure to saturated steam on the strength of different fibres (Technora Brochure)

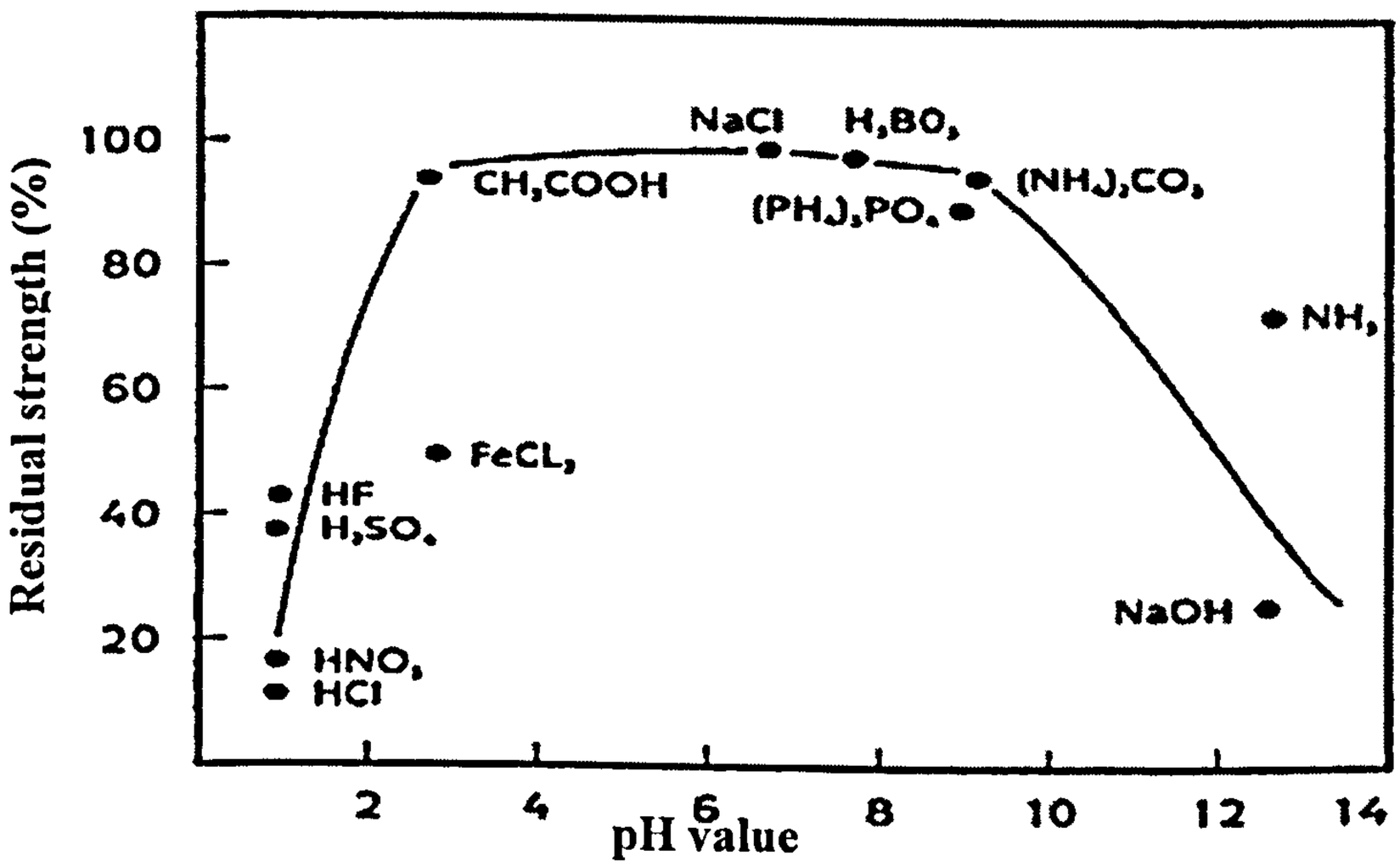

Figure 2.21 Effect of pH on the residual strength of Twaron fibre after 3 months exposure at room temperature (Twaron Technical Report QET 99023, 2001)

2.3.4 Ultraviolet Radiation Effects

It is known that UV light with wavelengths between 300 and 400nm is not absorbed by the atmosphere, and may be responsible for the degradation of polymers. Kevlar 49 has a strong absorption in the ultraviolet region around 250nm to 330nm (Penn, 1979).

Like other polymers, aramid fibres are sensitive to radiation from ultraviolet light and could photodegrade. Yarns exposed to ultraviolet light will lose some of their mechanical strength and darken in colour. Figure 2.22 shows the effect of outdoor exposure on Twaron aramid fibre, where strength is greatly reduced after only one year of exposure. However, two conditions must be fulfilled before this radiation can cause fibre degradation: firstly the absorption of the radiation by the polymer; and secondly the accumulation of sufficient energy to break the fibre's chemical bonds. These conditions are far from being fulfilled in artificial light sources or sunlight filtered by window glass. In addition, the deterioration of aramid fibres requires the presence of oxygen and is not enhanced by the presence of moisture or by atmospheric pollutants such as sulphur dioxide (Gibson, 2002).

Morgan et al (1983) reported that, in a study conducted by Harper and McAlister, the strength of bare Kevlar 49 yarn can decrease by more than 25% after one week of exposure to UV radiation.

Due to the self-screening property of these fibres, it is important to mention that UV degradation, when it occurs, it is usually limited to those filaments on the yarn's surface (du Pont, 2001). For example, when a very thin Kevlar 49 fabric was exposed directly to Florida sunlight for an extended period, it lost about half of its tensile strength. While in items like the 12.5 mm diameter rope, the majority of the yarns were protected by the outer layer and hence their strength loss was minimized (Bunsell, 1988).

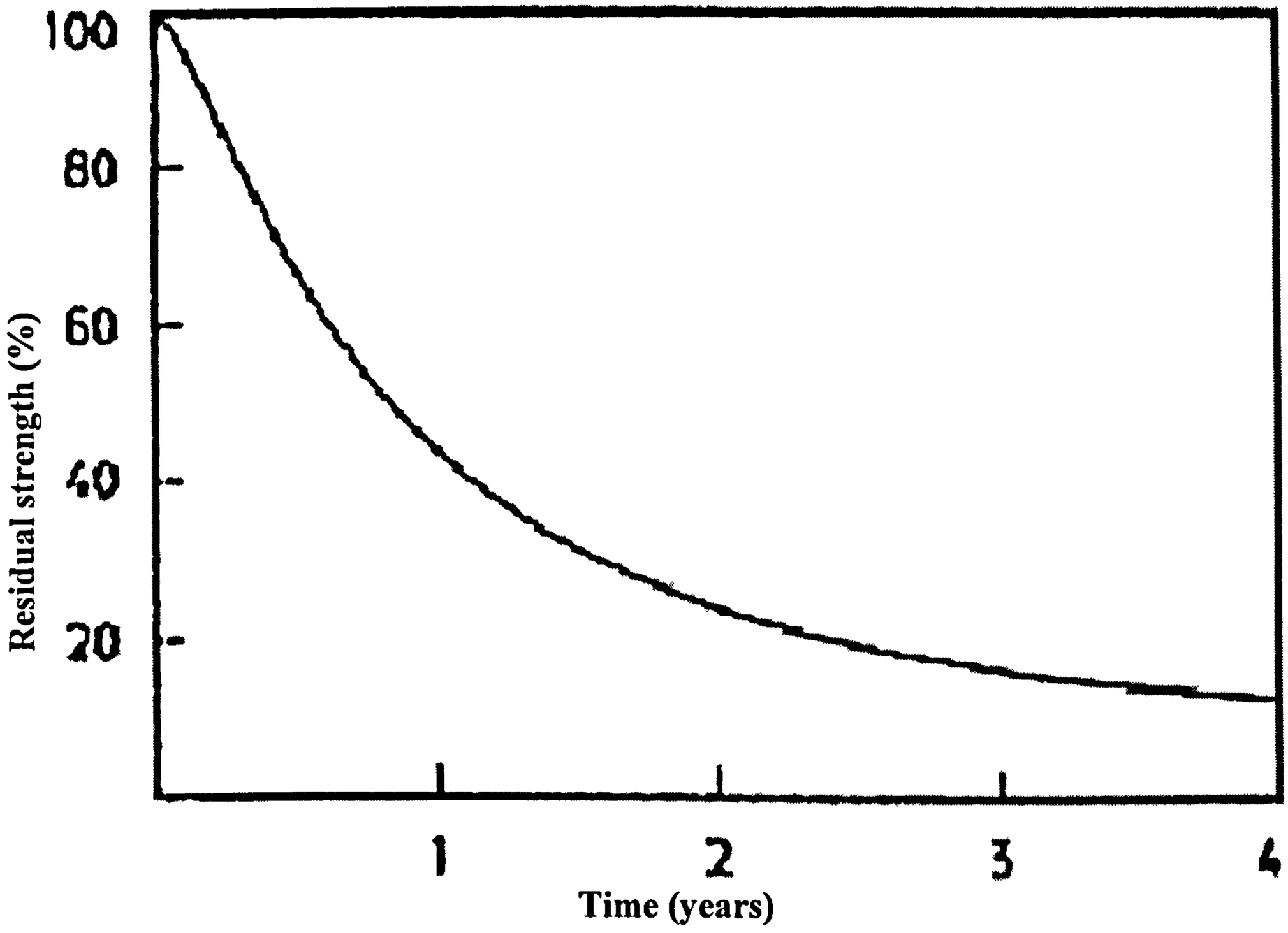

Figure 2.22 Influence of outdoor exposure (both UV and weather conditions) on the residual strength of Twaron aramid fibre (Twaron Technical Report QET 99023, 2001)

2.4 Aramid Fibre Stress Rupture Regression Behaviour

Stress rupture is the sudden failure of material while sustaining loads for long periods. It occurs as a result of the degradation of mechanical properties with time while under load.

Wilfong and Zimmerman (1977) compared the lifetime behaviour of Kevlar, Nylon 66 and Polyethylene in terms of time vs. load, where load was expressed as a fraction of normal breaking strength. They concluded that Kevlar fibre supports a larger fraction of its breaking load for a longer period of time than Nylon 66 or Polyethylene fibres.

Long-Term Behaviour of Aramid Fibre

In the literature, there are several studies and hypotheses of the factors that affect the long term load carrying performance of aramid fibres. For instant, Wilfong and Zimmerman (1977) and Gibson (2005) related yarn strength to yarn twisting, while Lafitte and Bunsell (1982) proved that the fibres contain serious defects along their length. It is believed that these defects could act as failure initiation sites that affect the long term load carrying capacity of these fibres.

In addition to their observations pertaining to fibre strength dependence on the yarn's twist level and the defects along its length, Wilfong and Zimmerman (1977) and Lafitte and Bunsell (1982) recorded some decline in fibre strength and Young's modulus when tested in high temperatures. The same observations were recorded in short-term tests conducted on Kevlar 29, where the slopes of the regression lines were found to increase with increases in test temperature (Gibson, 2002).

2.5 Stress Rupture Data Interpretation Methods

In the literature there are many regression-based interpretation procedures that can be used to process stress rupture test results. The outcome of these procedures is a value of pressure or stress for the system which should not be exceeded. The methods of interpretation used in this thesis are similar to those used previously for the processing of RTP pipe test results. This enables the comparison of tests results from both RTP pipes and aramid fibres; because for RTP, fibre failure is the key failure mechanism and hence when testing the fibres only, it is safe to assume that they will behave in the same way. Therefore, the relationship between the applied stress, σ and the time to failure, t_f that is applicable for RTP tests are also valid for aramid fibre tests.

One of the regression-based interpretation procedures used to process stress rupture test results is based on an empirical power law relationship between time to failure and pressure, with no particular assumptions made about the physical mechanisms involved in the creep and failure of the fibres. This is supported by the conclusions of Phoenix and Tierney (1983) and Wagner et al (1986), where they showed that the time to failure for constant stress conditions is most likely to follow a power law relation. Actually, this form

of relationship is assumed in almost all types of non-metallic pipe qualification procedures such as those used in this research work, ISO 9080, and others such as; ASTM-D 2837, ASTM-D 2992, and ISO 14692.

On the other hand, other workers have often employed models based on the theory of Eyring, which assumes creep deformation to consist of a series of thermally activated events. The Eyring model predicts a linear relationship between stress and $\log_{10}$ time to failure, instead of the relationship of empirical power law described earlier.

There is no especially strong argument in favour of either approach. Indeed both could be considered to fit the present results well. The Eyring model has the virtue of a sound theoretical origin but the activation volume has often been found to vary with both temperature and loading conditions. The power law model, on the other hand, has no theoretical basis, but fits the results equally well in the stress range of interest. It is worth noting that, when extrapolating a particular set of results to find a long-term value of 'design' strength, the power law ($\log_{10}$ stress vs $\log_{10}$ failure time) model will always give a more optimistic prediction than the Eyring approach (linear stress vs. $\log_{10}$ failure time).

Other statistical procedures used are described in ASTM-D 2837-98a, ASTM-D2992-96e1, ISO/DIS 14692-2. However, it should be noted that the procedure recommended in the present study is more conservative in its predictions, typically of the order of 3% in the LPL, compared to predictions from other standards (Gibson 2002).

2.5.1 The Multi-Regression Extrapolation Procedure ISO 9080 $\log_{10}$-$\log_{10}$

The standard multi-regression procedure recommended in ISO 9080 is an extrapolation procedure developed initially for thermoplastic pipes concerned with the long-term structural integrity of these pipes under operational stresses. This method was the result of numerous studies in the mid-1970s in the form of a technical report ISO/TR 9080:1992(E). Later, a new version was issued and designated as ISO/DIS 9080:1999(E) (Andersson, 2001). However, the report ISO/TR 9080:1992 was technically revised and replaced by ISO/TR 9080:2003, according to which this study was conducted. Based on 33 years of

experience with the long-term behaviour of plastic pipes in Bodycote (formerly Studsvik Polymer AB) in Sweden, Andersson (2001) believes that ISO/TR 9080:1992 is the most promising extrapolation method to describe the creep rupture performance of most materials.

The ISO 9080 procedure assumes that there is a linear relationship between the $\log_{10}$ of the time to failure and the $\log_{10}$ applied stress at each temperature. It also assumes that stress rupture curves are proportionally spaced depending on the reciprocal of the absolute temperature $\left(1/T\right)$, which is consistent with the creep and failure process being dominated by an Arrhenius-type process. Because the failure time exhibits power law dependence on stress, results are plotted on a $\log_{10}$-$\log_{10}$ scale. The method includes an extensive number of constant stress tests at several temperatures for the generation of creep rupture curves, followed by a multiple linear regression analysis in order to fit the data. From the regression data acquired (having a proper fit) a mean regression line is constructed and a statistical 97.5% lower confidence limit (two-sided 0.05 level of significance) curve is calculated and extrapolated to obtain the Lower Prediction Limit (LPL) at the design life. The 97.5% lower prediction limit is equivalent to the lower confidence limit of the 95% confidence interval of the predicted value, as shown in Figure 2.23. In other words, it is the line above which 97.5% of all new experimental points can be expected to lie.

In addition to the prediction of long term behaviour, ISO 9080 provides a method of testing for linearity which is used to confirm whether or not there is any change in behaviour (e.g. ductile-brittle or ductile-chemical degradation) or undesirable failure modes such as thermal oxidation over long periods or at high temperatures through what is called the 'Knee' detection method (Figure 2.24). The knee detection method will indicate any undesirable long term performance of the tested material. It worth noticing that including test data at temperatures higher than the intended design temperature is very important during the knee detection process. This is because undesirable failure mechanisms tend to occur after shorter times as test temperature is increased.

Long-Term Behaviour of Aramid Fibre

Since, for RTP, fibre failure is the key failure mechanism, the aramid fibres are also assumed to behave in the same way, so the following power law relationship applies between the applied stress, σ, and the time to failure, t_f.

$$\sigma = Ft_f^{-G}, \qquad [2.4]$$

where, F is the curve's intercept;

G is the slope of the regression line.

Or, alternatively,

$$\log\sigma = \log F - G\log t_f, \qquad [2.5]$$

where, F and G are power law constants, -G being the regression line slope.

The plastic pipes industry has considerable experience of modelling the stress rupture behaviour of pipe materials after long periods and over a range of temperatures, and has developed a very useful modelling and extrapolation protocol for failure data, in ISO 9080. This procedure has been recommended for use in modelling other types of failure data in addition to pipes, so it was adopted here. ISO 9080 assumes that the time to failure is given by an expression of the form

$$\log(t_f) = c_1 + \frac{c_2}{T} + c_3\log(\sigma) + \frac{c_4\log(\sigma)}{T}, \qquad [2.6]$$

where, t_f is time to failure in hours;

T is the test temperature in Kelvins,

σ is the stress level in megapascals, and

c_1, c_2, c_3, c_4 are the model fitting parameters.

At a particular temperature, this is equivalent to equation [2.4]:

$$\sigma = Ft_f^{-G}$$

with the regression constants being related to the ISO 9080 constants by

Long-Term Behaviour of Aramid Fibre

$$G = -\frac{1}{c_3 + \frac{c_4}{T}} \qquad \text{and} \qquad \log F = \frac{-c_1 - \frac{c_2}{T}}{c_3 + \frac{c_4}{T}}$$

The regression procedure obtains the best least squares fit of the constants based on the scatter in $\log t_f$, i.e. on the scatter in the horizontal direction. This has been shown to be more conservative than using the vertical scatter (i.e. the scatter in $\log \sigma$). Two versions of the protocol are available: the three parameter model ($c_4 = 0$) where all the regression lines have the same slope, and the four parameter model, where the slope varies with $1/T$. As will be shown in the result section, there is a small increase in this slope with increasing temperature; hence the '4-parameter' model only was used.

The calculations for the 4-parameters model and the computer code used to perform these calculations are given in Appendices A and B respectively.

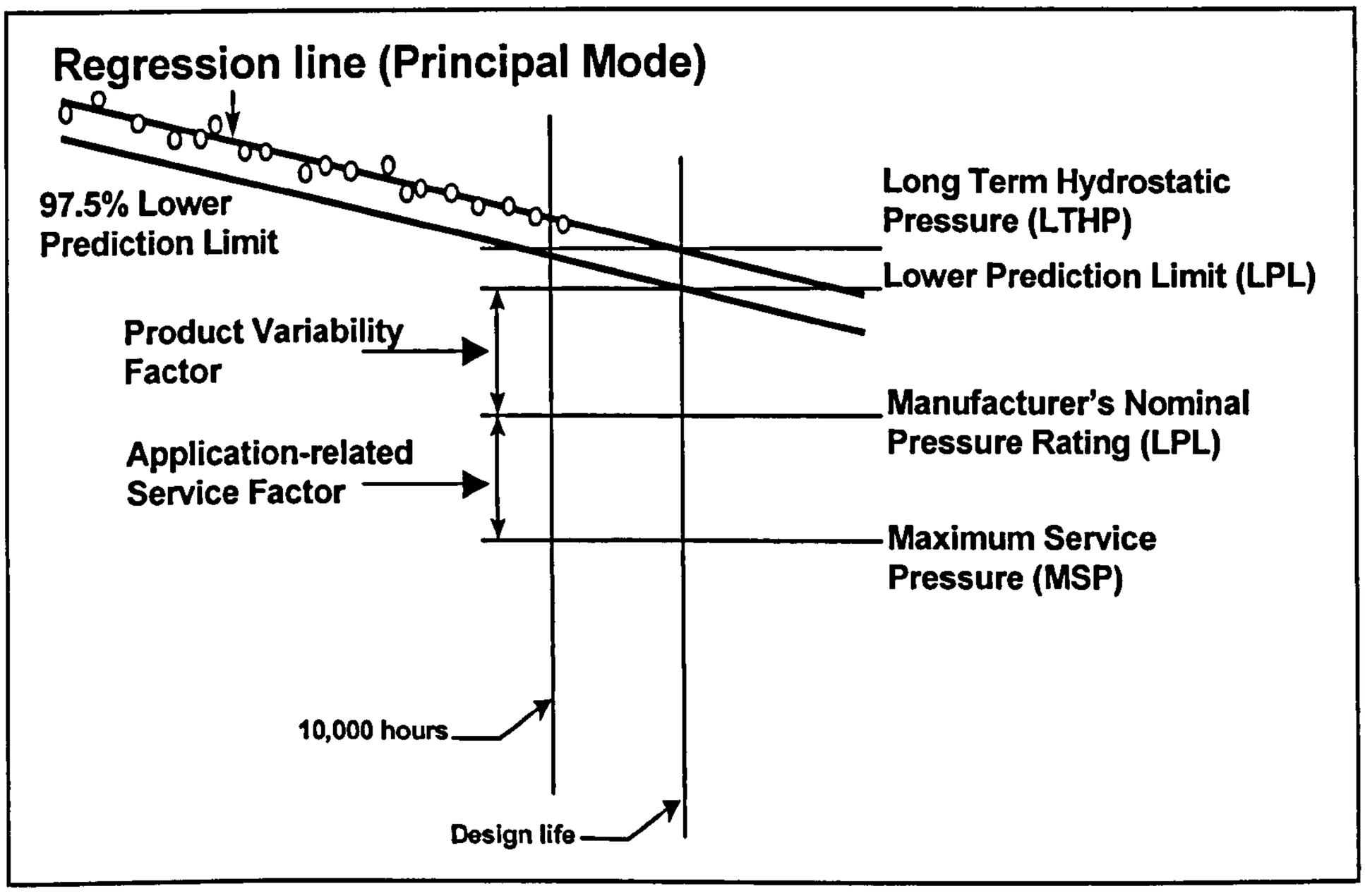

Figure 2.23 Schematic of pressure rupture relationship for Reinforced Thermoplastic Pipe, showing experimental results, mean line and extrapolation of the Lower Prediction Limit to design life.

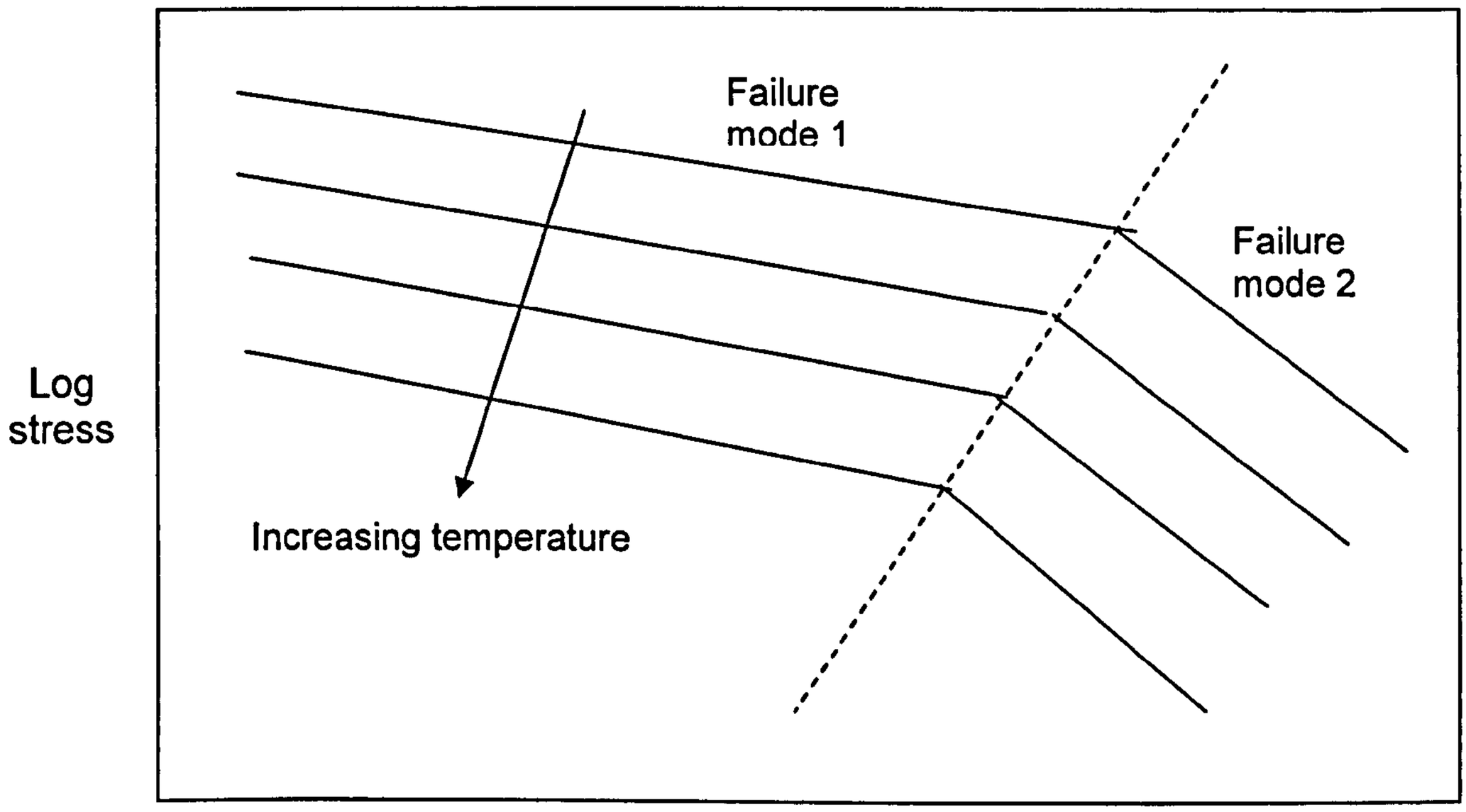

Figure 2.24 Schematic showing a possible undesirable failure mode

2.5.2 The Modified Multi-Regression Extrapolation Procedure ISO 9080 lin-log_{10}

Based on the theory of Eyring, which assumes creep deformation to consist of a series of thermally activated events, test results were modelled in a linear relationship between stress and log_{10}-time rather than the previously explained log_{10}-log_{10} relationship. In fact, in their published results for the study conducted on Twaron 1000 fibre, Akzo/Teijin presented a theoretical model for fibre behaviour that resulted in a linear relationship between applied stress and log_{10} failure time, based on an Arrhenius model relationship. To an extent, this appears to conflict with the power law relationship that has often been assumed to govern the regression behaviour of polymeric materials in general and both the reinforcement and the RTP pipes specifically. However, it should be borne in mind that the stress range of real interest for the design of RTP covers less than a decade and, when plotted over such a narrow range, the Twaron 1000 results published by Akzo/Teijin could probably be equally well-described by a log_{10}-log_{10} as by a log_{10}-linear relationship.

As the statistical procedure established in ISO 9080 is very reliable, as indicated earlier, it has been thought that it could be modified to accommodate other views and to enable the modelling of other forms of failure time to applied stress relationships. In the present case, the relationship is linear; hence, a modified ISO 9080 that relates linear stress and log_{10} time was applied.

2.5.3 Time-Temperature Superposition Procedure

The Time-Temperature Superposition (TTS) method provides a simple technique for relating different behaviour or properties at two or more different temperatures. It is based on the assumption that when data for a particular property at various temperatures are plotted on a logarithmic scale, then the property's curves versus time at each temperature should be the same if the underlying degradation mechanism that governs the property's relation with time and temperature is the same (Bernstein et al, 2004). Based on this assumption, there should be a shift factor by which the time for each set of data (at each temperature) can be multiplied to get all the data to overlap at one specified reference temperature. By definition, the shift factor at the reference temperature is unity.

Long-Term Behaviour of Aramid Fibre

The TTS method is often employed in the prediction of the long term behaviour of polymeric materials where a factor of $\log_{10}(a_T)$ provides the necessary horizontal shift to obtain the equivalent stress at temperature T_2 from temperature T_1 as shown in Figure 2.25, where J(t) is a time dependent variable such as stress.

The TTS principle can be applied to creep, stress relaxation, complex dynamic compliance and modulus data, as explained by Gol'dman (1994). The method used in the present research relies on the assumptions that the mechanism of deformation is the same throughout the time and temperature ranges and that a shift in logarithmic time is equivalent to a change in temperature (Gibson, 2005).

So, the increase in the temperature at which the ISO 9080 regression tests were carried out will help in revealing any change in the long term behaviour of aramid fibre material.

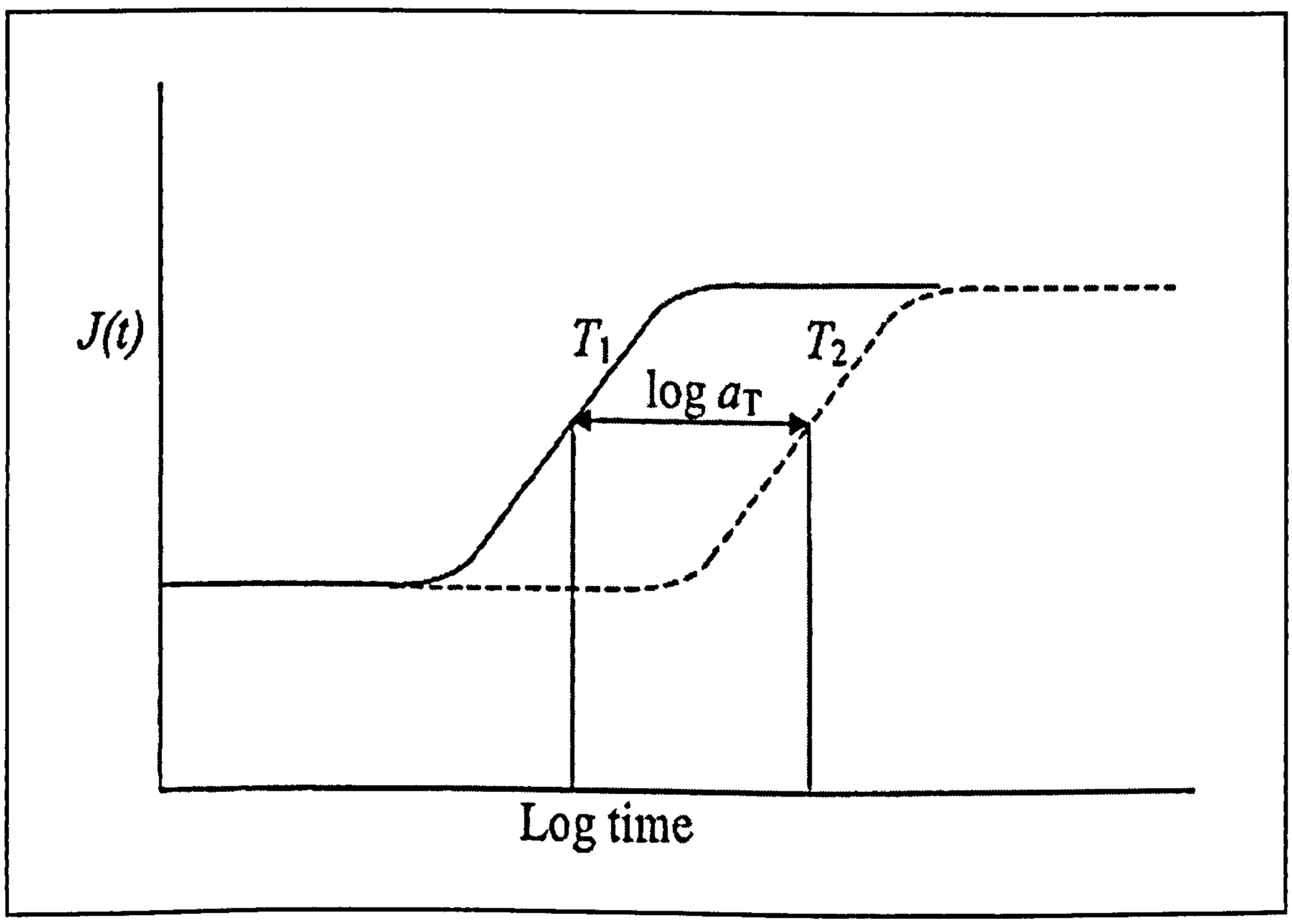

Figure 2.25 Schematics showing TTS principle applied to rupture stress

2.6 Aramid Fibre Creep Behaviour and Failure Model

2.6.1 Creep Behaviour of Polymeric Materials

Creep is the deformation that occurs over a period of time when a material is subjected to constant stress at constant temperature. In metals, creep usually occurs only at elevated temperatures; however, in plastics it is more common to occur at room temperature and is called cold flow or deformation under load. This effect is an indication of a general property of polymeric solids termed viscoelasticity. The solid is elastic, so it can recover; but it is viscous, so it can creep.

Creep is measured either by the increase in material sample length under tension over a period of time or by the stress reduction of material when held in a constant gauge length.

Polymers are viscoelastic at all temperatures, so that in considering the strains induced on them, it is important to take into account the applied stress level, application time and temperature.

Creep experiments are usually conducted under uniaxial constant loading conditions for a particular chosen test temperature. Measurements of extension are made at frequent time intervals until test sample fracture. Figure 2.26 shows a typical creep strain against time curve. Generally, there are four different regions in the curve:

- The initial creep region which is elastic in nature.
- The primary region, which indicates the early stage of creep and during which the creep rate decreases rapidly with time.
- The secondary region, in which the creep rate is almost constant when the system is in a steady state condition.
- The tertiary region, which denotes a rapid increase in strain and ends with fracture.

The overall increase in strain is believed to be due to microstructural instability from prolonged high temperature exposure and to a gradual increase in stress level which leads to complete fracture (Benham et al, 1996). It is also important to note that elongation to

fracture in creep is only a fraction of that usually obtained for continuous loading to fracture at high temperature.

It is argued that due to the very small gradient of the secondary stage of the creep process, that there might be a limiting creep level below which the strain rate will be almost equal to zero. This is one of the issues to be addressed in Chapter 6 of this thesis.

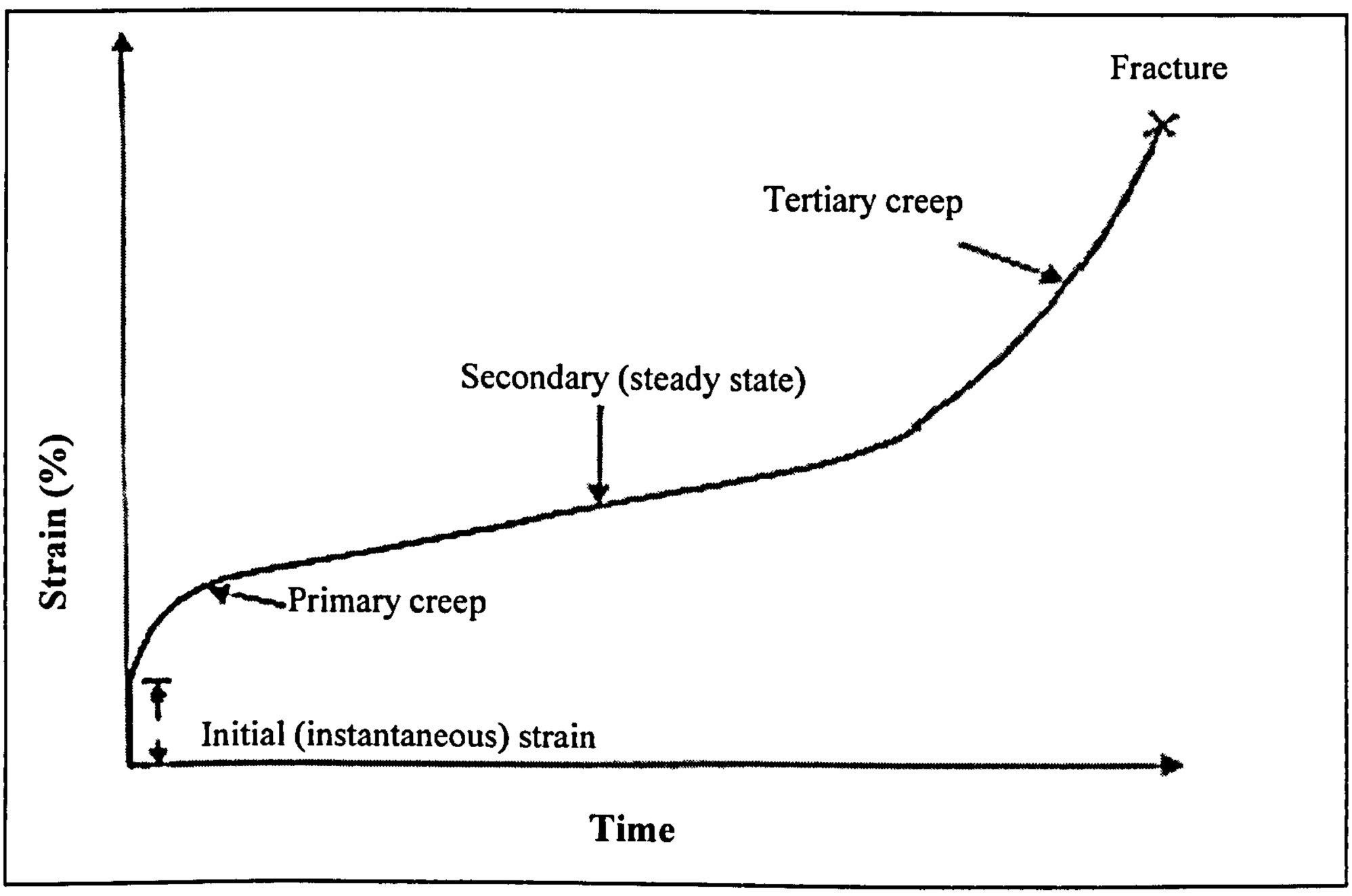

Figure 2.26 General creep curve for polymers

2.6.2 Aramid Fibre Creep Behaviour

Aramid fibre has very little creep, which is a phenomenon of stress relaxation when a fibre is held under stress because of its highly crystalline and anisotropic nature. However, its creep increases with increasing stress and temperature or when in contact with water as a result of the plasticization mechanism.

Cook's (1982) study of the creep behaviour of Kevlar 49 fibres under different loads, temperatures and environments supports the above observations with the conclusion that the overall creep in 10,000 hours was less than 0.5% in all cases. However, when compared with other reinforcements such as glass, boron, or graphite, Kevlar 49 fibre exhibited more creep, as was reported by Bunsell (Erickson, 1985).

It is noted (Kostikov, 1995) that the rate of creep rises as the applied stress increase. In contrary, Twaron Products bv reported (Twaron, 2000) that the creep rate of two different types Twaron yarns when measured has proven rather insensitive to stress level, temperature and moisture. An increase in rate from .016%decade to .020%decade was observed when the load was increased from the range of 10% to 40% of the breaking strength to a range of 50% to 60% for Twaron type 1055, while the increase was only from .016 to .022%decade in the case of Twaron 2200 when the loading was increased from 10 to 40% range. Also, the modulus of elasticity increases as the stress level increases, which is believed to be a consequence of crystallite rotation in the process of creep.

Maksimov and Plume's (2001) experimental data showed that the main part of the creep deformation of aramid SVM fibres was realized within the first five to seven months of the creep test. Then the creep rate of the fibres decreased considerably, but never stopped. Maksimov and Plume's observations disagree with those of Bunsell (1975) when testing the creep behaviour of Kevlar 49. Bunsell loaded the fibre to 85% of its expected breaking load, and his observations recorded little creep at the beginning of the test. After about 5 minutes of loading, the fibre stabilized, and no further measurable extension was observed.

Long-Term Behaviour of Aramid Fibre

In a study conducted by du Pont (on Kevlar 29) over a rather short time-scale at a range of temperatures, the results showed that the initial elastic strain that occurs on loading is followed by a slow rate of creep. It did appear that the creep rate at a particular stress declines with time, but it was not possible to conclude whether the creep slows down to a negligible rate over the observed timescale or whether it continues. Additionally, the results show that failure occurs when the overall strain reaches a value in the region of 0.032-0.035 (Gibson, 2002).

2.6.3 Aramid Fibre Failure Model

As described earlier, aramid fibre is a rigid rod polymer comprising stiff polymeric units arranged in a near-unidirectional crystalline phase. Figure 2.27 is a view of the structure which shows a unidirectional crystal containing imperfections corresponding to the ends of the individual crystal sequences. It is believed that the rod-like sequences shown here may correspond either to individual chains or to crystallites comprising a number of chains (Gibson 2005).

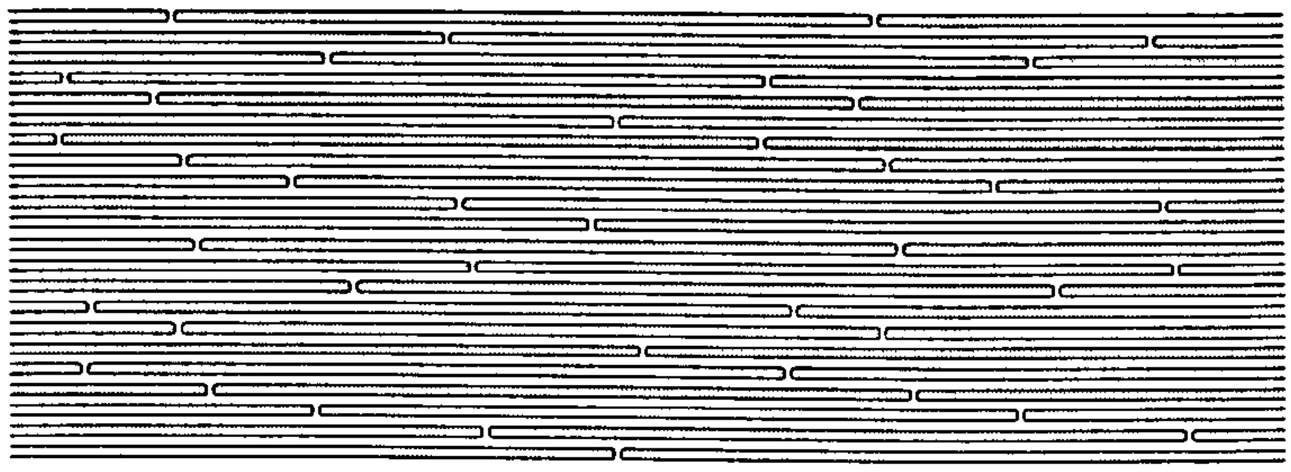

Figure 2.27 Schematic of the morphology of aramid fibre

It is generally accepted that the creep of aramid fibres under load involves plastic flow or movement parallel to the chain direction within the crystallites, and previous physical models for creep behaviour have been based on this approach.

Northolt (1980) summarized the fibre structure as being built-up of parallel aligned fibrils in which crystallites having a narrow orientation distribution relative to the fibre axis are linked end to end. Northolt models the strain as originating from the elastic extension of

the polymer chain and from the rotation of the chain or crystallite axis toward the fibre axis. The rotation is described as consisting of reversible (elastic) and irreversible (plastic) contributions, which accounts for the residual strain observed in the unloaded and unbroken fibre. The second tensile loading of a fibre is assumed to comprise elastic extension and rotation of the crystallites (Erickson, 1985). Clearly the deformation mechanism must also involve some imperfections in the crystal structure. Indeed it has been proposed that deformation could involve the relative movement of imperfectly aligned crystalline regions.

In their study of the relationship between the deformation of PPTA fibres and the molecular structure of their morphology, Northolt and van Aartsen (1977) concluded that, for a large part of the stress-strain curve, the macroscopic strain is brought about by elongation of the crystal lattice through valence angle deformation and the bond stretching of the polymer chain.

Wang et al (1992) also refer the elastic and viscoelastic deformations of aramid fibres to the crystallite rotation which is caused by the rod-like structure of the PPTA molecular chains and crystallites. So, during tensile loading, disoriented crystallites will rotate toward the direction of the fibre axis, originating both elastic and viscoelastic deformations. However, because the changes in crystallite angles are very small, it proved to be very difficult to measure such changes using techniques like x-ray scattering. Nevertheless, crystallite rotations can be measured using fibre elastic compliance which is related to the crystallite angle. The relationship between the rotation angles, or in other words the fibre elastic compliance, and the creep strain is directly proportional.

Erickson (1985) summarised other possible creep mechanisms, including:

- Fibre's internal stresses relaxation resulting from fibre fabrication.
- Molecular rearrangement due to changes in bond angles and bond lengths.
- Supramolecular or pleat structure associated with the hydrogen bonded sheets that introduce different crystalline structure by displacing the sheets relative to each other as they bend to form the pleats.

Long-Term Behaviour of Aramid Fibre

- Creep due to voids and cracks formation or growth that could influence the crystallite rotation mechanism mentioned above.

Based on the understanding that the strain observed under tension is a combined effect of the molecular elongation and the rotation of the chains, Chailleux and Davies (2003) proposed a model that describes the strain consisting of these two components.

A further possibility which will be examined here is deformation associated with the defect regions constituted by the ends of chains, or alternatively the ends of crystalline sequences involving several chains.

2.7 Aramid Fibre Microscopic Failure Analysis

As was the case with the physical structure failure studies, there have been few studies on the microscopic failure process of aramid fibres.

Morgan et al (1983) reported that, when in the form of unimpregnated yarns, aramid fibres fail in tension by axially splitting. This is because when an anisotropic solution such as that of aramid fibres is subject to shear or elongation flow, its domains deform and orient along the direction of flow/shear in ordered arrangements. But at high shear or elongation rates, the boundaries of these domains may be partly destroyed and may link up to form the fibrillar structure (Yang, 1992). The splitting phenomenon could also be attributed to internal cracks and defects in the fibre during the manufacturing process (Dobb et al, 1979).

In their views of the structural fibre splitting and failure process, Morgan et al (1983) proposed that crack propagation can readily occur parallel to the fibre's longitudinal axis because this only requires rupture of the H-bonds. However, failure transverse to the fibre direction could occur by two possible mechanisms. The crack transverses a path that follows the original macromolecular chain ends inherent in the fibre, or additional chain ends are produced under stress by chain scission, thus producing additional paths for transverse crack propagation.

Long-Term Behaviour of Aramid Fibre

In his study of Kevlar-49 and Kevalr-29, Bunsell (1975) suggested that it is the high drawn ratio employed in the manufacturing of these fibres that probably results in a low radial strength. This weak radial bonding may then account for some of the surface layers becoming detached and resulting in a large amount of surface swarf which can be seen on the fibre. In addition, Bunsell suggested that fracture of the fibre under stress is initiated by these splits or possibly some internal flaw. Separation of these fibrils leads to the formation of nodular surface flaws that contribute to subsequent axial splitting (Kerr, 2005).

Lafitte and Bunsell (1982) noticed no difference in the fracture morphology in fibre breaks from simple tensile, fatigue, and creep conditions.

Chapter 3 Experimental Procedure

The tests were conducted on ten specially-designed rigs, as shown in Figures 3.1 and 3.2. Air tests were conducted on the horizontal test rigs shown in Figures 3.1a and 3.2 a while environmental tests were conducted on the vertical rigs (Figures 3.1b and 3.2 b).

Each rig was composed of three major systems: the load application system, the environment control system, and the data acquisition system.

The load application system has a dead weight lever arm loading mechanism. This was made from aluminium rectangular tube measuring 50.8 x 76.2 mm. The lever sat on an angled steel block, allowing it to move as the fibre elongated. Yarn samples at both ends were gripped using 'capstan' type grips made of 19.05 mm aluminium bar around which they were wrapped several times. In this way, all elements of the yarn were tensioned equally and the minimum possible local stress concentration was put across the roller grips. No evidence of grip slippage or local damage at the grips was noted, and fibre failures were within the gauge length as shown in Figure 3.3. Failure results were ignored if it occurred at the grip. The weights on the lever were added manually with great care taken not to cause instantaneous failure. Samples were held under constant tension until failure occurred. In order to maintain a consistent and constant load throughout the test, the lever arm was adjusted to maintain a horizontal level as the fibre elongated.

A load cell was used to check the calculated lever arm loading ratio, which is used to determine the exact load experienced by the fibre after loads were applied on the lever arm. Both calculated and measured lever arm loading ratios were found to be identical. So it can be claimed that using the load cell has provided an accurate calibration for the dead-weight experimental setup used. The linearity error in the used load cell was ±3%.

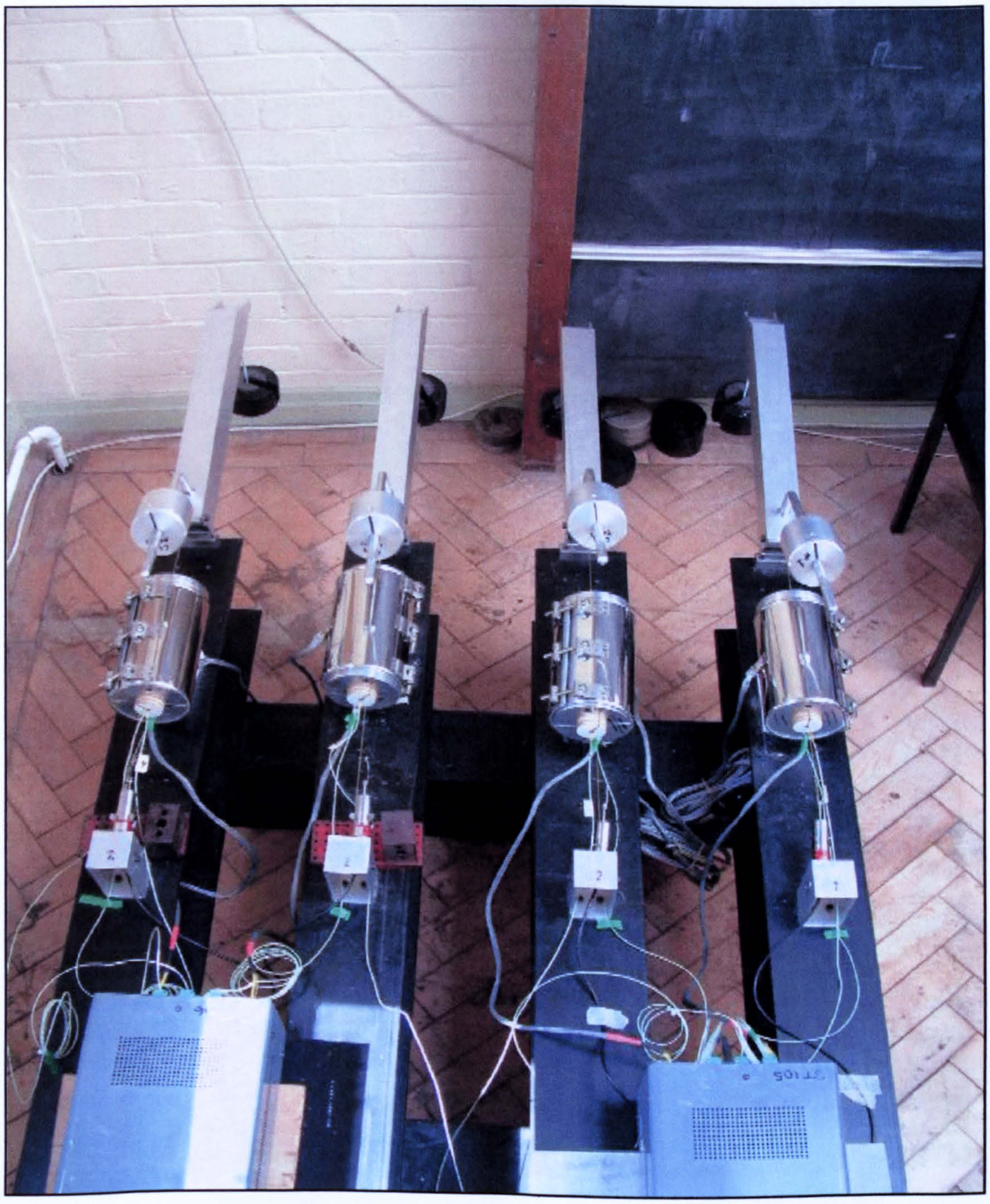

Figure 3.1 Photograph of: **(A)** the Horizontal rigs for testing in air

Figure 3.1 Photograph of: **(B)** the Vertical rigs for environmental testing

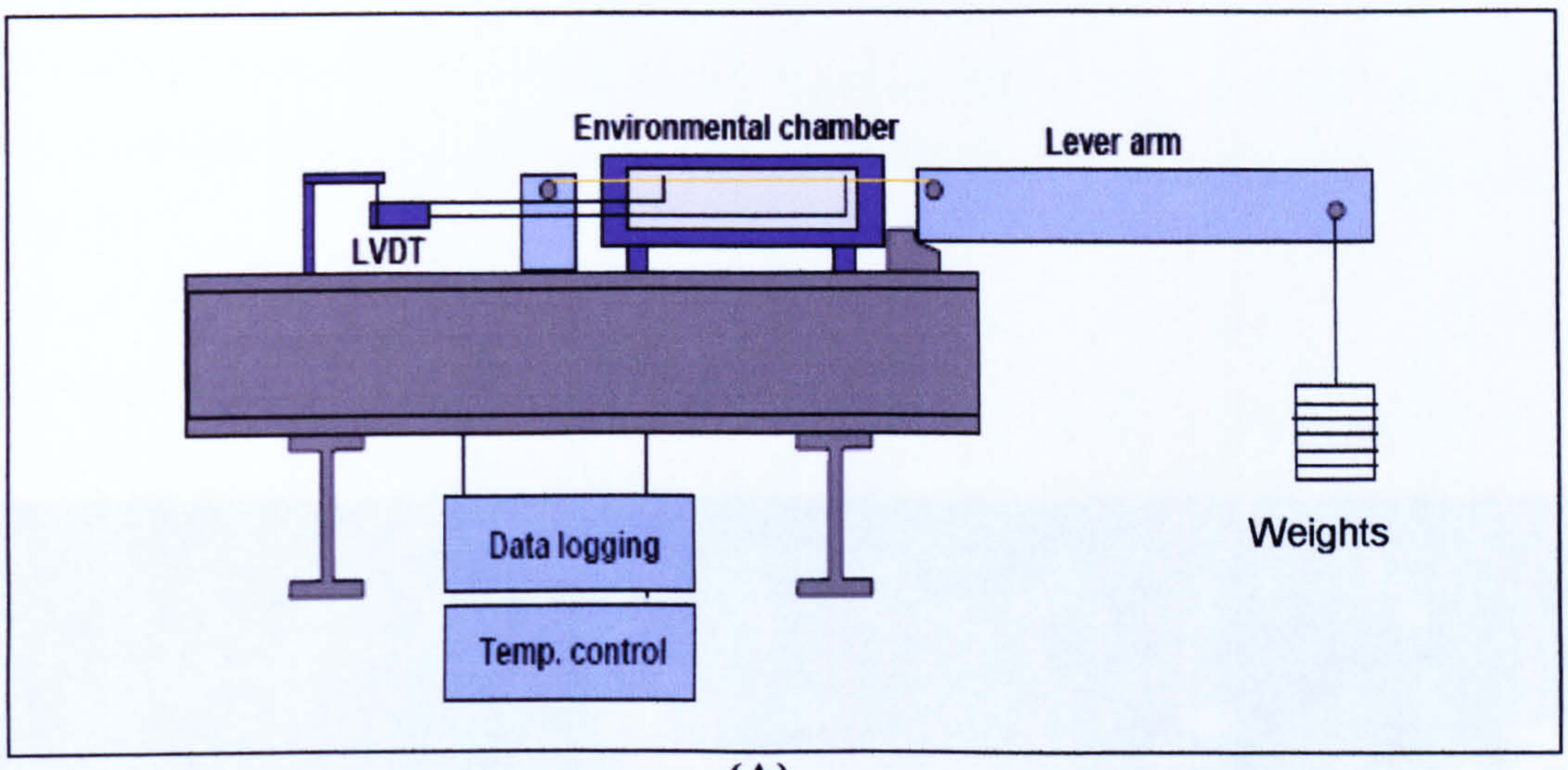

(A)

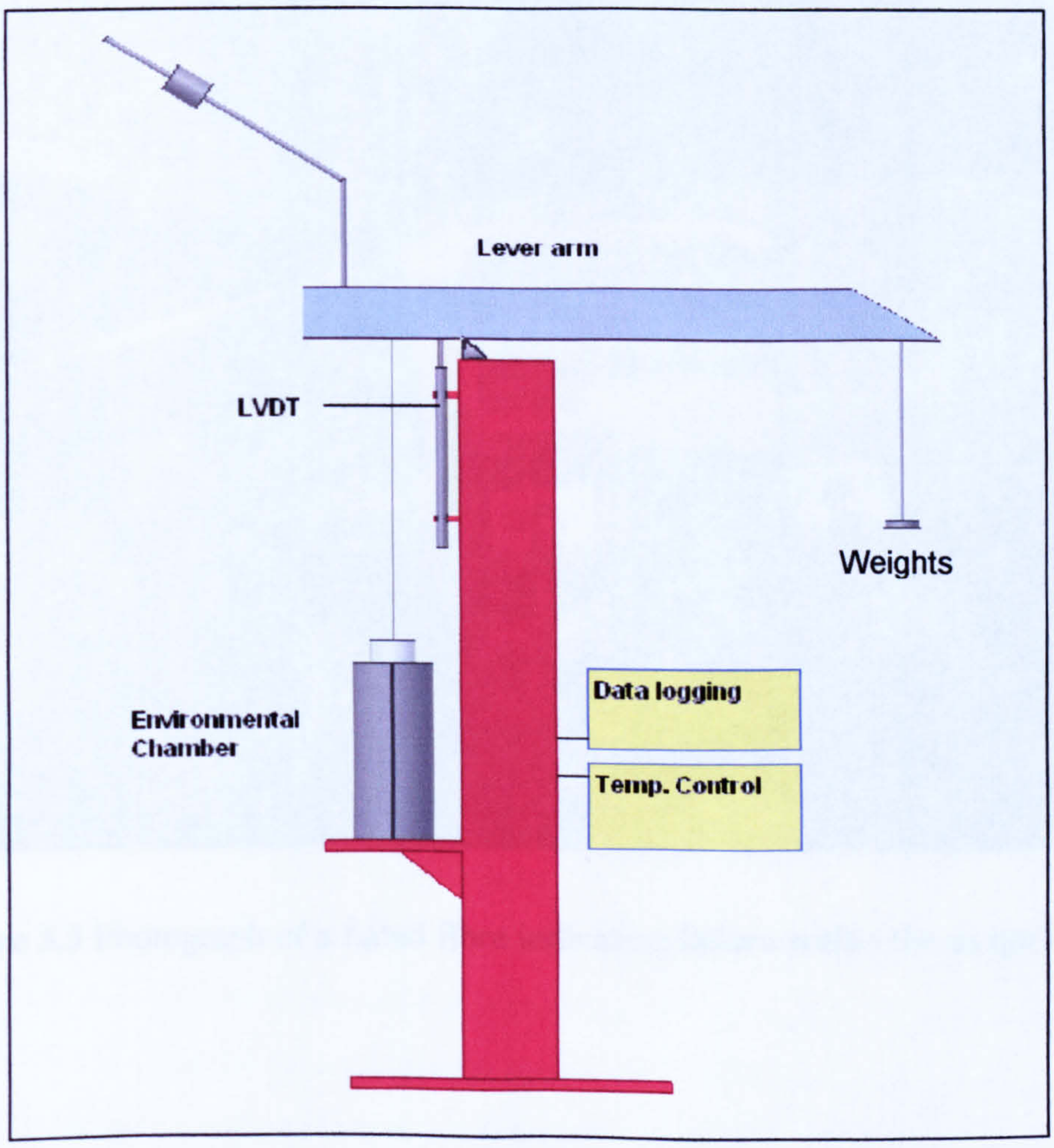

(B)

Figure 3.2 Stress rupture testing machines: **(A)** Horizontal machines for testing in air **(B)** Vertical machine for environmental testing

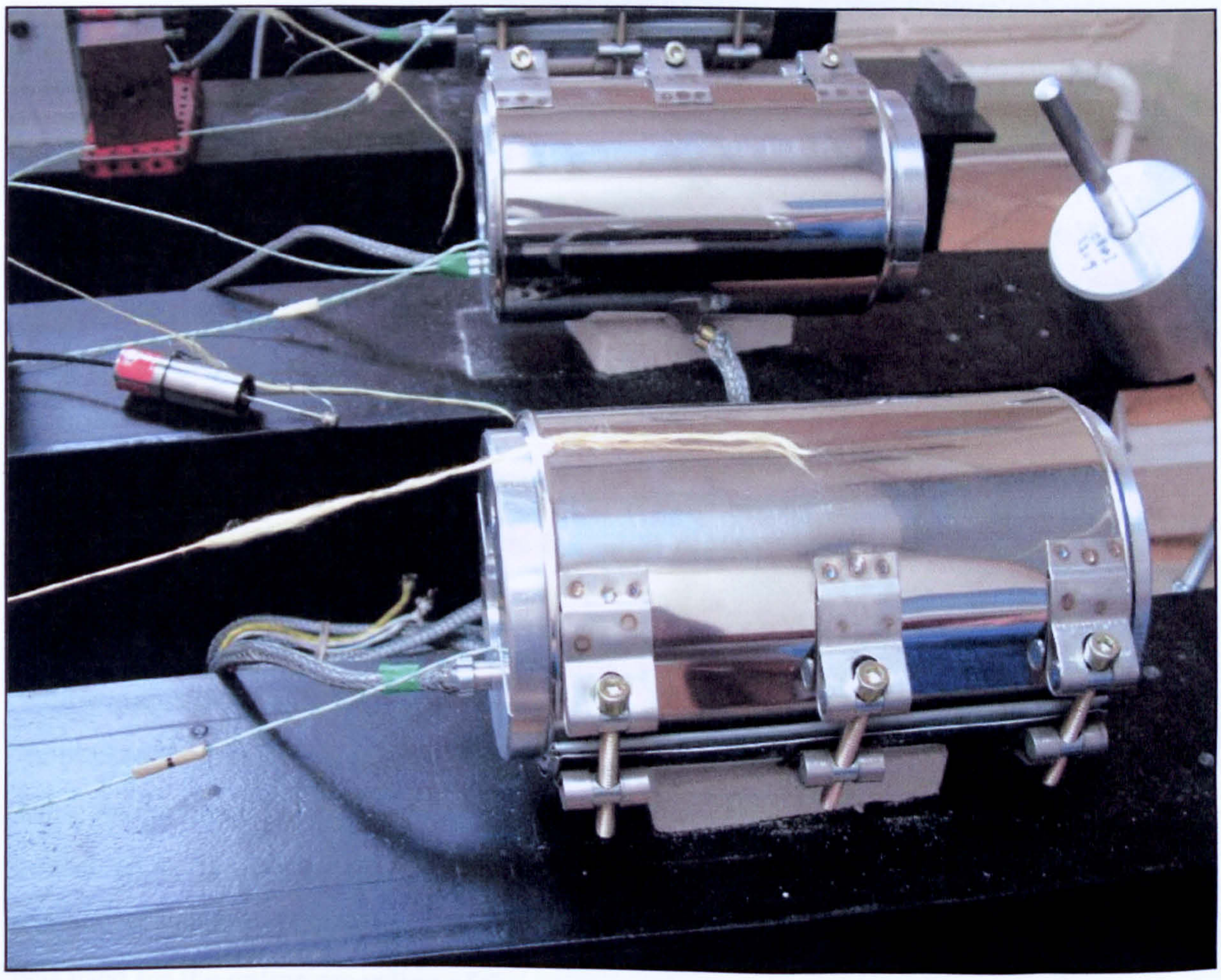

Figure 3.3 Photograph of a failed fibre indicating failure within the gauge length

Long-Term Behaviour of Aramid Fibre

In the environment control system, the tested gauge length of the yarn was subjected to various combinations of test temperatures and environments (air, water, low pH water, and crude oil).

High temperature tests were conducted using an air oven made of a bored 150.24mm diameter aluminium block which was heated using either cartridge heaters or heater mats. The centre bore was 76.2 mm in diameter and it was capped at both ends to maintain a consistent air temperature along the sample's gauge length throughout the test period, hence minimizing the effect of fibres gauge length sensitivity. Temperature along the gauge length was controlled within ± 2°C utilizing a control system described below. A similar environmental control system was used for the vertical test rigs, the main difference being that vertical PTFE-lined cylinders were used to hold the heated test environments. The pH level in the low pH water environment was measured daily using a pH meter.

For the environmental tests, liquid levels were topped up as necessary to ensure continuous exposure to the test environment across the gauge length of the tested samples.

Finally, the control and data acquisition system was responsible for controlling the test temperatures to within ± 2°C using specially-designed heater controllers. This system also monitored the test temperatures online, and detected the time to failure of each sample using the mounted linear variable differential transformer (LVDT). Yarn samples were connected to the LVDT using a 26 x 0.53mm pin glued with a drop of super-glue. A personal data acquisition system (IOtech Personal Daq/55) linked to a personal computer was used for the online recording of the test events.

Tests at each stress level were repeated at least twice to reduce the influence of fibre variability and experimental scatter. In both horizontal and vertical arrangements, test samples were set in the test position and left for a sufficient length of time to precondition in the environment and so that the temperature stabilized before load application. Stabilization periods varied depending on the test temperature and environment, but never

exceeded 30 minutes. All tests were conducted in an area protected from direct sunlight, and yarn spools were always kept covered to protect them from light degradation.

Samples that did not fail for extended periods (>1000 hrs or >10,000 hrs) were broken using a computer controlled hydraulic Instron mechanical testing machine model 8511 (Figure 3.4) using a 20KN load cell and different loading rates. The same Instron machine was used to conduct a number of the short term tests lasting up to 100 hours. The load was held constant during the tests, and samples were gripped using capstan grips similar to those used in the dead weight lever setup. High temperature environments for tests conducted on the Instron machine were achieved using a temperature controlled oven as shown in Figure 3.5, which also shows the arrangement used for creep testing. For creep tests, sample gauge length was around 145mm, and the strain was measured with an LVDT arrangement as shown. Strain rate data from the LVDT was obtained during the load application and during the initial part of the creep test at much faster rates compared to the rest of the test.

Fractographic analysis was conducted on failed fibres using an environmental scanning electron microscope (ESEM) XL30 ESEM-FEG as shown in Figure 3.6.

Figure 3.4 Computer controlled hydraulic Instron mechanical testing machine used to break the samples in tests of very long duration

Figure 3.5 Close-up of the temperature controlled oven used for high temperature tests on the hydraulic Instron mechanical testing machine

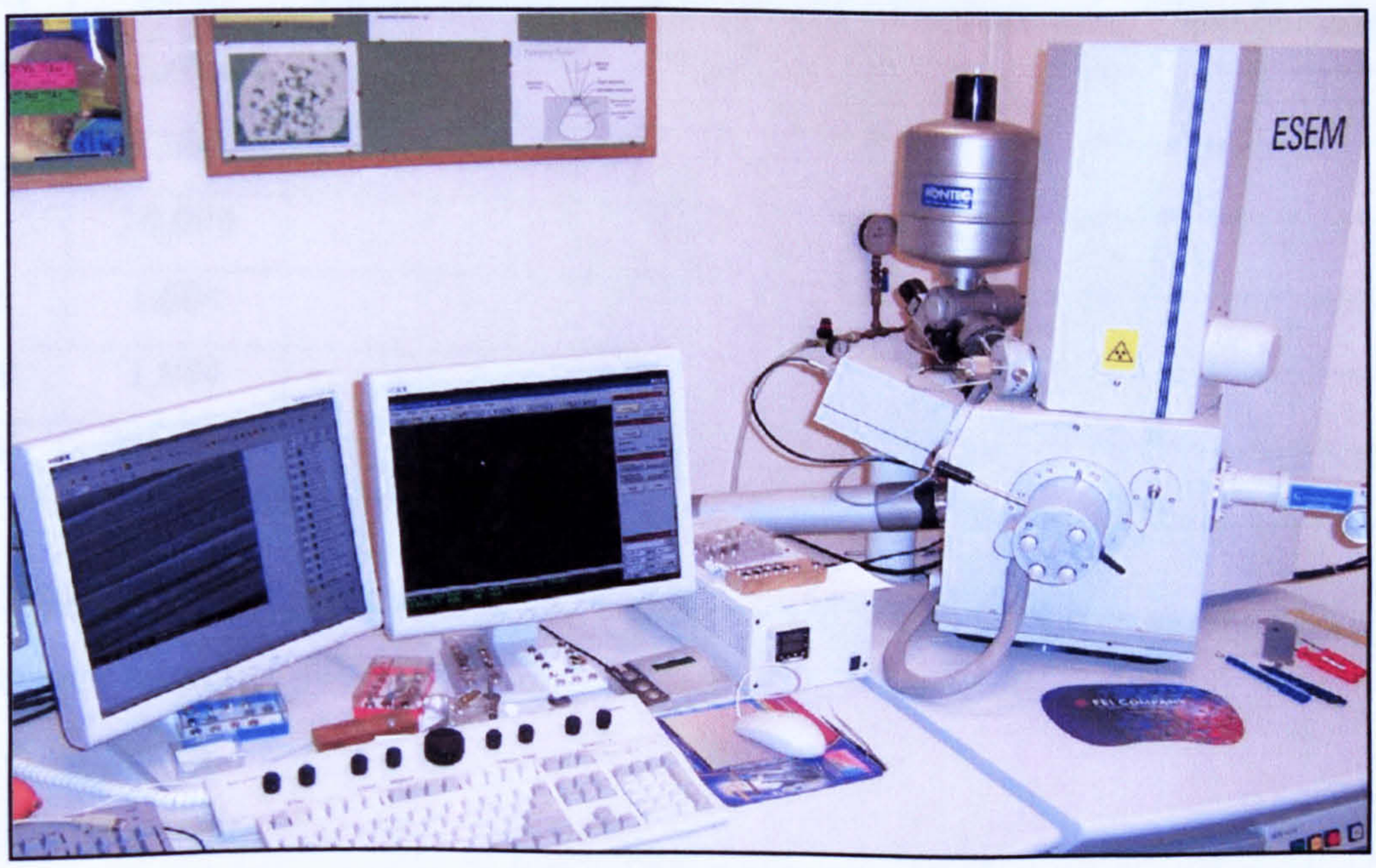

Figure 3.6 Photograph of the fei XL30 ESEM-FEG used in the fractographic analysis of the filed aramid fibre yarns

Long-Term Behaviour of Aramid Fibre

The experimental programme in this study involved performing long term stress rupture tests on the following aramid fibre yarns: Kevlar 29 1670 dtex z80 twist (manufactured by du Pont), Twaron 1000 1680 dtex z80 twist and Technora T200 1670 dtex z80 (manufactured by Teijin). Kevlar and Twaron are acknowledged to be very similar in performance and effectively interchangeable. Table 3.1 summarizes the dimensional and physical parameters of the three fibres involved in the test programme.

Table 3.1 Dimensional and physical parameters of the fibre yarns tested

Fibre Type	Density [g/cm^3]	Tensile Strength [GPa]	Young's Modulus [GPa]	% Elongation at Break
Kevlar 29	1.44	2.9	75	3.5
Twaron 1000	1.44	3	71	3.5
Technora T200	1.39	3.4	71	4.4

Table 3.2 Stress rupture test matrix

Temp (°C)	Time (hr) up to	Air Environment	Water Environment	Low pH Environment	Oil Environment
25	**1,000**	✓	×	×	×
65	**1,000**	✓	✓	✓	✓
	10,000	✓	✓	✓	✓
95	**1,000**	✓	×	×	×
120	**1,000**	✓	×	×	×
140*	**1,000<**	✓	×	×	×

Table 3.2 summarizes the test matrix. As indicated, tests were conducted in four different environments, namely:

1. Air environment.
2. Regular tap water.
3. Low pH water prepared by dissolving 1.878g of potassium hydrogen tartrate in 1000ml of pure tap water. The solution had a pH of around 4.

4. Saudi Arabian and Iranian crude oil of API 38.5 and H_2S content of less than 0.1% supplied by Saudi Aramco and Shell oil companies respectively.

Due to safety regulations, the low pH water environment was used to replace the crude oil environment with high H_2S concentration originally proposed for testing.

Test temperatures ranged from 25°C to 140°C. The highest temperature (140°C) was included in the test programme to improve the predictions generated by the Time Temperature Superposition Model used for the interpretation of the results, as explained in Chapter 4. Test duration ranged from one hour to 10,000 hours.

Applied loads generally ranged between 40 to 85% of the fibre's tensile strength. One of the difficulties encountered while performing the rupture tests was predicting the stress level (load) corresponding to an expected time to failure. This could be due to the statistical variation in strength due to the distribution of flaws or weak points in the fibre's morphology. As a consequence, a scatter in the time to failure was imposed, as explained in the results and discussion below.

The fibre's cross sectional area (diameter) as determined using the following equation [2.1]:

$$A = \frac{LD}{\rho} \times 10^{-4}$$

where, A is the cross sectional area in mm^2;

ρ is density in g/cm^3;

LD is linear density in dtex.

Chapter 4 Long-Term Behaviour of Aramid Fibres in Air under Different Temperatures

4.1 Introduction

Sudden material failure while sustaining large loads for long periods is known as creep-rupture, stress-rupture, or static fatigue. This phenomenon, which happens in various materials, may occur at any significant stress given enough time because the mechanical properties of the material are thought to degrade with time while under loading. So, when the material's residual strength becomes equal to the applied load, stress rupture occurs. In metals, stress rupture is noticed at high temperatures, while in most polymeric materials it occurs at room temperature.

The design life usually required from materials is tens of years, but it is not feasible to conduct qualification tests for such periods. Neither it is possible to simply extrapolate short-term test results to predict long-term behaviour since there could be changes in failure modes after long periods. Hence, the long term suitability of a particular material is best determined by tests and interpretation methods that simulate, accelerate, and extrapolate long-term behaviour. Among these methods are those which characterise the material's performance under stress, taking into account the service conditions (e.g. temperature, environment, etc). Generally, the lifetime of a material is controlled by the material itself, the surrounding environment, and the loading conditions it is under.

In this part of the thesis the results of tests are presented on the regression behaviour of three different fibre yarns for times between 100 and 10,000 hours. These data were collected at different temperatures for the three commercially available aramid fibres. Test temperatures were 25°C, 65°C, 95°C, and 120°C, and the test environment was air. It is clear from the discussion in section 2.3.1 that, for the maximum operating temperature specified currently for RTP (65°C), the temperature dependence of aramid should not be a huge concern because of the limited effect of temperature on its strength properties in the 65°C temperature range, especially during the short-term tests conducted by the

manufacturers. However, tests are required for longer periods and particularly at higher temperatures to accelerate undesirable failure modes, if any, into the qualification test period.

The following are the specific aims of this section:

- To establish values of regression line gradients and 20 year design parameters for the fibre yarns and to compare them to those of RTP.
- To determine whether there is any evidence of long term changes in the failure mode that could affect the reliability of the material or the generated data.
- To verify and cross-check the results obtained using different modelling methods.

4.2 Stress Rupture Experimental Results and Discussions:

Three methods, as outlined in Chapter 2, were used to process and interpret the results obtained from the stress rupture tests.

The first was the multi-regression extrapolation procedure of the standard ISO 9080. As indicated in Chapter 2, the ISO 9080 procedure assumes that there is a linear relationship between the $\log_{10}$ of the time to failure and the $\log_{10}$ applied stress at each temperature. It also assumes that stress rupture curves are proportionally spaced depending on the reciprocal of the absolute temperature. Results are plotted on a $\log_{10}$-$\log_{10}$ scale because it is thought that the failure time exhibits power law dependence on stress. The method includes an extensive number of constant stress tests at several temperatures for the generation of creep rupture curves, followed by a multiple linear regression analysis in order to fit the data. From the regression data acquired a mean regression line is constructed and a statistical 97.5% lower confidence limit curve is calculated and extrapolated to obtain the Lower Prediction Limit (LPL) at the design life.

The second method used to process and interpret the results of the stress rupture tests was the modified standard ISO 9080. In this method a linear relationship between applied stress and $\log_{10}$ failure time, based on the theory of Eyring and an Arrhenius relationship, is used to enable the modelling of their relationship. Similar to the previous ($\log_{10}$-$\log_{10}$) method,

this method includes an extensive number of constant stress tests at several temperatures for the generation of creep rupture curves, followed by a multiple linear regression analysis in order to fit the data. From the regression data acquired a mean regression line is constructed and a statistical 97.5% lower confidence limit curve is calculated and extrapolated to obtain the Lower Prediction Limit (LPL) at the design life.

The third method used was the time-temperature superposition technique, which is based on the assumption that when data for a particular property in various temperatures are plotted on a logarithmic scale, then the property's curves versus time at each temperature should be the same if the underlying degradation mechanism that governs the property relation with time and temperature is the same. Based on this assumption, there should be a shift factor by which the time for each set of data (at each temperature) can be multiplied to get all the data to overlap at one specified reference temperature.

4.2.1 Behaviour in Air as Modelled by ISO 9080 (log_{10}-log_{10})

Figures 4.1, 4.2, and 4.3 show the stress rupture results of the different yarns in air at 25°C, 65°C, 95°C and 120°C as modelled by the standard log_{10}-log_{10} ISO 9080 procedure. The regression constants and the 20 year LPL values were calculated according to the ISO 9080 procedure and are given in Table 4.1.

For Kevlar and Twaron, the values of the regression line slope, *G*, are near to the values measured by the manufacturers of RTP pipe (Gibson et al, 2004), and they are very similar to each other although there have been marginal more scatter in Kevlar compare to Twaron. This is interesting, as it had been anticipated that the regression line slopes for the yarns by themselves might be a little flatter. Indeed, had the slopes been shallower, then any small statistical variation in the material's properties can result in large variations in the time to failure. Hence, it will be very difficult to know when a sample under particular stress will fail when tested especially with long-term tests like the +10,000 hours failure time required by the qualification procedures. There is no such data available in literature for the third fibre (Technora) to compare with.

Long-Term Behaviour of Aramid Fibre

The fact that aramid fibre regression line slopes are quite similar to those of RTP pipe supports the idea of utilizing stress rupture tests conducted on the fibre yarns in the prediction of RTP behaviour, and hence reduces the need for expensive long term tests on pipe samples needed for qualification. Additionally, this proves that these products (i.e. RTP) are well-manufactured from the viewpoint of strain balance and distribution among all loaded yarns, as it is believed that such an effect has been the result of an effective manufacturing process in converting the yarns into reinforcing tapes as well as in incorporating the tapes into the RTP. Additionally, it was concluded in the RTP JIP that one of the consequences of strain imbalances between yarns would be an increase in the regression line slope. Hence, the pressure regression test is therefore a good test of RTP quality.

The results show only small differences between Kevlar and Twaron yarn types when tested in air, confirming that the products are, for most purposes, effectively interchangeable. It is clear that the ISO 9080 procedure has been effective in correlating the behaviour at different times and temperatures.

Increasing the test temperature caused an evident decline in strength with time, as was anticipated, where the slopes of the regression lines were found to increase with increases in test temperature. This is very clear in the case of Kevlar and Twaron fibres. The temperature effect is not very much evident in the case of Technora fibre, however, it should be noted that this conclusion is based on very limited number of data points.

It can be seen from figures 4.1 to 4.3 that the scatter of failure points for the individual yarns is significant, and much greater than that observed when testing RTP spool samples under pressure. This is probably due to the fact that along the length of a fibre there is a variation in statistical strength due to the distribution of flaws or weak points in its morphology. Additionally, when a pipe is tested, the behaviour of several hundred yarns is effectively averaged, which greatly reduces the scatter.

Long-Term Behaviour of Aramid Fibre

The mechanical behaviour of yarns is strongly influenced by the level of twist, and as indicated earlier, along the length of a fibre there is a variation in statistical strength due to the distribution of flaws or weak points in its morphology. With untwisted fibres, therefore, test results depend on the gauge length. Hence, it is required to maintain the gauge length at a minimum so that its sensitivity effect is kept to minimum as well. Twisted yarns eliminate this problem by allowing stress to be shared, through friction, between adjacent filaments when a particular filament fails. This is why yarn twisting usually results in more consistency in measurements of the breaking strength and elongation at break, because of the distribution of tensile forces between the yarn's filaments. This is similar in some respects to the 'composite' effect achieved when fibres are impregnated by a rigid resin matrix.

Finally, there is no evidence of any 'knee' in the curves either after long periods or when the higher temperatures test data were added to help in accelerating the undesirable failure mechanisms (if any) to a shorter time period. This was checked both visually and using the mathematical procedure recommended in ISO 9080. This suggests that there will be no change of failure mechanism after long periods at the RTP pipe maximum design temperature of 65°C, which gives confidence in the qualification procedure proposed by the JIP for RTP products containing aramid fibre. This also supports the idea of utilizing the fibre stress rupture tests as an alternative to the expensive long term tests on pipe samples needed for qualification.

Table 4.1 Regression test results, stresses in GPa

	25°C			
	G	***F***	**20 yr Mean Stress**	**20 yr LCL**
Kevlar	-0.03682	2.2085	1.4159	1.283
Twaron	-0.04237	2.2278	1.3656	1.226
Technora	-0.05044	2.4890	1.35371	1.226

	65°C			
	G	***F***	**20 yr Mean Stress**	**20 yr LCL**
Kevlar	-0.04919	2.0958	1.1572	1.018
Twaron	-0.05402	2.1961	1.1440	1.001
Technora	-0.05514	2.4976	1.2835	1.137

	95°C			
	G	***F***	**20 yr Mean Stress**	**20 yr LCL**
Kevlar	-0.06179	1.9867	0.9422	0.774
Twaron	-0.06485	2.1228	0.9703	0.801
Technora	-0.05845	2.5037	1.23629	1.027

	120°C			
	G	***F***	**20 yr Mean Stress**	**20 yr LCL**
Kevlar	-0.07569	1.8730	0.7511	0.521
Twaron	-0.07573	2.0518	0.8223	0.600
Technora	-0.06107	2.5086	1.20006	0.901

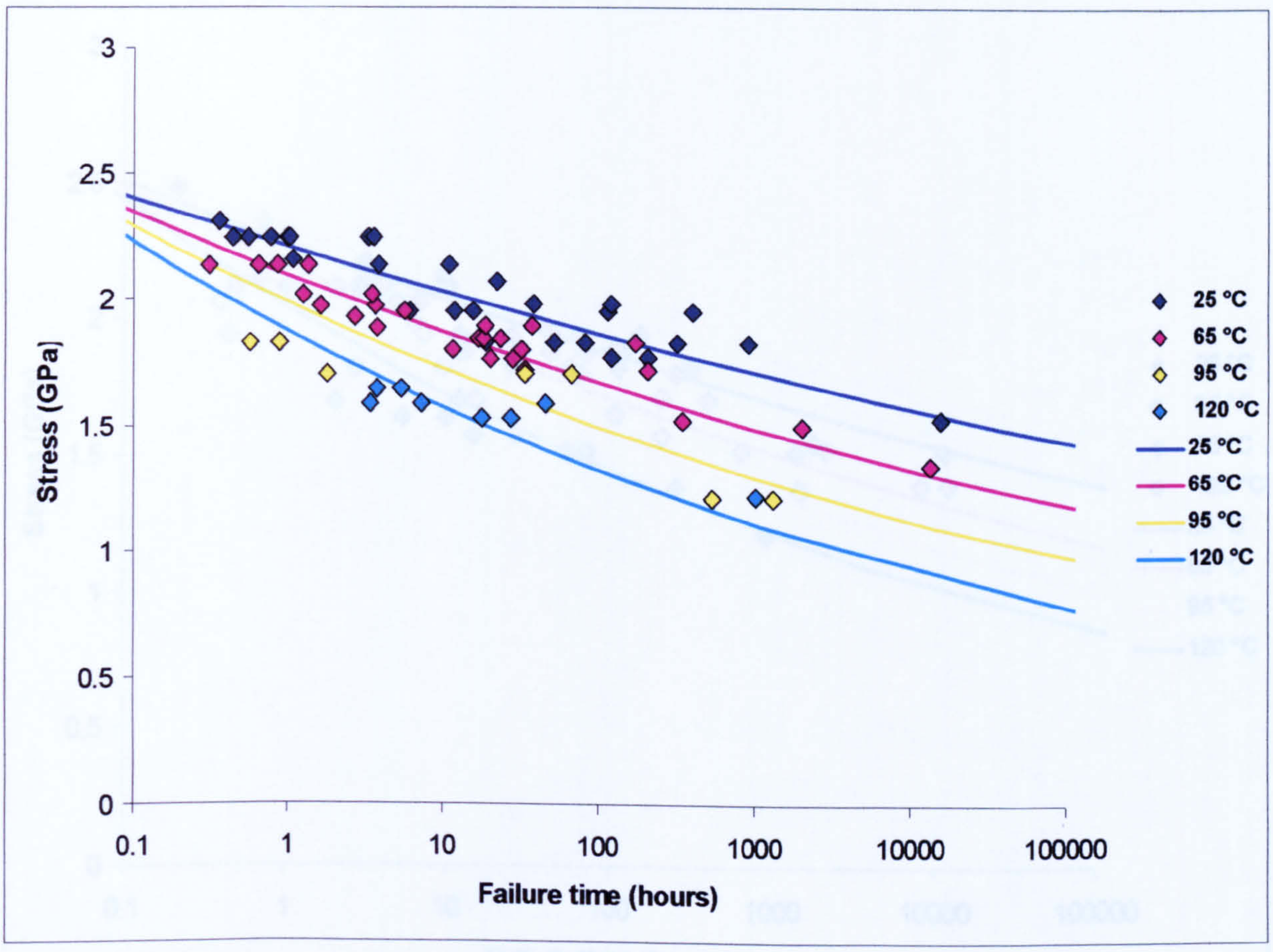

Figure 4.1 Results of Kevlar 29 yarn in air.

Continuous lines are the predictions of the ISO 9080 4-parameter model

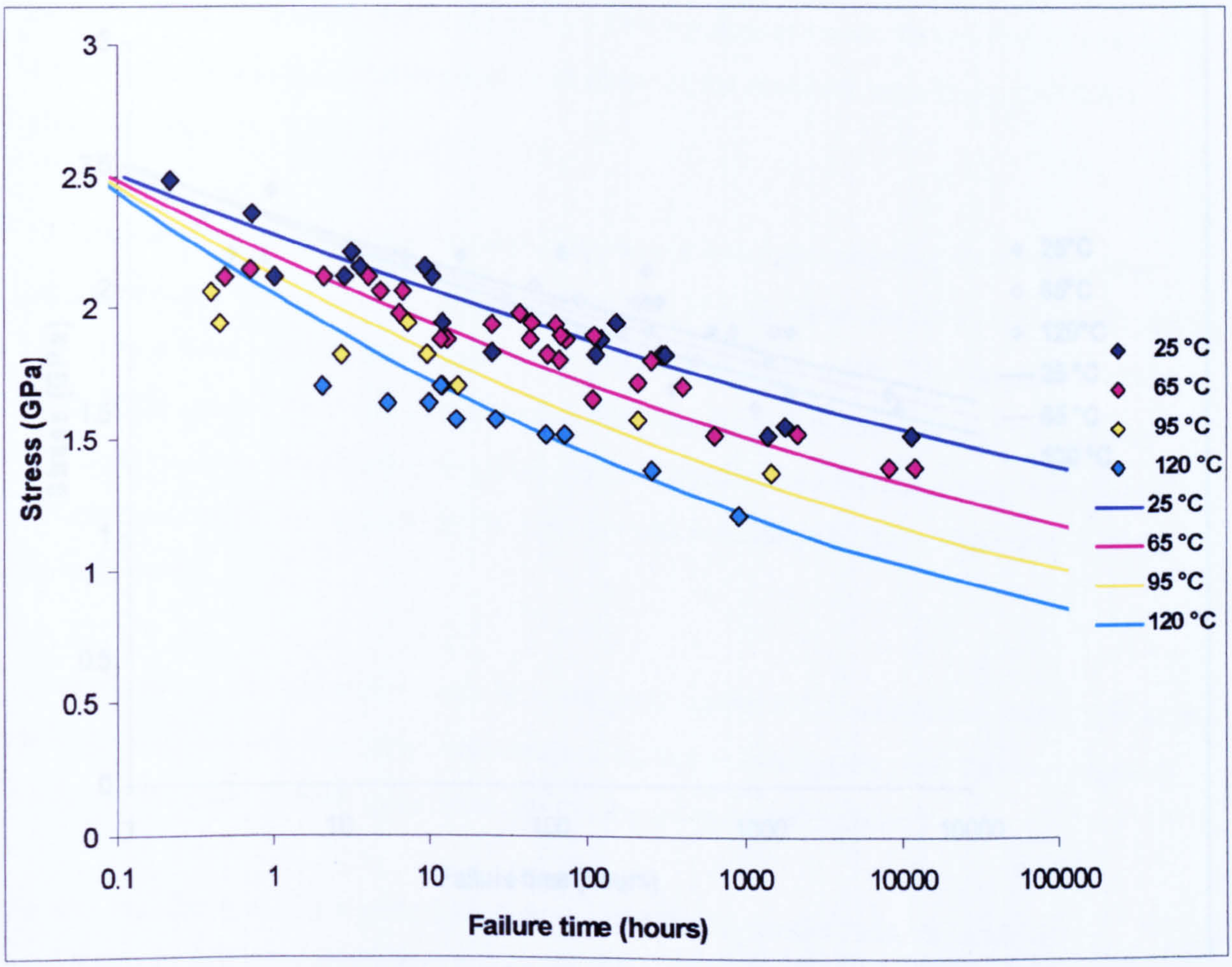

Figure 4.2 Results of Twaron 1000 yarn in air.

Continuous lines are the predictions of the ISO 9080 4-parameter model

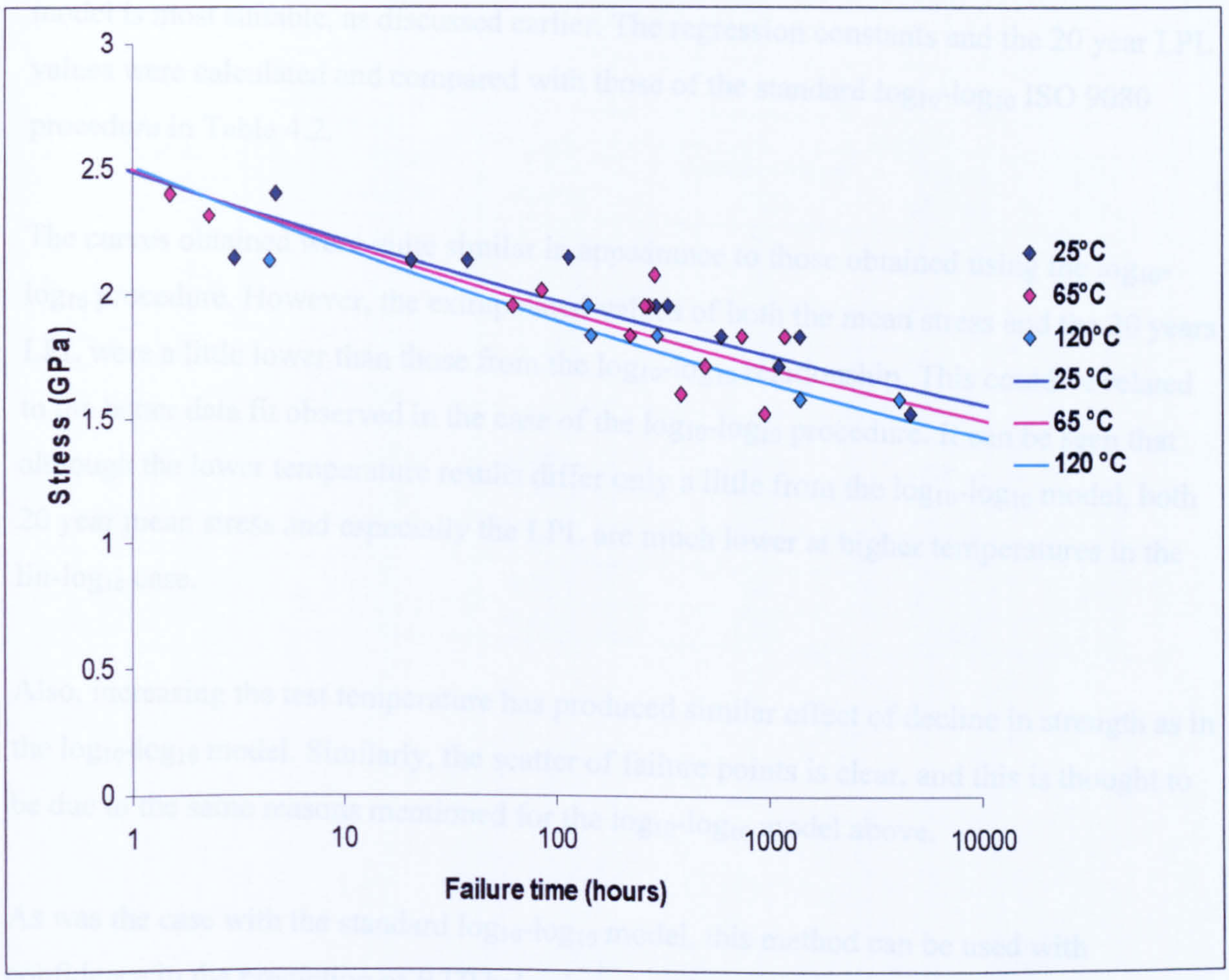

Figure 4.3 Results of Technora T200 yarn in air.
Continuous lines are the predictions of the ISO 9080 4-parameter model

4.2.2 Behaviour in Air as Modelled by the Modified ISO 9080 (lin-log_{10})

Figures 4.4 and 4.5 show the stress rupture results on the different yarns in air at 25°C, 65°C, 95°C and 120°C as modelled by the modified lin-log_{10} ISO 9080 procedure. This was conducted by replacing the log_{10} stress function with linear stress, to determine which model is most suitable, as discussed earlier. The regression constants and the 20 year LPL values were calculated and compared with those of the standard log_{10}-log_{10} ISO 9080 procedure in Table 4.2.

The curves obtained were quite similar in appearance to those obtained using the log_{10}-log_{10} procedure. However, the extrapolated values of both the mean stress and the 20 years LPL were a little lower than those from the log_{10}-log_{10} relationship. This could be related to the better data fit observed in the case of the log_{10}-log_{10} procedure. It can be seen that although the lower temperature results differ only a little from the log_{10}-log_{10} model, both 20 year mean stress and especially the LPL are much lower at higher temperatures in the lin-log_{10} case.

Also, increasing the test temperature has produced similar effect of decline in strength as in the log_{10}-log_{10} model. Similarly, the scatter of failure points is clear, and this is thought to be due to the same reasons mentioned for the log_{10}-log_{10} model above.

As was the case with the standard log_{10}-log_{10} model, this method can be used with confidence in the prediction of RTP behaviour, and hence reduces the need for expensive long term tests on pipe samples, especially at low temperatures.

Table 4.2 Comparisons of the 20 year mean and LPL from the log_{10}-log_{10} and lin-log_{10} models

Log₁₀-Log₁₀				***Linear-Log₁₀***		
Kevlar				**Kevlar**		
Temperature (°C)	**Mean (GPa)**	**LPL (GPa)**		**Temperature (°C)**	**Mean (GPa)**	**LPL (GPa)**
25	1.416	1.283		25	1.328	1.135
65	1.157	1.018		65	1.016	0.790
95	0.942	0.774		95	0.762	0.453
120	0.751	0.521		120	0.534	0.073
Twaron				**Twaron**		
Temperature (°C)	**Mean (GPa)**	**LPL (GPa)**		**Temperature (°C)**	**Mean (GPa)**	**LPL (GPa)**
25	1.365	1.226		25	1.277	1.068
65	1.144	1.001		65	0.995	0.757
95	0.970	0.801		95	0.773	0.456
120	0.822	0.600		120	0.580	0.125

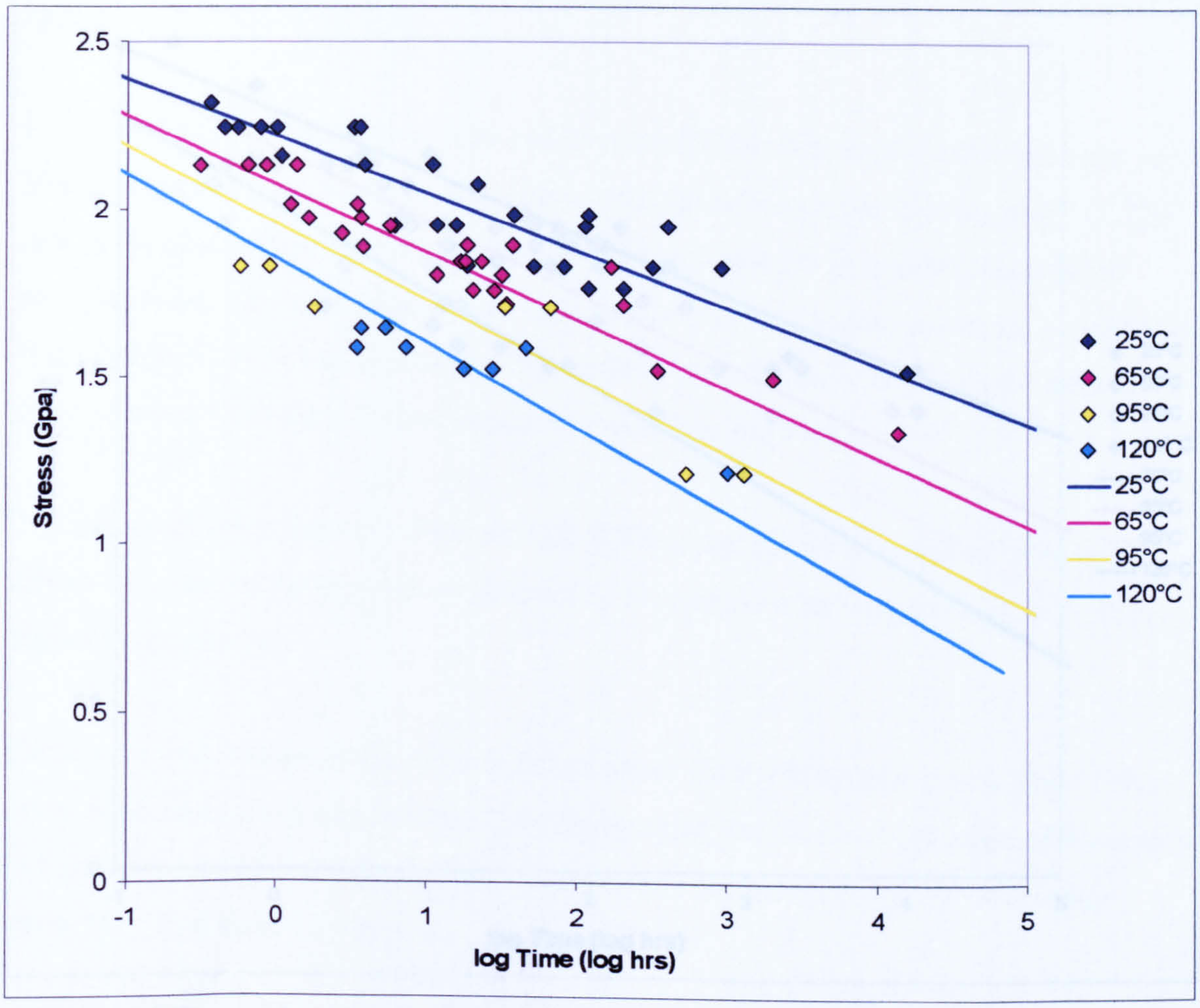

Figure 4.4 Regression test results for Kevlar yarns at 25, 65, 90 and 120°C (ISO 9080, modified to fit the lin-$\log_{10}$ relationship)

Long-Term Behaviour of Aramid Fibre

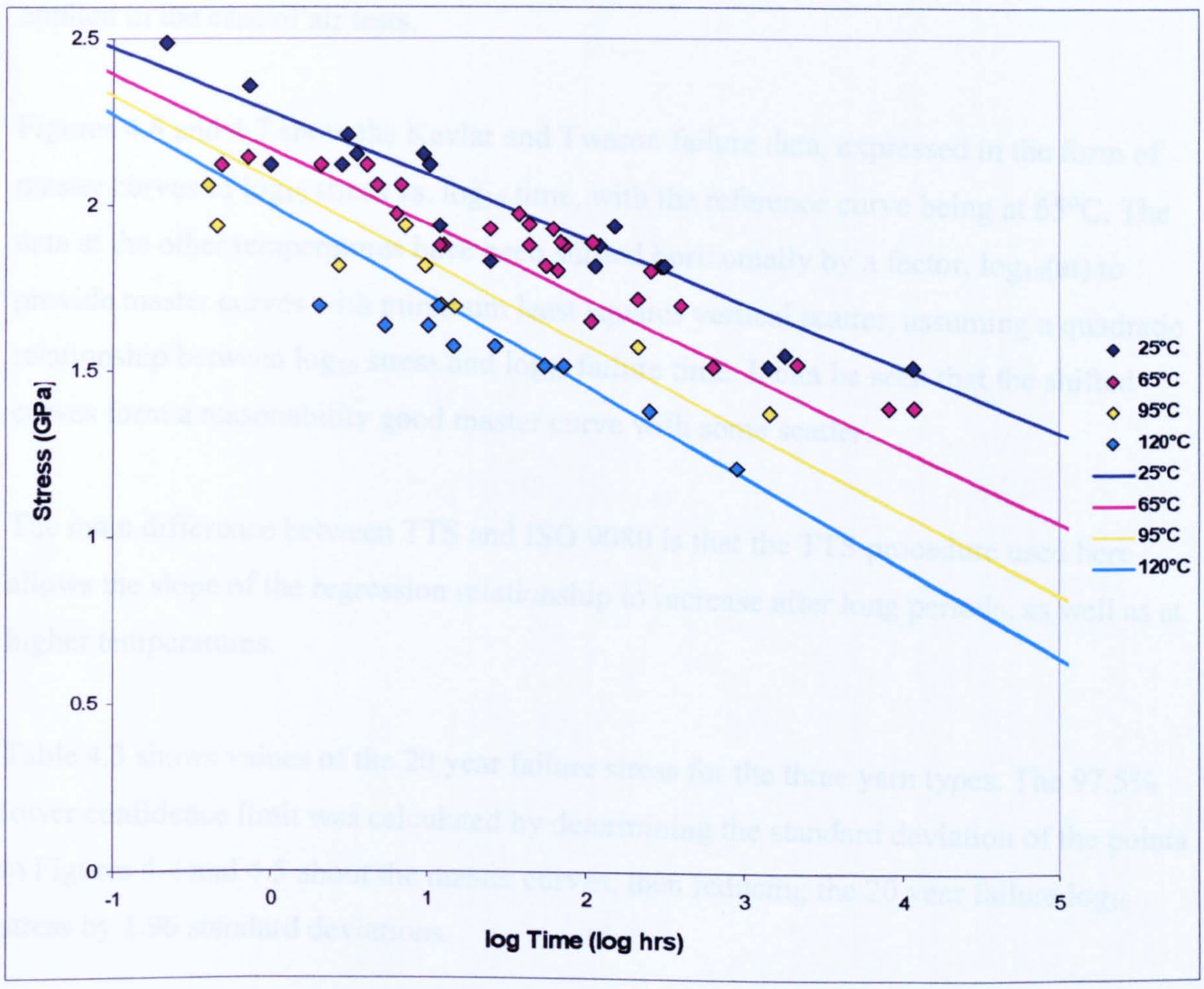

Figure 4.5 Regression test results for Twaron yarns at 25, 65, 90 and 120°C (ISO 9080, modified to fit the lin-$\log_{10}$ relationship)

4.2.3 Behaviour in Air as Modelled by Time-Temperature Superposition

From the standard ISO 9080, it has been shown that there is no change in the underlying degradation or failure mechanism that governs strength in relation to time and temperature. Hence, the basic assumption for using the TTS analysis method has been met, and it can be applied in the case of air tests.

Figures 4.6 and 4.7 show the Kevlar and Twaron failure data, expressed in the form of master curves of $\log_{10}$ stress vs. $\log_{10}$ time, with the reference curve being at 65°C. The data at the other temperatures have been shifted horizontally by a factor, $\log_{10}(at)$ to provide master curves with minimum least squares vertical scatter, assuming a quadratic relationship between $\log_{10}$ stress and $\log_{10}$ failure time. It can be seen that the shifted curves form a reasonability good master curve with some scatter.

The main difference between TTS and ISO 9080 is that the TTS procedure used here allows the slope of the regression relationship to increase after long periods, as well as at higher temperatures.

Table 4.3 shows values of the 20 year failure stress for the three yarn types. The 97.5% lower confidence limit was calculated by determining the standard deviation of the points in Figures 4.4 and 4.5 about the master curves, then reducing the 20 year failure $\log_{10}$ stress by 1.96 standard deviations.

It can be seen that the Twaron values are comparable with the data generated from the standard ISO 9080 procedure, but the predicted Kevlar data are rather more favourable as they are higher than those predicted using the standard ISO 9080.

Table 4.3 20 year mean failure stress and 20 year LPL at 65°C, determined from time-temperature superposition

	20 year mean failure stress (GPa)	**20 year LPL stress (GPa)**
Kevlar	1.643	1.505
Twaron	1.184	1.098

Long-Term Behaviour of Aramid Fibre

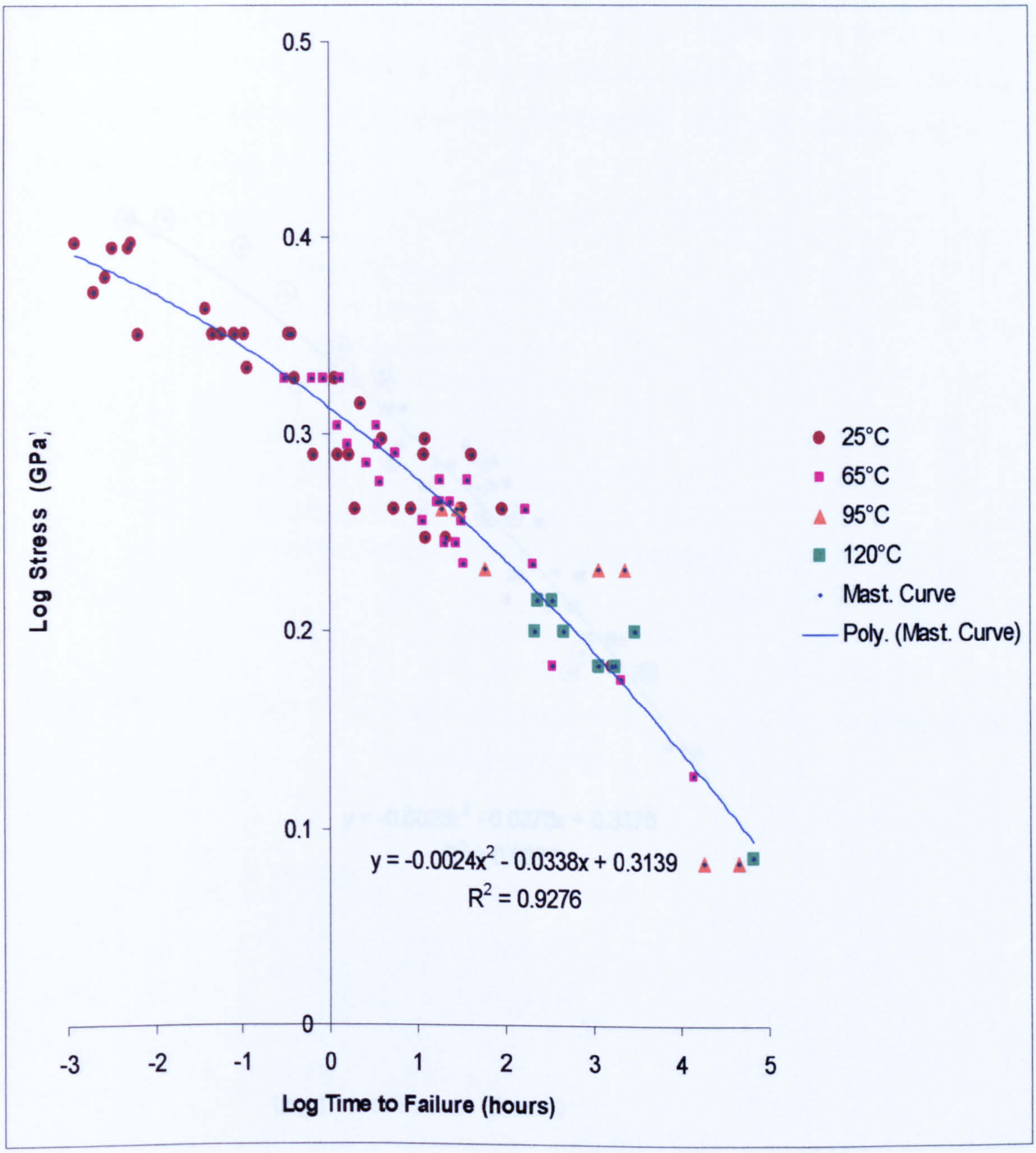

Figure 4.6 Time temperature superposition master curve of stress vs. $\log_{10}$ time to failure for Kevlar yarns at 65°C.

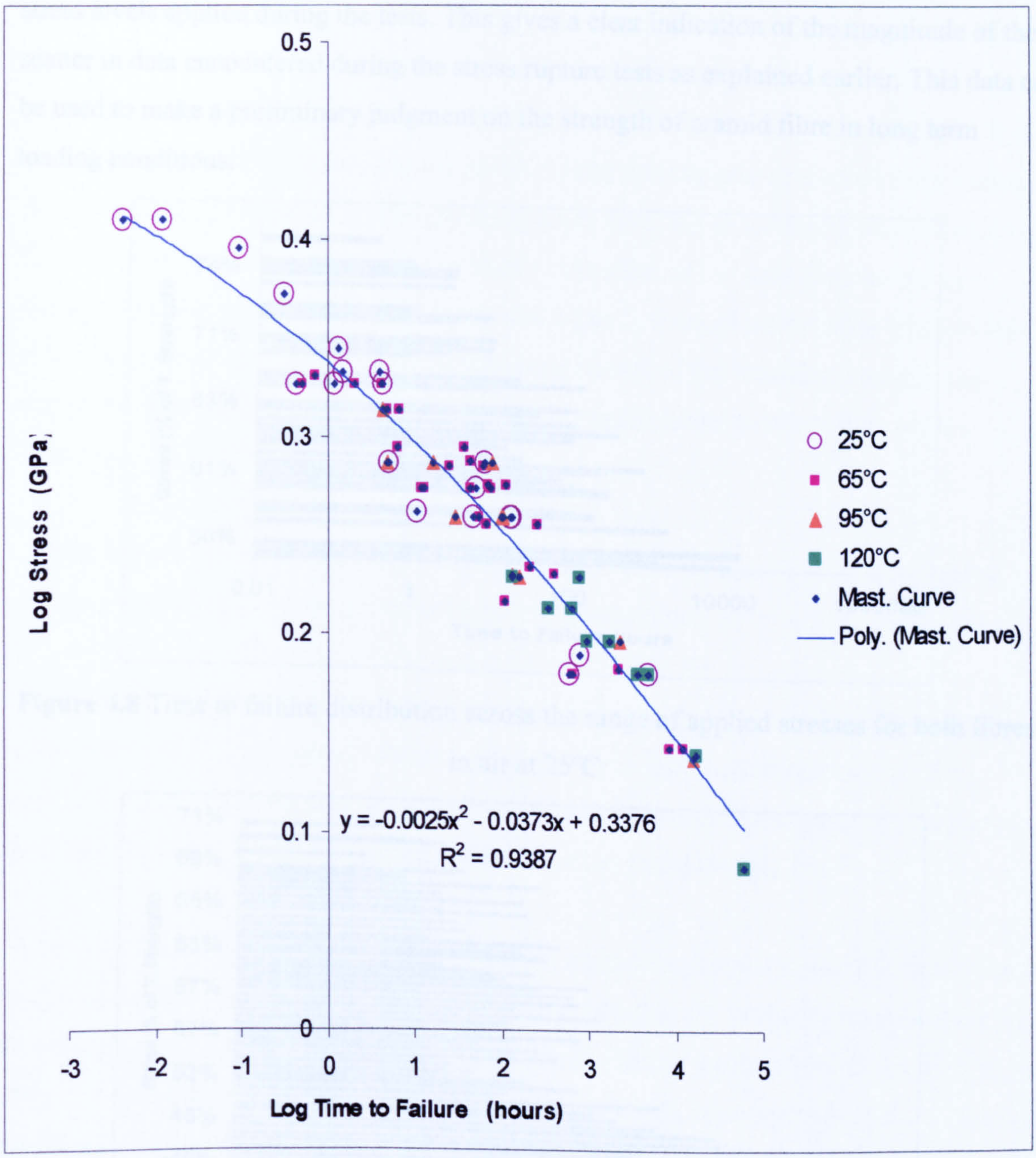

Figure 4.7 Time temperature superposition master curve of stress vs. $\log_{10}$ time to failure for Twaron yarns at 65°C.

4.2.4 Range of Time to Failure at Different Stresses

Figures 4.8 and 4.9 are plots of the range of times to failure (TTF) observed at the different stress levels applied during the tests. This gives a clear indication of the magnitude of the scatter in data encountered during the stress rupture tests as explained earlier. This data can be used to make a preliminary judgment on the strength of aramid fibre in long term loading conditions.

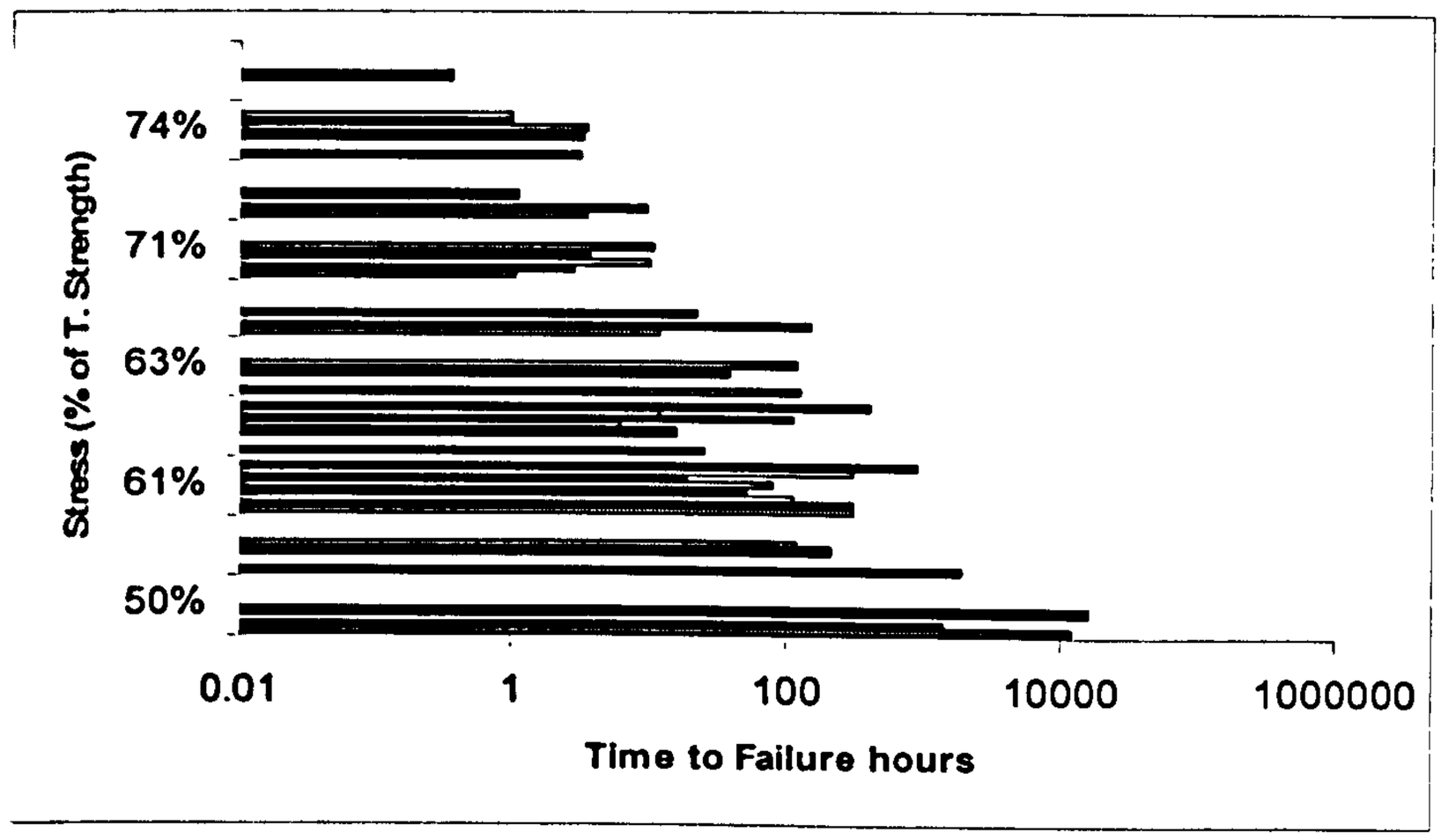

Figure 4.8 Time to failure distribution across the range of applied stresses for both fibres in air at 25°C

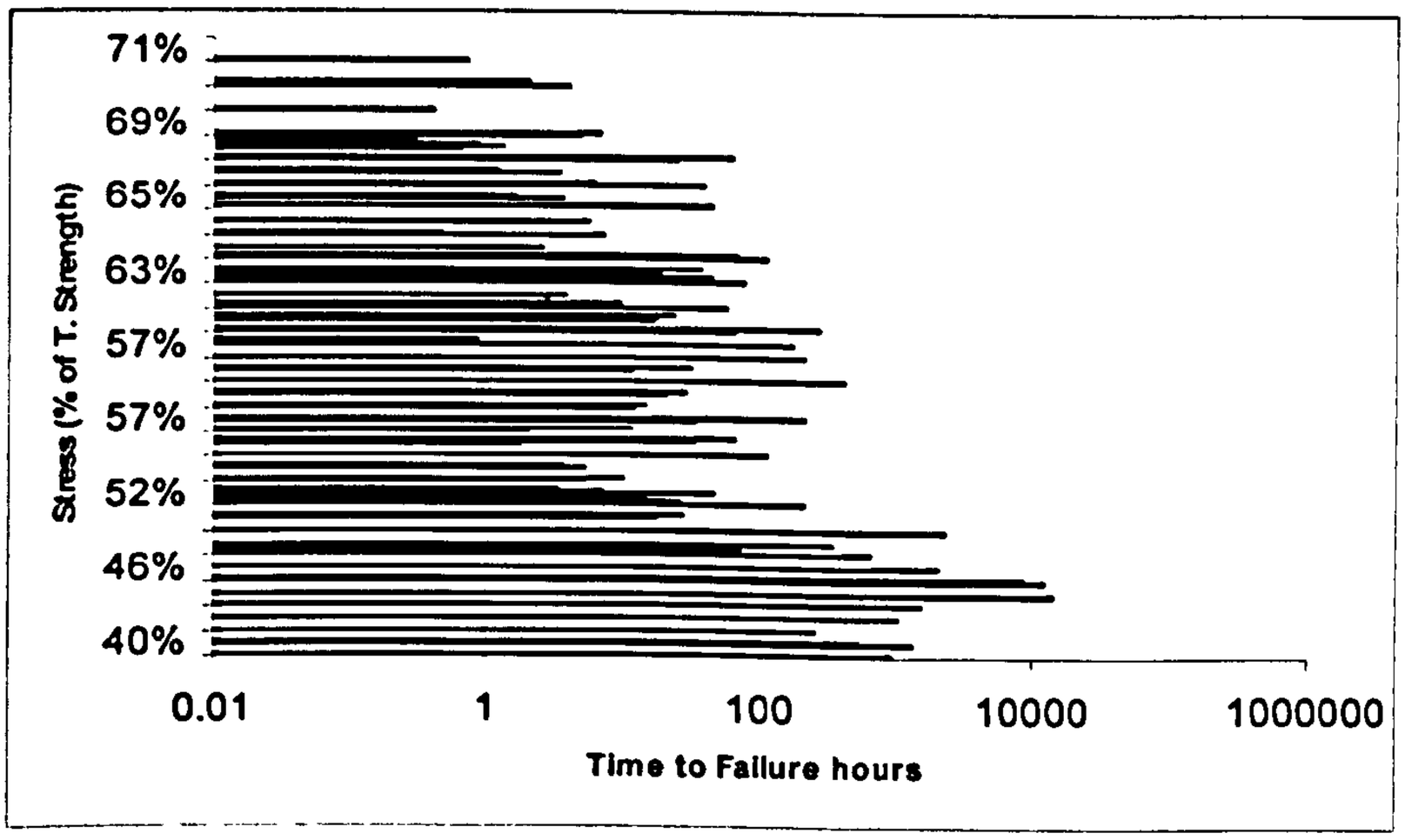

Figure 4.9 Time to failure distribution across the range of applied stresses for both fibres in air at 65°C

4.3 Conclusions

The most notable feature in the results curves presented is the scatter of data points, which is significantly greater than that for the RTP pipe tests reported by Gibson et al (2005) and others. This is probably due to the fact that when a pipe is tested; the behaviour of several hundred yarns is effectively averaged, which greatly reduces the scatter. In addition, it is believed that the fibres contain serious defects along their length; as a result there should be some statistical variation in strength along each fibre, due to a distribution of these flaws or weak points. Additionally, the tensile properties of the yarn samples are not identical in all cases, due to the dependence of a yarn's strength on twisting level which will usually result in more consistency in measurements of the breaking strength and elongation at break because of the distribution of tensile forces between the yarn's filaments.

Despite this scatter, the actual failure parameters for the two main fibres studied were similar, confirming that they are effectively interchangeable.

Generally, all synthetic fibres lose their load bearing capacity when under load and high temperature over a long period of time, and as has been shown in the present results, aramid fibres are no exception to this general rule. This is demonstrated by the increase in regression lines slope with increasing test temperature and duration.

There is no evidence of a knee in any of the yarn regression curves, suggesting that there is no change in failure mode after long periods when tested in air, probably because there is no environmental interaction apart from the limited effect of temperature on the fibre's strength rather than on the failure mechanism. This gives more confidence in the method used and its predictions, particularly at low temperatures such as 25°C.

It can be concluded that the creep rupture measurements have successfully characterised the long-term failure behaviour of the aramid fibre yarns, and have provided data that can be used as the basis for future design in tensile applications, including for RTP. The different yarn types showed similar regression parameters.

The following conclusions were drawn from the work:

- All three prediction methods gave similar predictions for the 20 year mean stress and the 20 year LPL stress.
- Due to the scatter in properties among individual fibre samples it was necessary to conduct a large number of tests in order to reduce the scatter effect under each test condition. This scatter is thought to be due to the fact that along the length of a fibre there is statistical variation in strength due to the distribution of flaws or weak points in its morphology.
- The $\log_{10}$-$\log_{10}$ plots, by their shape, give a more optimistic prediction of the long term behaviour of aramid fibres than the lin-$\log_{10}$ plots.
- The values of the regression line slope, *G*, for both fibres were near to the values measured by the manufacturers of RTP pipe. This is interesting, as it had been anticipated that the regression line slopes for the yarns by themselves might be a little flatter. This supports the idea of utilizing stress rupture tests conducted on the fibre yarns in the prediction of RTP behaviour, and hence reduces the need for expensive long term tests on pipe samples needed for qualification.
- Considerable tensile strength reductions were observed over long testing periods at different temperatures.
- Tests results showed only small differences between the yarn types when tested in air, confirming that the products are, for most purposes, effectively interchangeable.
- The results suggest that there is unlikely to be a change in failure mechanism after long periods, which lends confidence to the use of aramid fibre in highly loaded long term tensile applications.
- Regardless the loss of strength encountered as a result of long-term loading, aramid fibres performance is sufficiently high and they can be used in many applications where high strength is required.

Chapter 5 Long-Term Behaviour of Aramid Fibres under Different Temperature & Environmental Conditions

5.1 Introduction

Although it is generally believed that aramid fibres are resistant to most chemicals, experimental results from this study have shown some reduction in strength as a result of exposure to different environments.

The aim of this chapter is to determine the effect of various environments on yarn behaviour during the test period, and to determine whether or not there was any evidence of long term changes in the failure mode that could affect the reliability of the data generated.

An explanation of the mechanism of degradation as well as the results of the long-term stress rupture regression analysis is presented below for Kevlar and Twaron aramid fibres. The data presented were collected at combinations of a temperature of 65°C and different environments; namely pure tap water, low pH water, and crude oil.

When polymers are exposed to different fluid environments, the absorption of species from these fluids results in plasticization which reduces strength and stiffness as a result of changes in free volume. Another form of change could be caused by chemical reactions between the absorbed species and the polymer resulting in loss of molecular weight through chain scission in the form of hydrolysis. As indicated in Chapter 2, because water molecules are small and polar, they can approach the hydrogen bonding sites and disrupt the original hydrogen bonds. Chain scission could also occur as a result of the prolonged periods of load application in the form of stress-induced chain scission, or as a result of exposure to UV radiation.

However, although such form of degradation will lead to loss of strength; this was not very drastic as will be demonstrated in the sections below. This confirms the findings of Cook et al (1982), Morgan et al (1984) and Cantrill (2002).

It should be stressed that the noticeable reductions in the load-bearing capability of the yarns when tested in crude oil and water (both pure and low pH) environments is not only time dependent. Rather it is also a function of the test environment and possibly also of temperature, which leads to certain forms of degradation in the material tested.

Exposure to both crude oil and water (pure and low pH) resulted in more rapid decays in stress compared to exposure to air. As a result, the horizontal shift factor cannot be applied and the results for air and other environmental conditions cannot be superimposed. This suggests the existence of different failure mechanisms as a result of changing the test environment, which therefore means that the principles of superposition no longer apply.

5.2 Stress Rupture Experimental Results and Discussions

5.2.1 Behaviour in Crude Oil at 65°C as Modelled by ISO 9080 (log_{10}-log_{10})

The results of the regression tests in crude oil at 65°C are shown in Figures 5.1 and 5.2. It can be seen that crude oil immersion has a small but significant effect. With both Kevlar and Twaron the slope of the crude oil measurements is a little shallower than that of the regression data in air. This implies that there may be some initial plasticization effect, which has less influence as time goes on.

On this basis it is relevant to calculate a factor relating to crude oil immersion. This was conducted for each crude oil experimental point. This factor is the failure stress in crude oil divided by the failure stress in air at the same time to failure as predicted by the ISO 9080 model. The average values taken for all the experimental points at 65°C were 0.93 and 0.91 for Kevlar and Twaron respectively. A reasonable factor to allow for the effect of crude oil on reinforcement, therefore, would be 0.90. This is probably conservative, given the fact that the regression lines appear to converge after long periods.

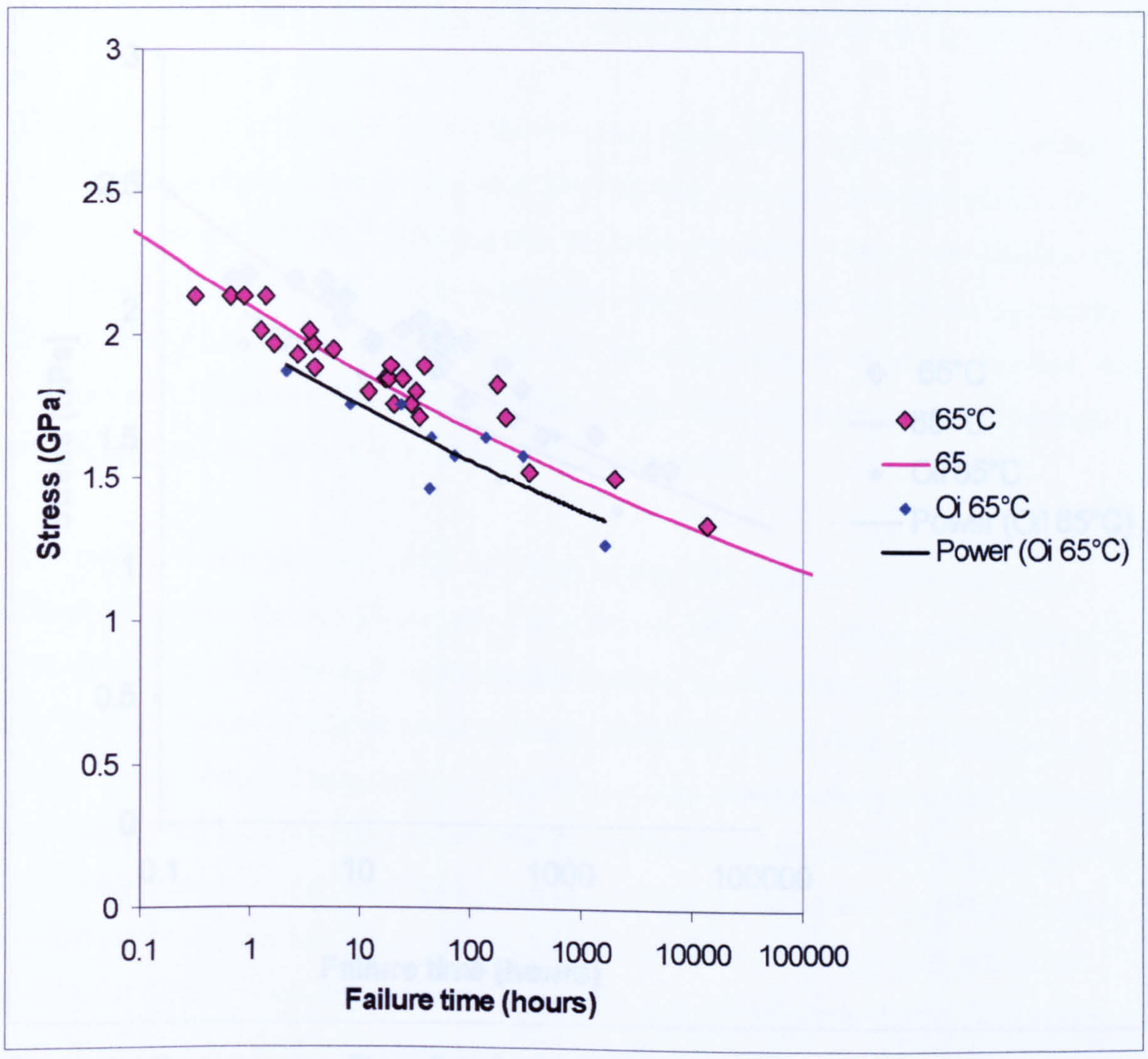

Figure 5.1 Kevlar yarn: effect of testing in crude oil at 65°C. Key: Upper curve and pink points represent the ISO 9080 fit and 65°C points for testing in air. Lower curve and black points represent tests in crude oil. Average ratio for all crude oil points = 0.93.

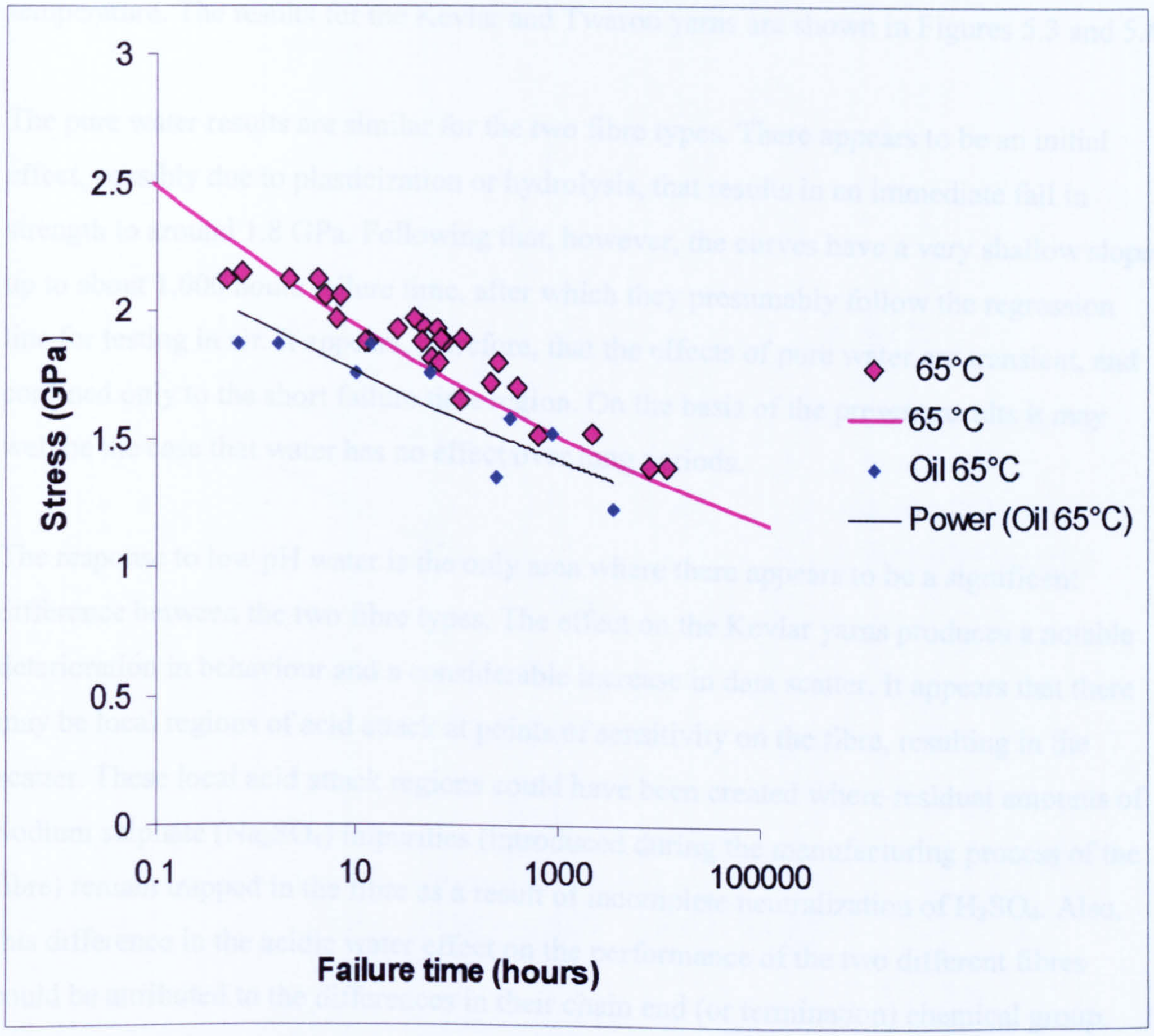

Figure 5.2 Twaron yarn: effect of testing in crude oil at 65°C. Key: Upper curve and pink points represent the ISO 9080 fit and 65°C points for testing in air. Lower curve and black points represent tests in crude oil. Average ratio for all crude oil points = 0.91.

5.2.2 Behaviour in Water at 65°C as Modelled by ISO 9080 (log_{10}-log_{10})

Tests were carried out in both pure water and low pH (acidic) water at 65°C. For the low pH water tests a buffer solution was prepared by dissolving 1.878g of potassium hydrogen tartrate in 1000ml of pure tap water. The solution had a pH of around 4 at the test temperature. The results for the Kevlar and Twaron yarns are shown in Figures 5.3 and 5.4.

The pure water results are similar for the two fibre types. There appears to be an initial effect, possibly due to plasticization or hydrolysis, that results in an immediate fall in strength to around 1.8 GPa. Following that, however, the curves have a very shallow slope up to about 1,000 hours failure time, after which they presumably follow the regression line for testing in air. It appears, therefore, that the effects of pure water are transient, and confined only to the short failure time region. On the basis of the present results it may well be the case that water has no effect over long periods.

The response to low pH water is the only area where there appears to be a significant difference between the two fibre types. The effect on the Kevlar yarns produces a notable deterioration in behaviour and a considerable increase in data scatter. It appears that there may be local regions of acid attack at points of sensitivity on the fibre, resulting in the scatter. These local acid attack regions could have been created where residual amounts of Sodium sulphate (Na_2SO_4) impurities (introduced during the manufacturing process of the fibre) remain trapped in the fibre as a result of incomplete neutralization of H_2SO_4. Also, this difference in the acidic water effect on the performance of the two different fibres could be attributed to the differences in their chain end (or termination) chemical group. Aramid fibres chain may end either with (—COOH) or (—NH_2), which will have different interactions with the test environment in the form of acid-induced chain hydrolysis (Morgan et al, 1983).

By contrast, the effect of the acidic water on the Twaron yarn appears no different from that of pure water.

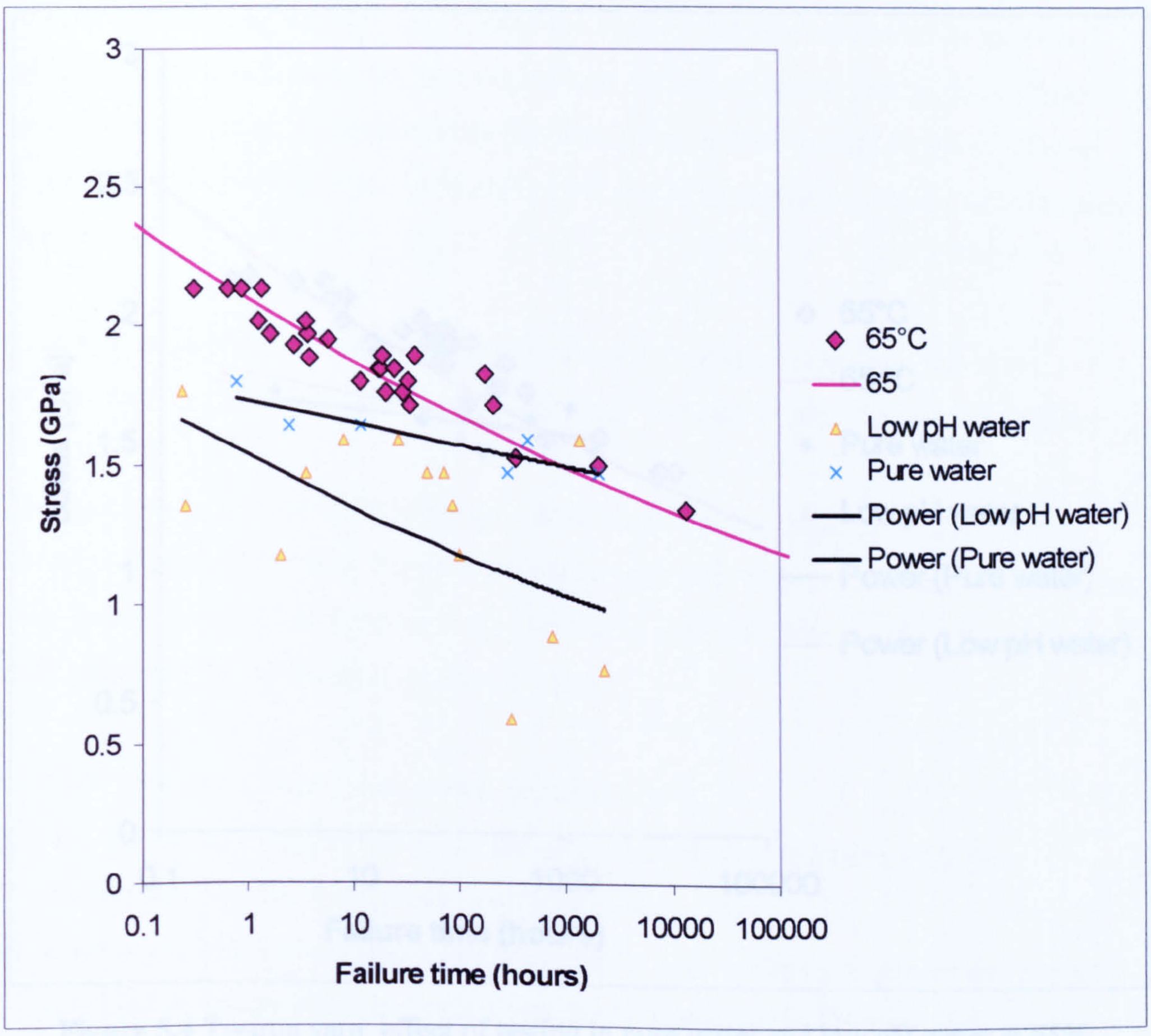

Figure 5.3 Kevlar yarn: effect of testing in pure water and low pH water at 65°C.

Key: Upper curve and pink points represent the ISO 9080 fit and 65°C points for testing in air. Middle curve, and blue points represent tests in pure water. Lower curve and yellow points represent tests in low pH water.

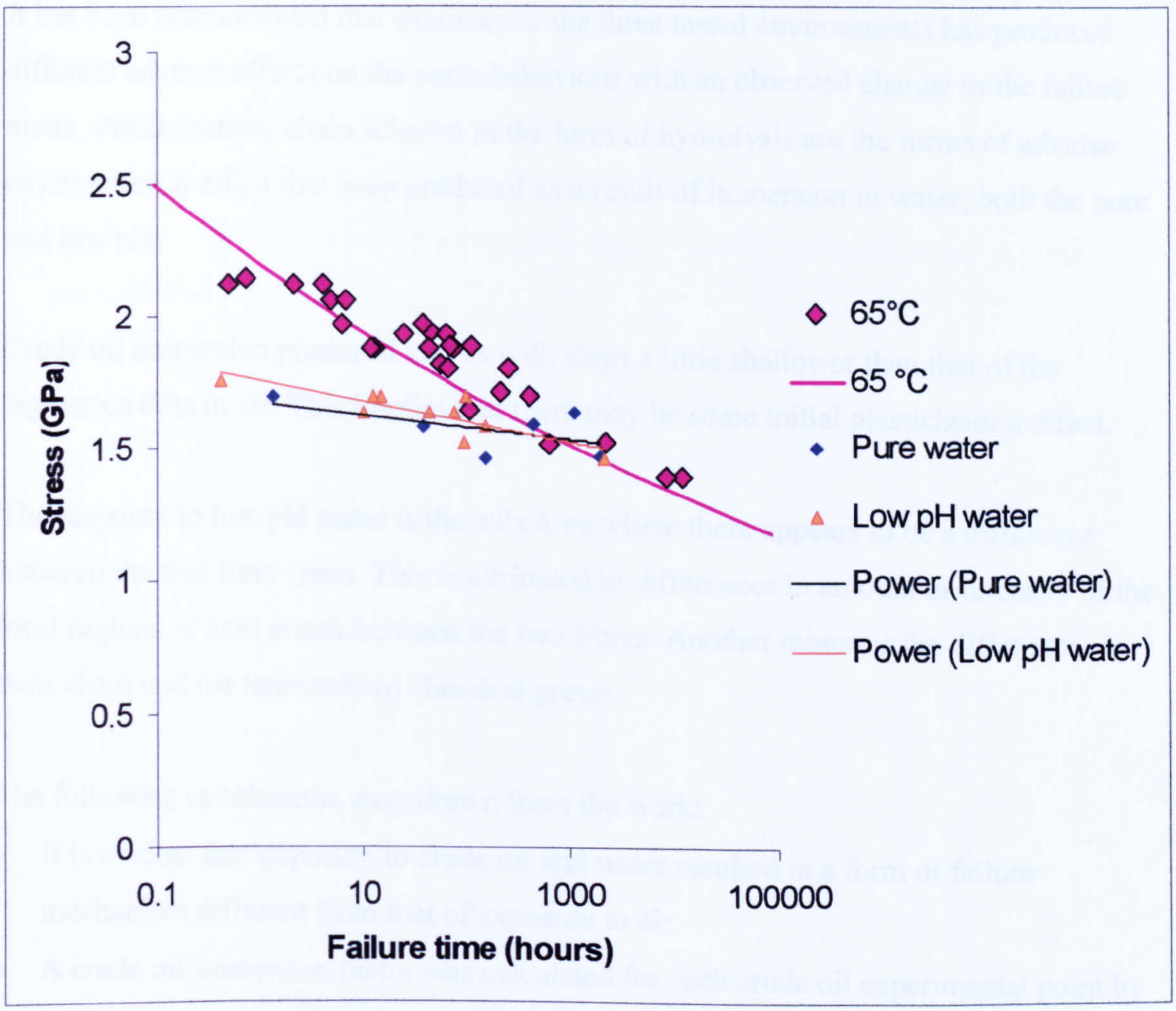

Figure 5.4 Twaron yarn: effect of testing in pure water and low pH water at 65°C.

Key: Upper curve and pink points represent the ISO 9080 fit and 65°C points for testing in air. Black curve and points represent tests in pure water. Orange curve and points represent tests in low pH water.

5.3 Conclusions

The programme of environmental experiments carried out on the Kevlar and Twaron types of aramid fibres gave useful data relevant to their long-term regression.

It has been demonstrated that exposure to the three tested environments has produced different adverse effects on the yarns behaviour with an observed change in the failure mode. Plasticization, chain scission in the form of hydrolysis are the forms of adverse environmental effect that been produced as a result of immersion in water, both the pure and low pH.

Crude oil immersion produced curves with slops a little shallower than that of the regression data in air. This implies that there may be some initial plasticization effect.

The response to low pH water is the only area where there appears to be a difference between the two fibre types. This is attributed to differences in amount or intensity of the local regions of acid attack between the two fibres. Another reason is the differences in their chain end (or termination) chemical group.

The following conclusions were drawn from the work:

- It is evident that exposure to crude oil and water resulted in a form of failure mechanism different from that of exposure to air.
- A crude oil immersion factor was calculated for each crude oil experimental point by dividing the failure stress in crude oil by the failure stress in air at the same time to failure, as predicted by the ISO 9080 model. The average values taken for all the experimental points were 0.93 and 0.91 for Kevlar and Twaron respectively.
- Due to the decay in stress as a result of exposure to crude oil and water compared to air, it is believed that different failure mechanisms are taking place as a result of changing the test environment, which therefore means that the principles of superposition no longer applies in the case of these environmental tests.
- Water immersion resulted in plasticization and chain scission in the form of hydrolysis.

Long-Term Behaviour of Aramid Fibre

- No significant difference between the effect of pure water and low pH water was noticed in the case of the fibres. It is believed that deterioration in strength when exposed to these environments is dominated by hydrolysis, and that the low pH has very little influence.
- Difference in low pH water effect between the two fibres is attributed to either differences in intensity of the local regions of acid attack or differences in the chain end (or termination) chemical group.
- Plasticization, chain scission in the form of hydrolysis are the forms of adverse environmental effect that been produced as a result of immersion in water, both the pure and the low pH.

Chapter 6 Aramid Fibre Creep Behaviour and Failure Model

6.1 Introduction

As indicated in chapter one, in order to accurately predict fibre durability it is necessary to have a detailed understanding of the physical structure of the fibre, and how its structure is related to the deformation and failure process. To facilitate such understanding, a model has been proposed for the fibre failure mechanism and relating the stress to time to failure and estimating the strain to failure based on the material's properties.

6.2 Aramid Fibre Failure Model

Aramid fibre is a rigid rod polymer comprising stiff polymeric units arranged in a near-unidirectional crystalline phase. One view of the structure, as in Figure 2.26 (page 48), shows a unidirectional crystal containing imperfections corresponding to the ends of individual crystal sequences. The rod-like sequences shown in Figure 2.26 may correspond either to individual chains or to crystallites comprising a number of chains. Figure 6.1 gives a clearer view of the structure, showing the fibre consisting of cylindrical crystallites with some degree of structural continuity in fibre direction. Also the non-random distribution of the macromolecular ends within the crystallites is illustrated.

It is generally accepted that the creep of aramid fibres under load involves plastic flow or movement parallel to the chain direction within the crystallites. One problem is the identification of the actual deformation mechanism, which is difficult to envisage in a system where the chains are almost perfectly aligned within the crystalline phase.

One of the proposed possibilities for explaining the actual deformation mechanism associated with the creep of aramid fibres under load is deformation associated with the defect regions constituted by the ends of chains or alternatively the ends of crystalline sequences involving several chains. Such regions of chain end concentration align laterally between crystallites to form planes that contain a greater concentration of chain ends than would be the case in a random chain-end distribution. These regions of chain-end

concentration within the fibre, as anticipated by Morgan et al (1983), are the primary critical physical structural parameters that control deformation and failure.

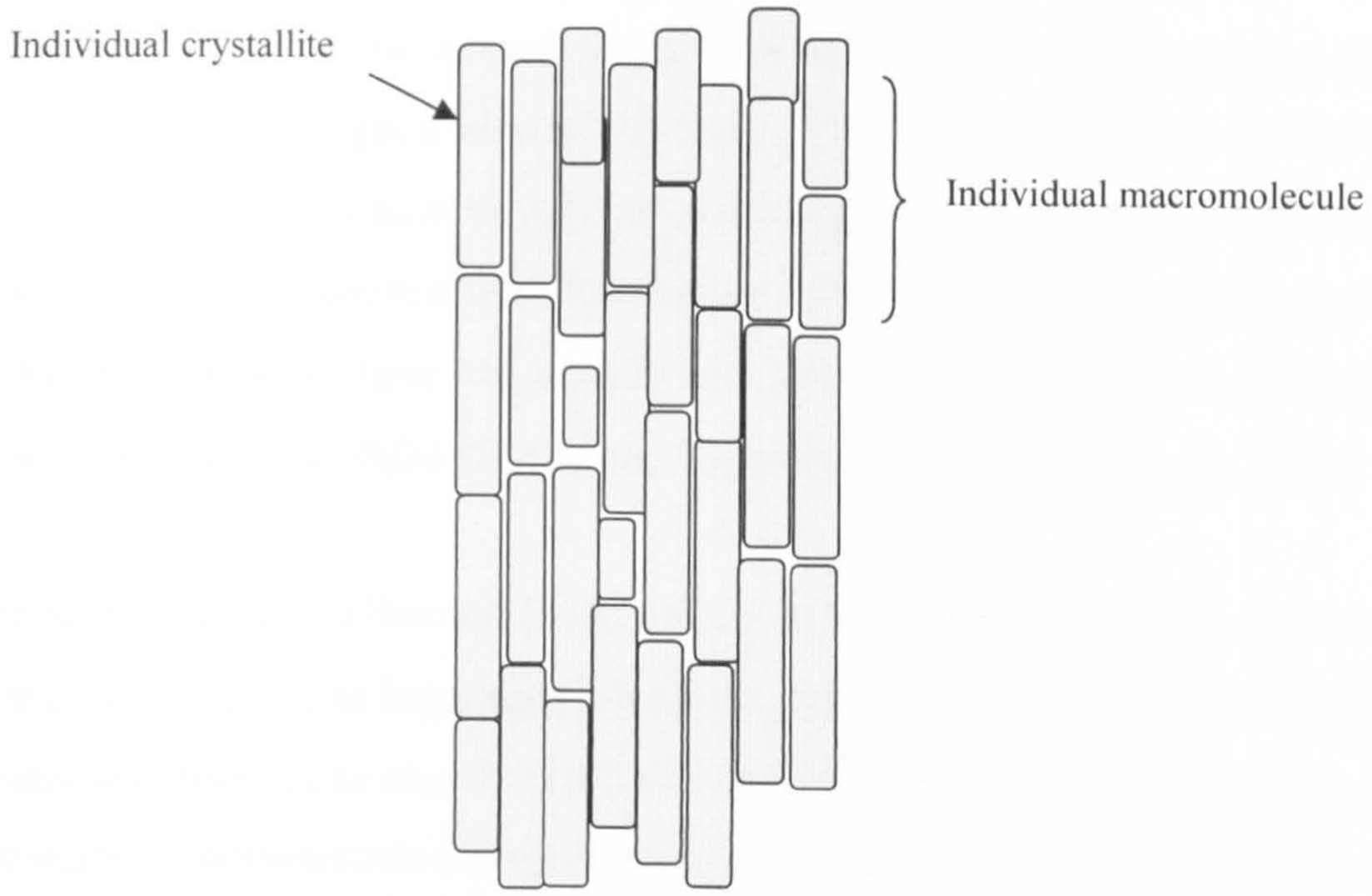

Figure 6.1 Schematic model of chain-end distribution in aramid fibre (Morgan et al, 1983)

6.3 Aramid Fibre Creep Behaviour

Figures 6.2 to 6.5 are the outcomes of the experimental tests at 25°C and 65°C in both linear and logarithmic scales. The curves were displaced because it was difficult to record the initial strain readings due to non-ideal loading conditions and instrument limitations.

As noticed from the figures, the aramid yarns showed a short 'primary' creep period of deformation following the application of the load. This lasted for less than 0.1 hours, after which the creep rate fell to a slow steady value during the 'secondary' creep period that lasted throughout most of the test until the rupture of the yarn's fibres. The figures also show that in some samples there was a slight increase in creep rate prior to failure. In others there was little or no indication of any increase in creep rate prior to failure.

It was argued by Lafitte and Bunsell (1985), Cook et al (1982), and Erickson (1985) that creep is generally linear with $\log_{10}$ time. However, from a comparison between the linear and logarithmic curves it can also be claimed that this relationship is also linear with time on a linear scale, as demonstrated in the figures mentioned above and as will be explained in the following discussions.

With the present limited result it is rather very difficult to reach a definite conclusion on which form (the logarithmic or the linear) is best for describing the relation between strain and time. More data collected over longer periods and a wider range of stresses should assist in reaching such conclusion.

It should also be noted that the total creep failure strain observed in these creep tests is less than that reported in the literature and by the fibre manufacturers under simple tensile tests for some stress levels. This is true for both the 25°C and 65°C tests.

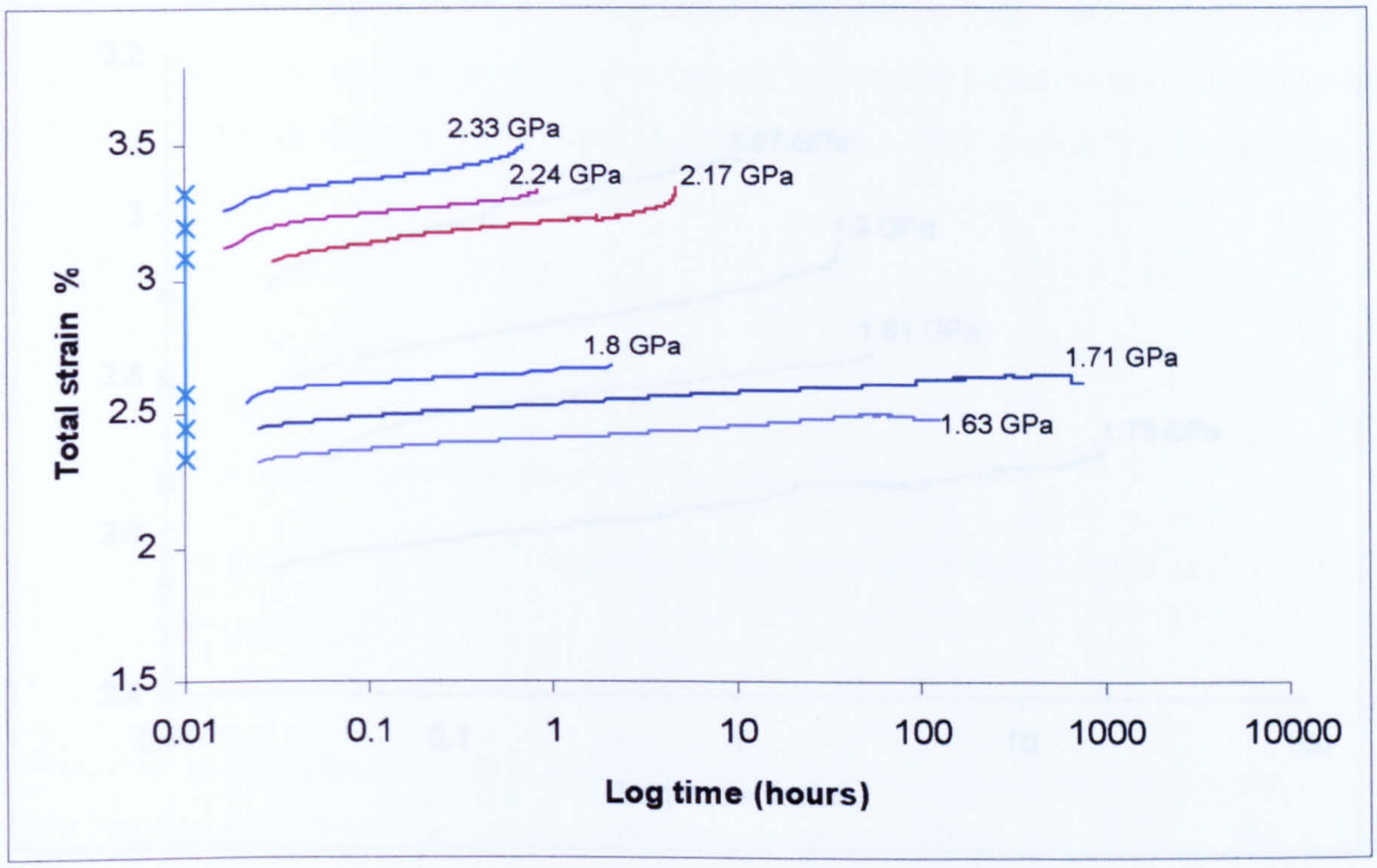

Figure 6.2 Total stain vs. $\log_{10}$ time at different stress levels and 25°C

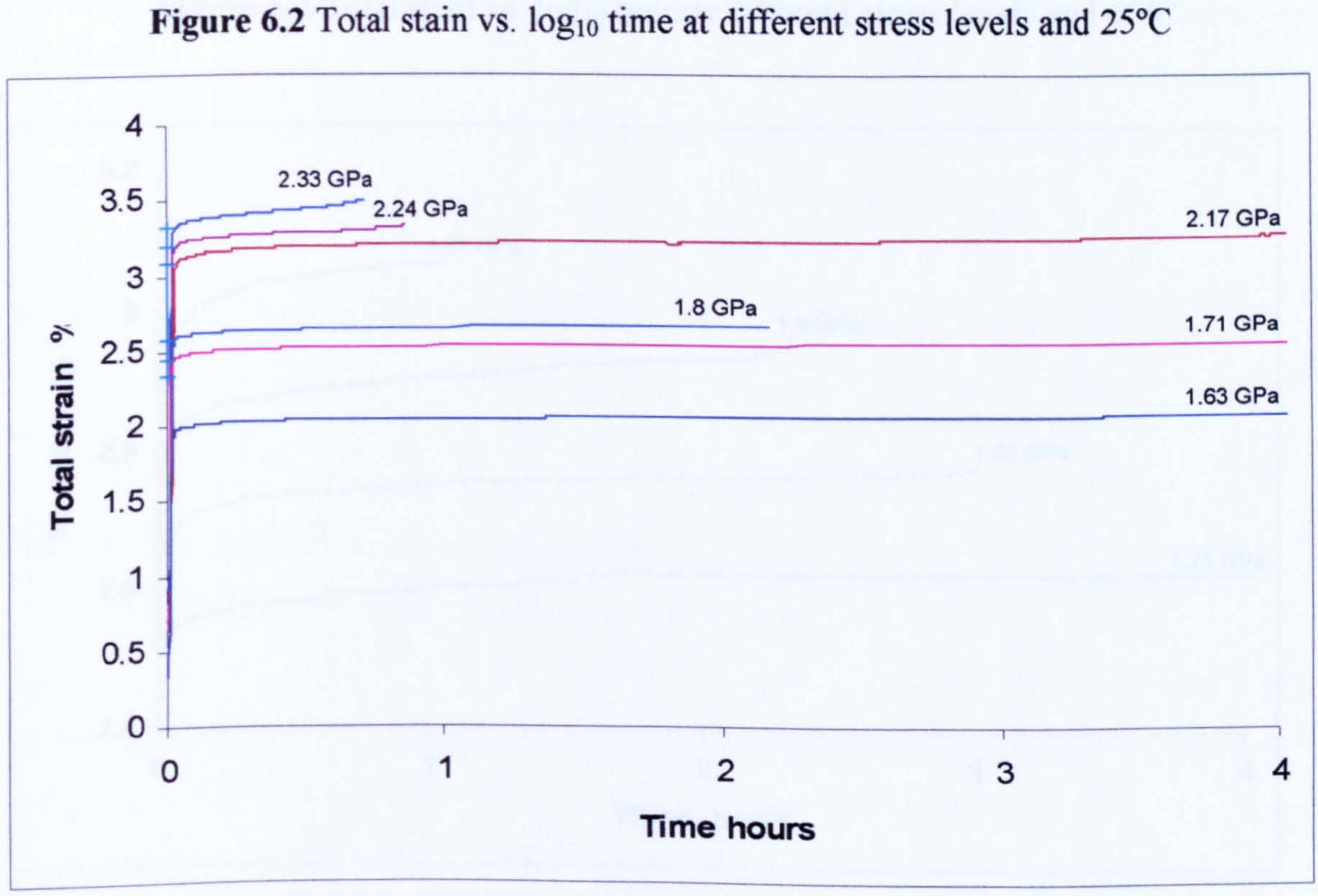

Figure 6.3 Total stain vs. time at different stress levels and 25°C

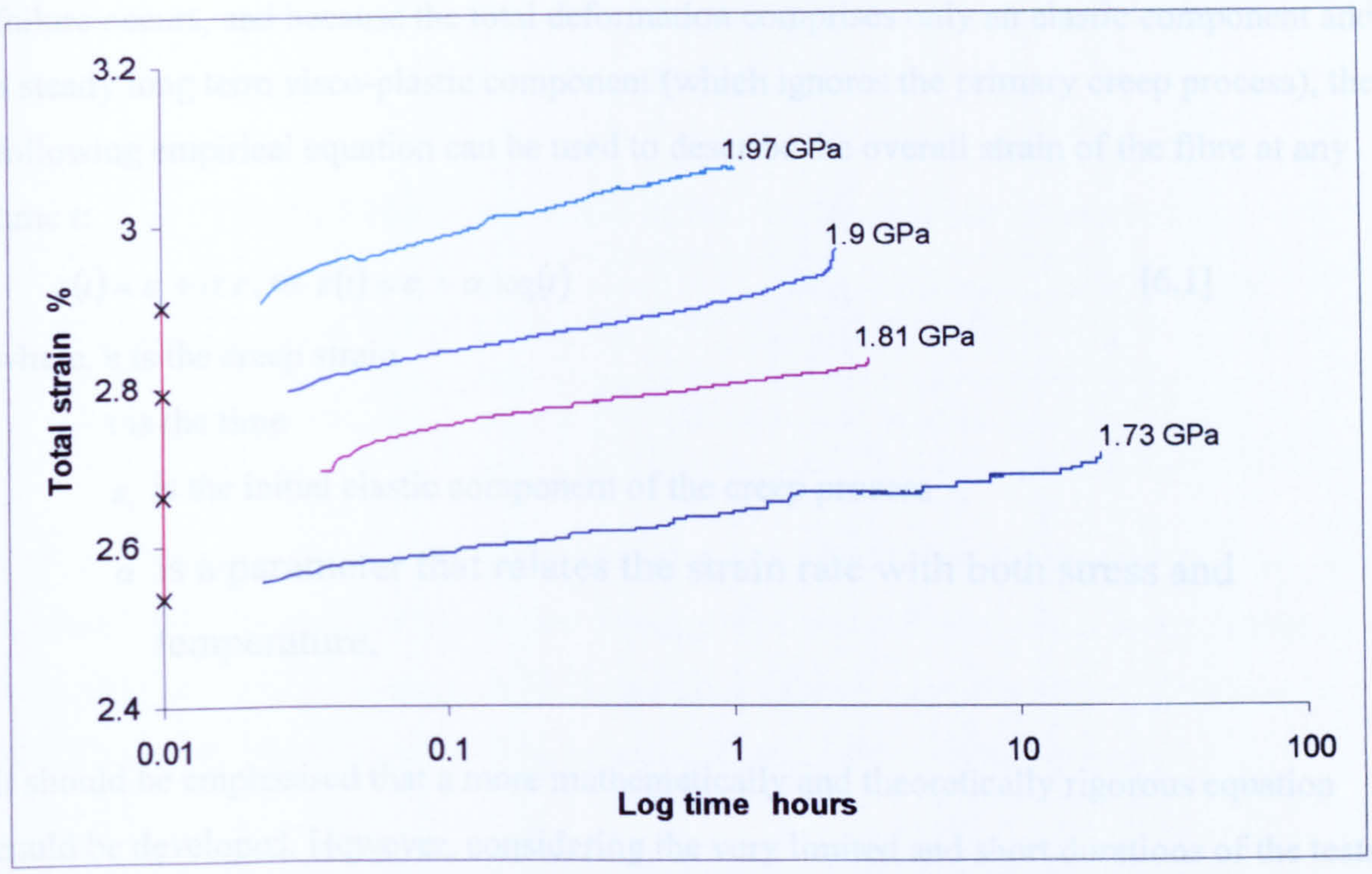

Figure 6.4 Total stain vs. $\log_{10}$ time at different stress levels and 65°C

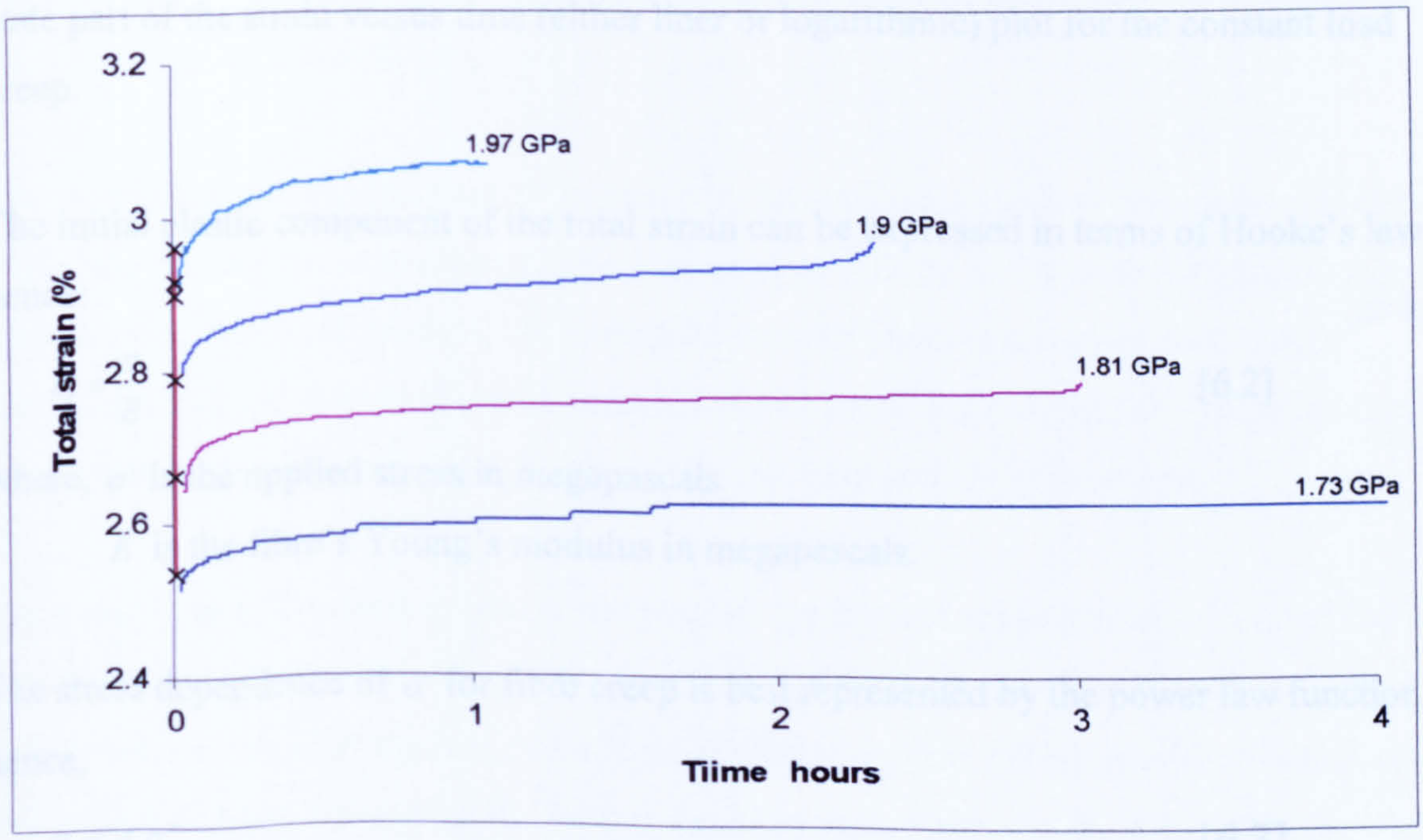

Figure 6.5 Total stain vs. time at different stress levels and 65°C

Long-Term Behaviour of Aramid Fibre

Considering the linear trend of strain with both time and $\log_{10}$ time which continues until failure occurs, and because the total deformation comprises only an elastic component and a steady long term visco-plastic component (which ignores the primary creep process), the following empirical equation can be used to describe the overall strain of the fibre at any time *t*:

$$\varepsilon(t) = \varepsilon_i + \alpha\, t \text{, or } \varepsilon(t) = \varepsilon_i + \alpha \log(t) \qquad [6.1]$$

where, ε is the creep strain

t is the time

ε_i is the initial elastic component of the creep process

α is a parameter that relates the strain rate with both stress and temperature.

It should be emphasised that a more mathematically and theoretically rigorous equation could be developed. However, considering the very limited and short durations of the tests conducted here, it is believed that the accuracy of the empirical equation [6.1] is sufficient, and that it is particularly convenient to use since the creep rate is the slope of the steady-state part of the strain versus time (either liner or logarithmic) plot for the constant load creep.

The initial elastic component of the total strain can be expressed in terms of Hooke's law, hence:

$$\varepsilon_i = \frac{\sigma}{E} \qquad [6.2]$$

where, σ is the applied stress in megapascals

E is the fibre's Young's modulus in megapascals.

The stress dependence of α for fibre creep is best represented by the power law function, hence,

$$\alpha = A\,\sigma^n \qquad [6.3]$$

Long-Term Behaviour of Aramid Fibre

The values of the parameters A and n are listed in Table 6.1 for the 25°C and 65°C tests from both the logarithmic and the linear representations. These numerical values correspond to stresses expressed in GPa and times in hours.

Table 6.1 Numerical values of the fibre's strain rate parameters

Linear Scale Values				***Logarithmic Scale Values***		
Temperature (°C)	**A**	**n**		**Temperature (°C)**	**A**	**n**
25	$10^{-7.05}$	17.1		25	$10^{-2.24}$	2.21
65	$10^{-7.82}$	22.4		65	$10^{-2.92}$	4.99

Figures 6.6 and 6.7 are comparison of the logarithmic and linear strain predictions as per equation [6.1] extrapolated to hundred thousand hours at different stress levels. Values of the constants A and n, in equation [6.3], are from Table 6.1 and the Material's Young's Modulus equals 73 GPa and 68 GPa for the 25°C and 65°C tests respectively.

The figures confirm the observation that the creep behaviour can be described using either the logarithmic or linear relationship especially for the tests conducted at 65°C. The only difference between the two descriptions is towards the end of the sample's life where there has been some uncertainty.

The very small and limited gradual increase in the strain rate suggests that some internal molecular movement or readjustment is taking place similar to the annealing process in metals. After this readjustment, the molecular structure becomes locked and further movement under the applied load is almost inhibited, and the progressive failure from the local weakness in the individual fibres reaches its limit and fracture occurs.

The exact time to failure does not correspond to the applied stress levels, which reflects the scatter of strength data for these fibres found earlier. Nevertheless, there has been a clear correlation between the applied stress, time to failure and the failure strain as demonstrated in Figure 6.8. Also, notice that the failure strain increases with the increase in the applied stress level.

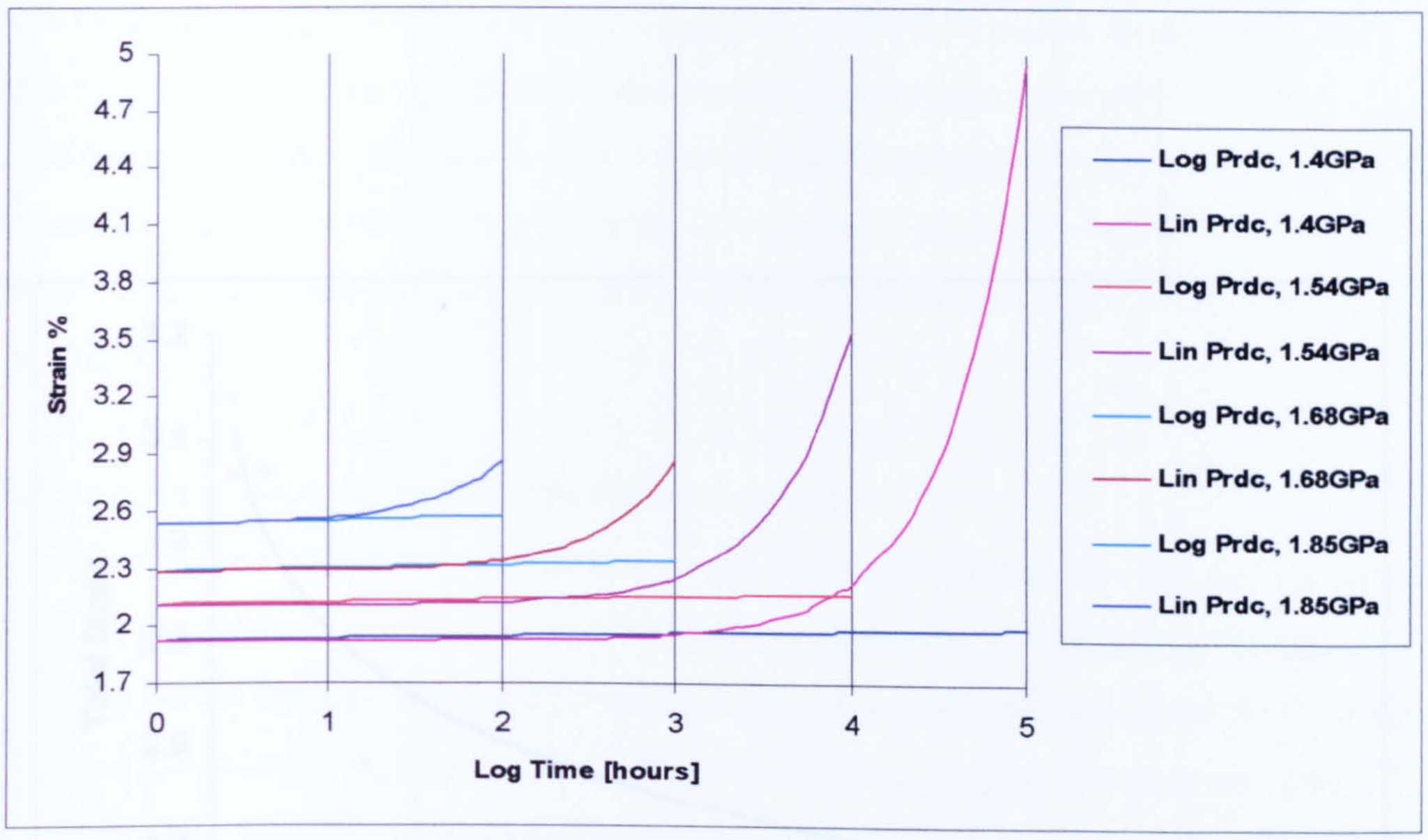

Figure 6.6 Total stain predictions vs. $\log_{10}$ time at different stress levels and 25°C

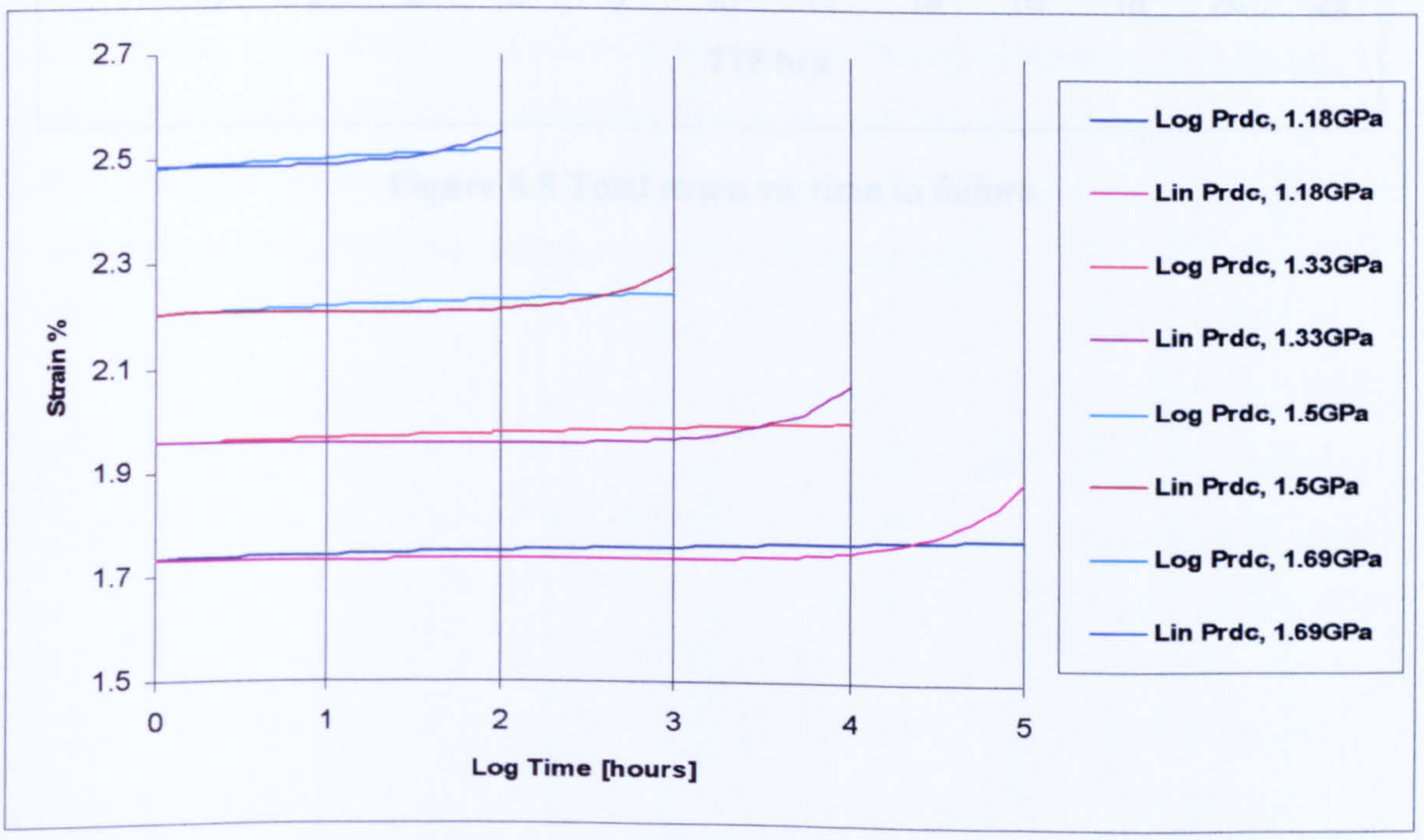

Figure 6.7 Total stain predictions vs. $\log_{10}$ time at different stress levels and 65°C

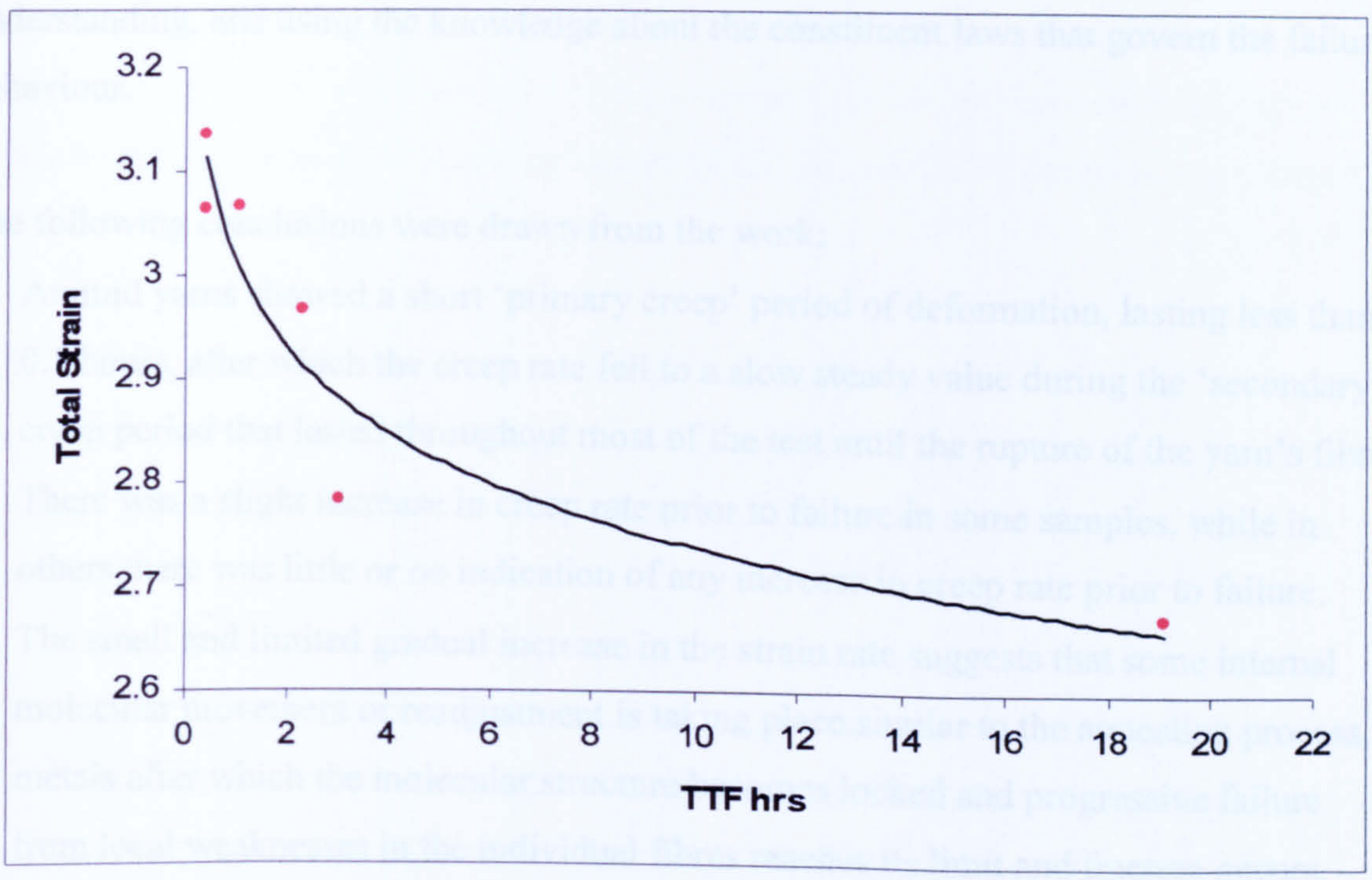

Figure 6.8 Total strain vs. time to failure

6.4 Conclusion

Aramid fibres are unidirectional crystals containing imperfections corresponding to the ends of individual crystal sequences. When loaded, deformation involves sliding or plasticity around defect regions. A model was proposed for relating stress to time to failure and estimating the strain to failure based on the material's properties based on this understanding, and using the knowledge about the constituent laws that govern the failure behaviour.

The following conclusions were drawn from the work:

- Aramid yarns showed a short 'primary creep' period of deformation, lasting less than 0.1 hours, after which the creep rate fell to a slow steady value during the 'secondary' creep period that lasted throughout most of the test until the rupture of the yarn's fibres.
- There was a slight increase in creep rate prior to failure in some samples, while in others there was little or no indication of any increase in creep rate prior to failure.
- The small and limited gradual increase in the strain rate suggests that some internal molecular movement or readjustment is taking place similar to the annealing process in metals after which the molecular structure becomes locked and progressive failure from local weaknesses in the individual fibres reaches its limit and fracture occurs.
- Both the logarithmic and linear representation of the relationship between creep strain and time well described the behaviour within the sample life.

Chapter 7 Aramid Fibre Failure Mechanism (Structural Behaviour)

7.1 Introduction

Following the explanation of physical structure in Chapter 6; it was also thought that a microstructural analysis of fibre failure was necessary for a better understanding of its behaviour and durability. A Scanning Electron Microscope (SEM) analysis was utilized to assist with the microstructural investigation.

7.2 SEM Characterization to Assess the Failure Modes

The appearance of aramid fibre under SEM was generally a uniform smooth cylindrical profile (Figure 7.1), with minor surface roughness and variations in diameter along the same fibre.

Figure 7.2 shows different degrees of magnification at the fractured end of a tested aramid fibre. In the first two SEM photographs, the splitting and fibrillating morphology are clear. The other three high magnification SEM photographs show some striation marks in a parallel direction to the fibre's axis. These striation marks are believed to be the result of the suggested plastic flow or movement within the crystallites in a direction parallel to the chain direction, as was suggested in the physical failure model.

The fibres tend to split and fibrillate upon failure under tensile loading, making the splitting and fibrillating the major characteristics of fracture morphology observed in the SEM analysis of the failed samples. The fibrillar bundle projects from the surface of the fractured fibre into several directions; hence it can not be related to the direction of extrusion or winding on the package. It is believed that tensile failure initiates at fibril ends and propagate via shear failure between the fibrils (Pigliacampi, 1995). It is worth re-emphasising that the fibres, in fact, consist of hundreds of filaments that are made of many identical fibrils as described in the aramid fibre manufacturing process in chapter 2.

Long-Term Behaviour of Aramid Fibre

Figures 7.3 and 7.4 compare failed samples that indicate splitting and fibrillating with some cut fibres that demonstrate sharp edge ends.

The splitting and fibrillating phenomenon could be attributed to one or a combination of the following causes:

- The high drawn ratio employed in the manufacturing of these fibres probably caused low radial strength. This weak radial bonding may then account for some of the surface layers becoming detached, resulting in a large amount of surface swarf which can be seen on the fibre. Fracture of the fibre under stress could be initiated by these splits. After the initiation a split would easily develop in a longitudinal direction because of the low radial strength, and failure would occur when the load bearing cross-sectional area is sufficiently reduced so as to cause failure under the maximum applied load.
- Internal cracks and defects in the fibre during the manufacturing process. It is assumed that cracks initiate at these defects or as a result of the breakage of hydrogen bonds in the transverse direction. Cracks propagate along the fibre's axis leading to delamination and further crack propagation until failure.
- The highly anisotropic structure of the fibre with a low transverse strength.

Figure 7.5 is a two dimensional schematic illustration of the crack initiation and propagation process. Assuming crack initiation is due to one of the reasons mentioned above, the crack progresses parallel to the fibre direction (longitudinal) as more H-bonds are ruptured, while it propagates in a traversal direction following the chain end concentration regions.

It is worth mentioning that the presence of moisture worsens the situation because it disrupts the hydrogen bonding between the fibrils, making it easer to initiate and propagate longitudinal splitting. Also, the distribution and aggregation of impurities such as Na_2SO_4 throughout the fibre will affect the packing of the macromolecules in the transverse fibre direction and hence enhance the fibrillation process.

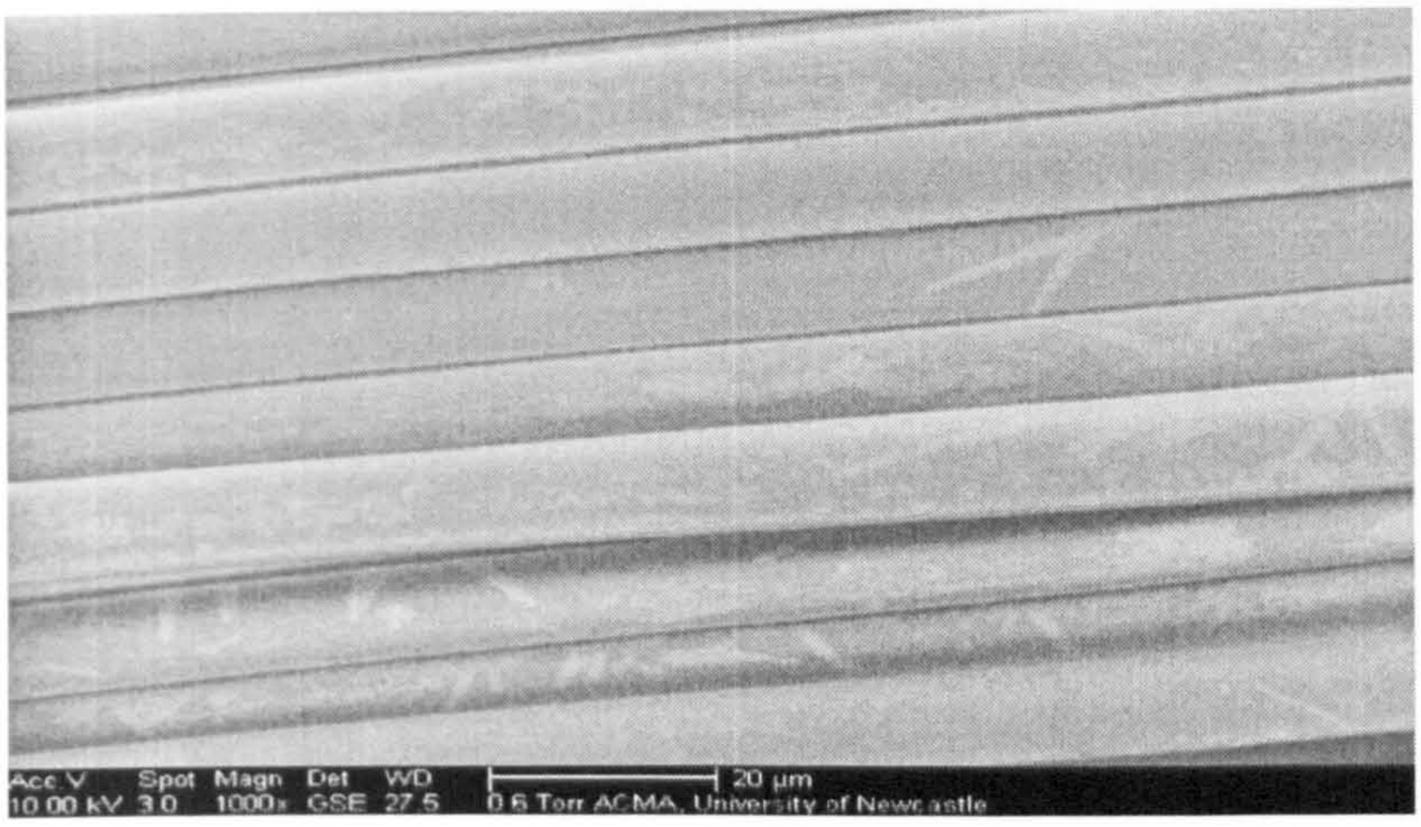

(a) 1000X

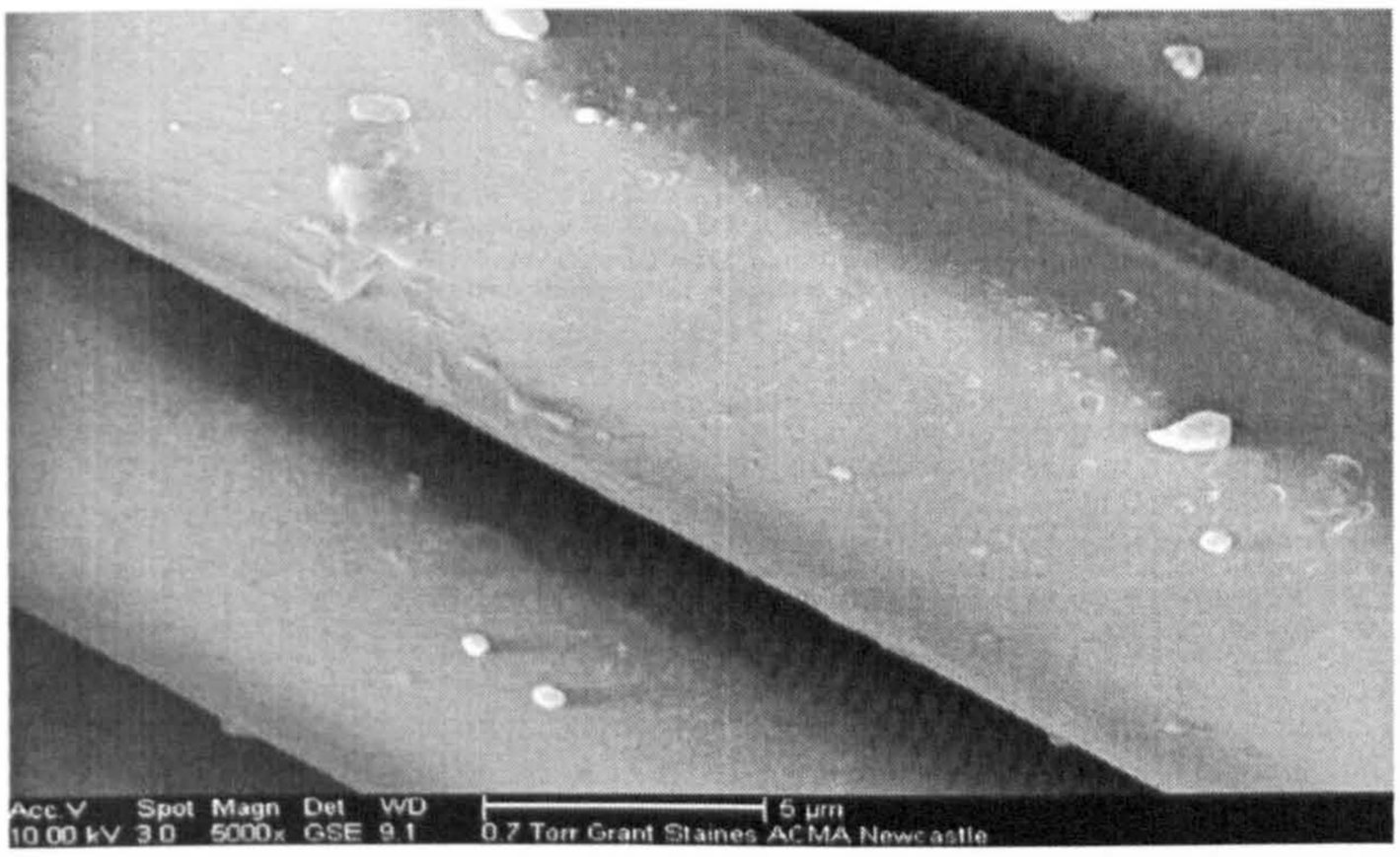

(b) 5000X

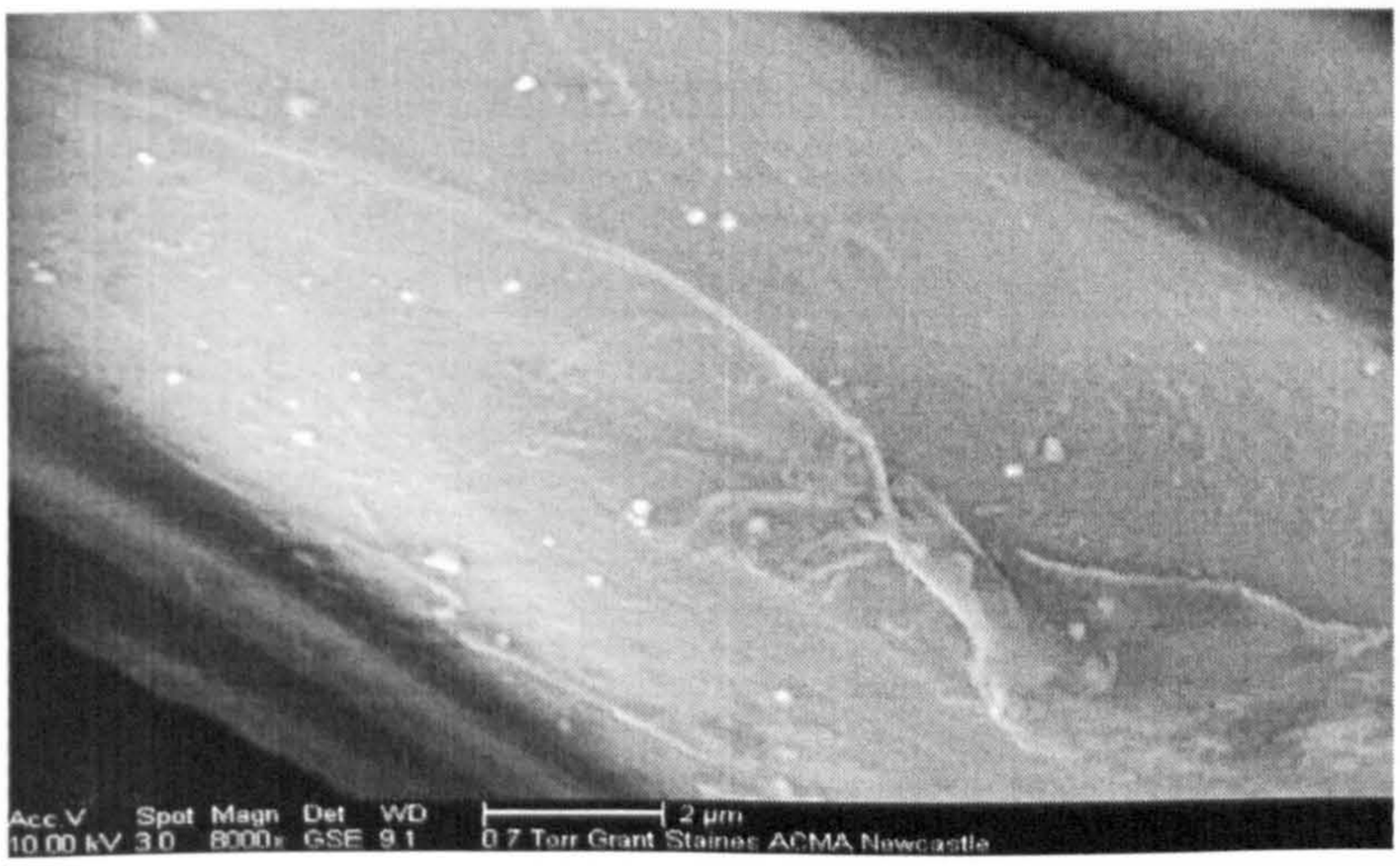

(c) 8000X

Figure 7.1 SEM photographs of aramid fibres under different magnifications

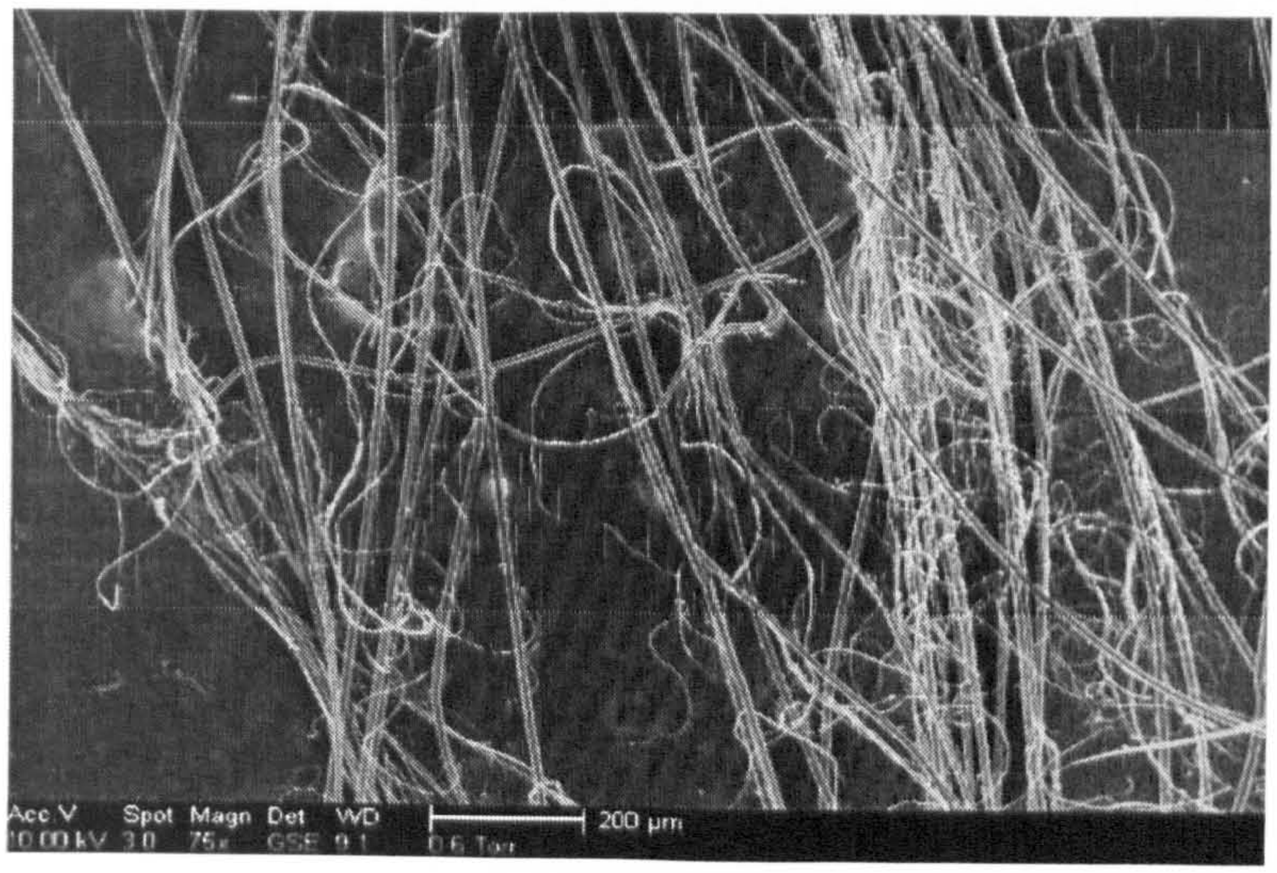

(a) Fibrillating at fractured end, X75

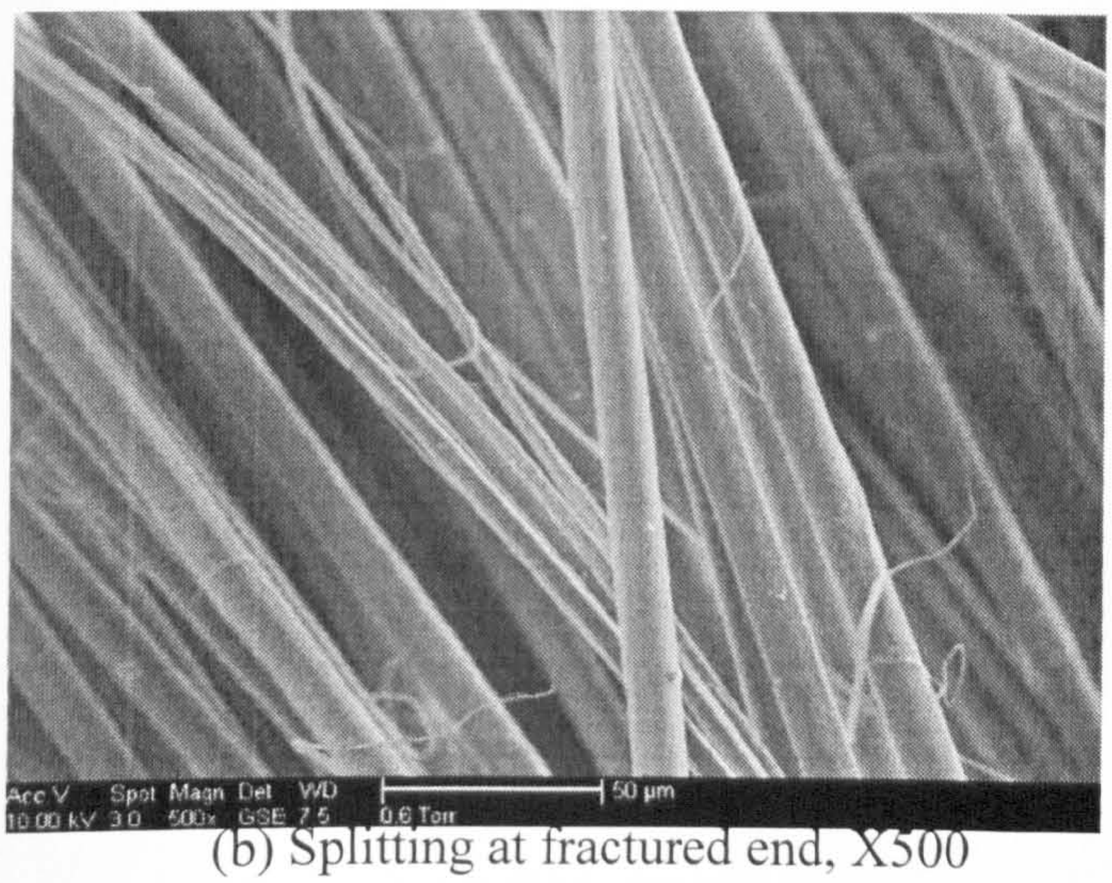

(b) Splitting at fractured end, X500

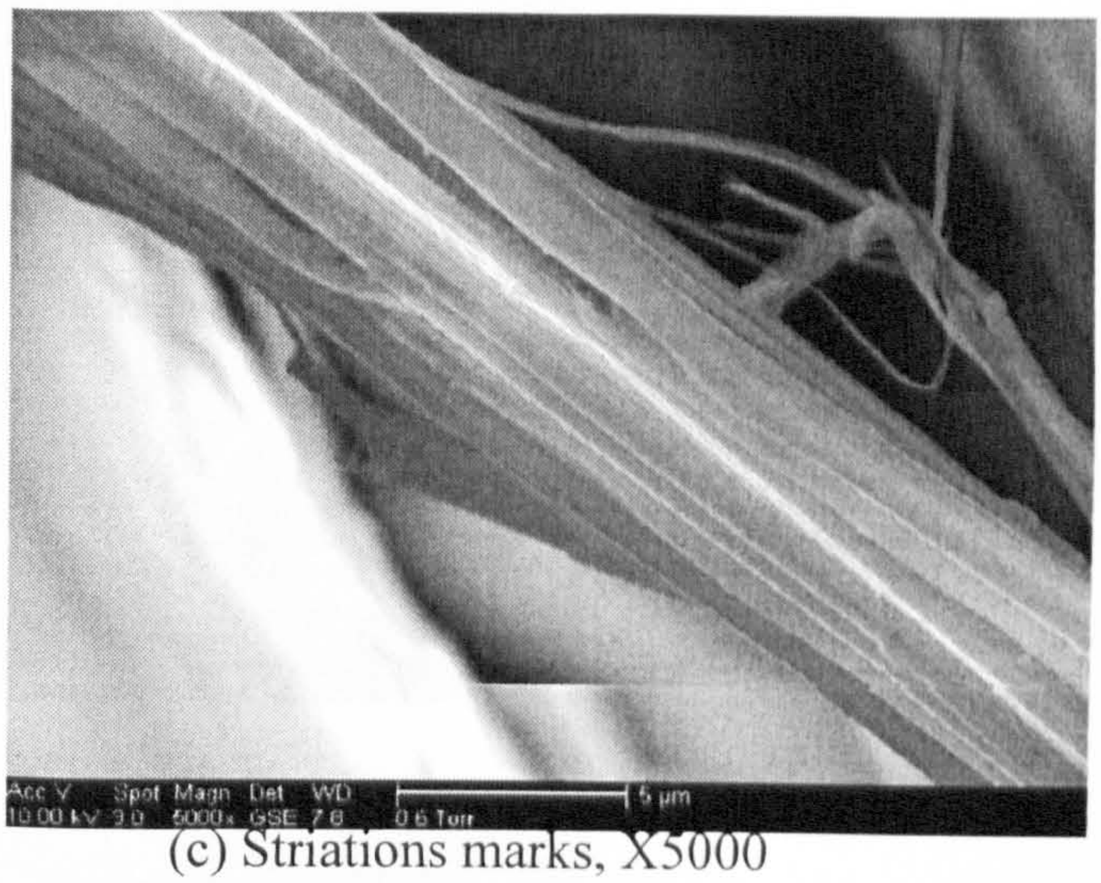

(c) Striations marks, X5000

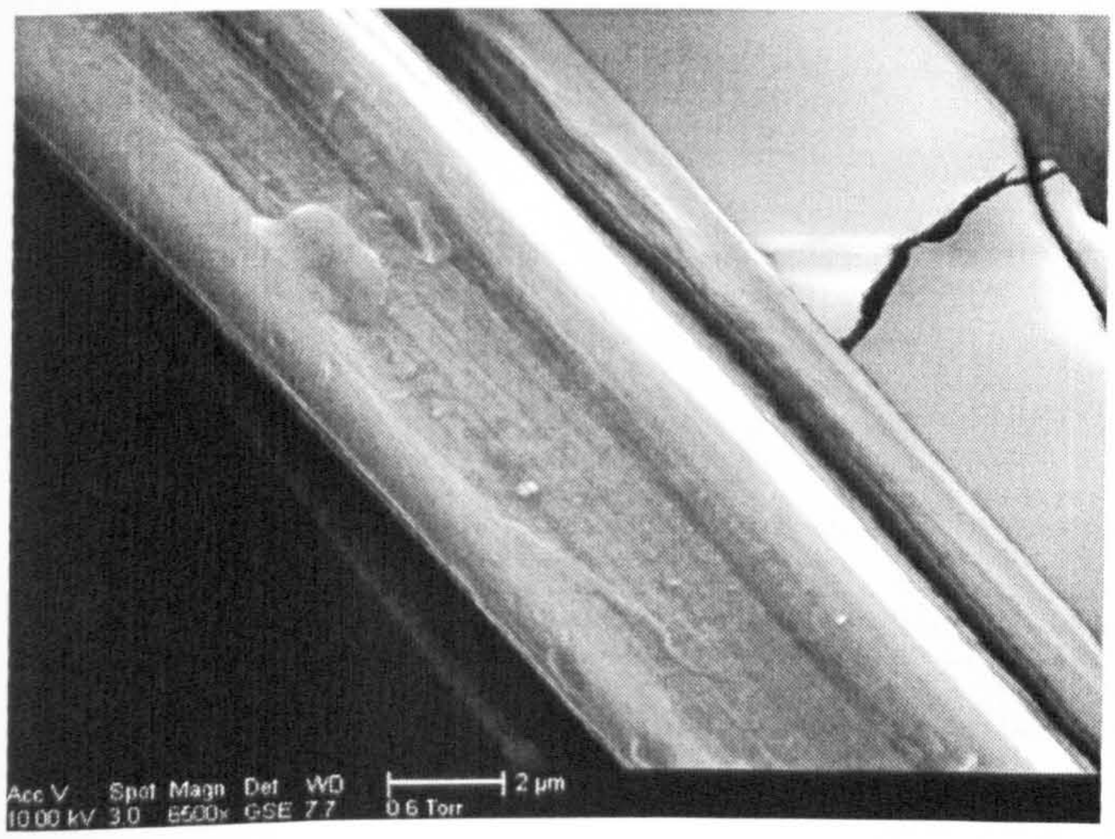

(d) Striations marks, X6500

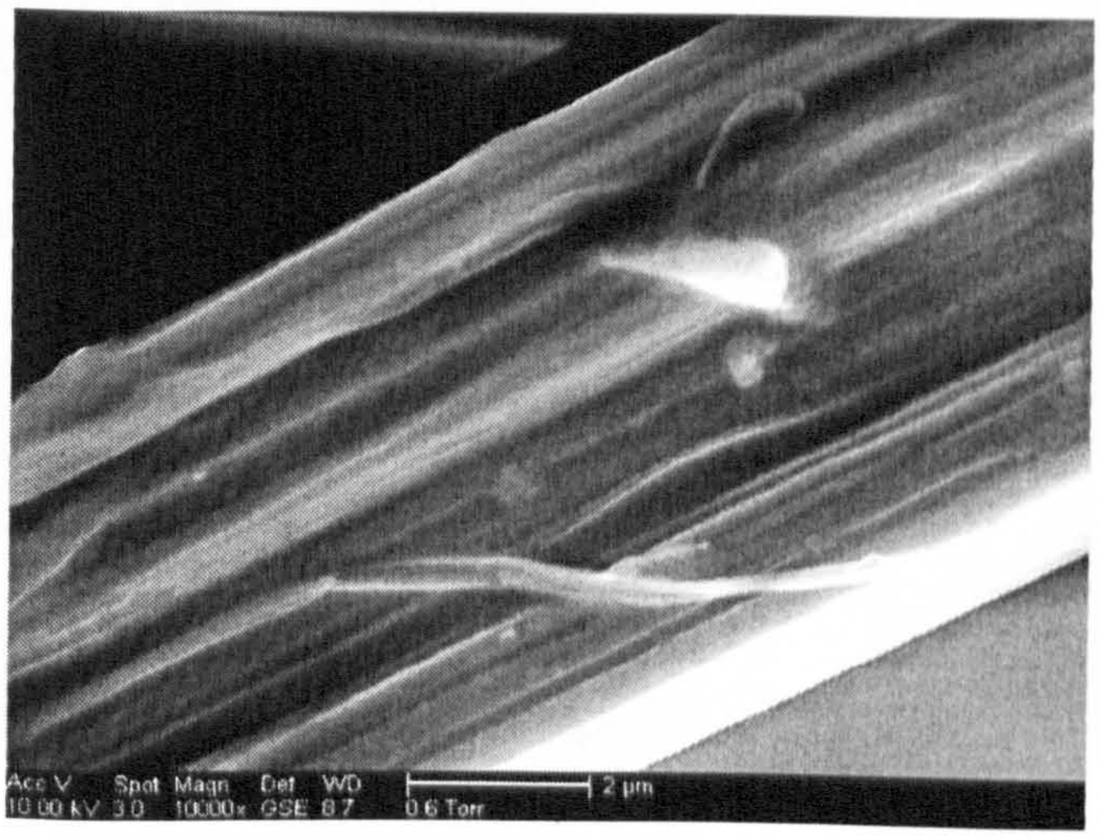

(e) Striations marks, X10000

Figure 7.2 SEM photographs of the fractured end of a fibre under different magnifications

(a) 250X

(b) 500X

(c) 230X

Figure 7.3 Splitting and fibrillating of failed fibres under SEM

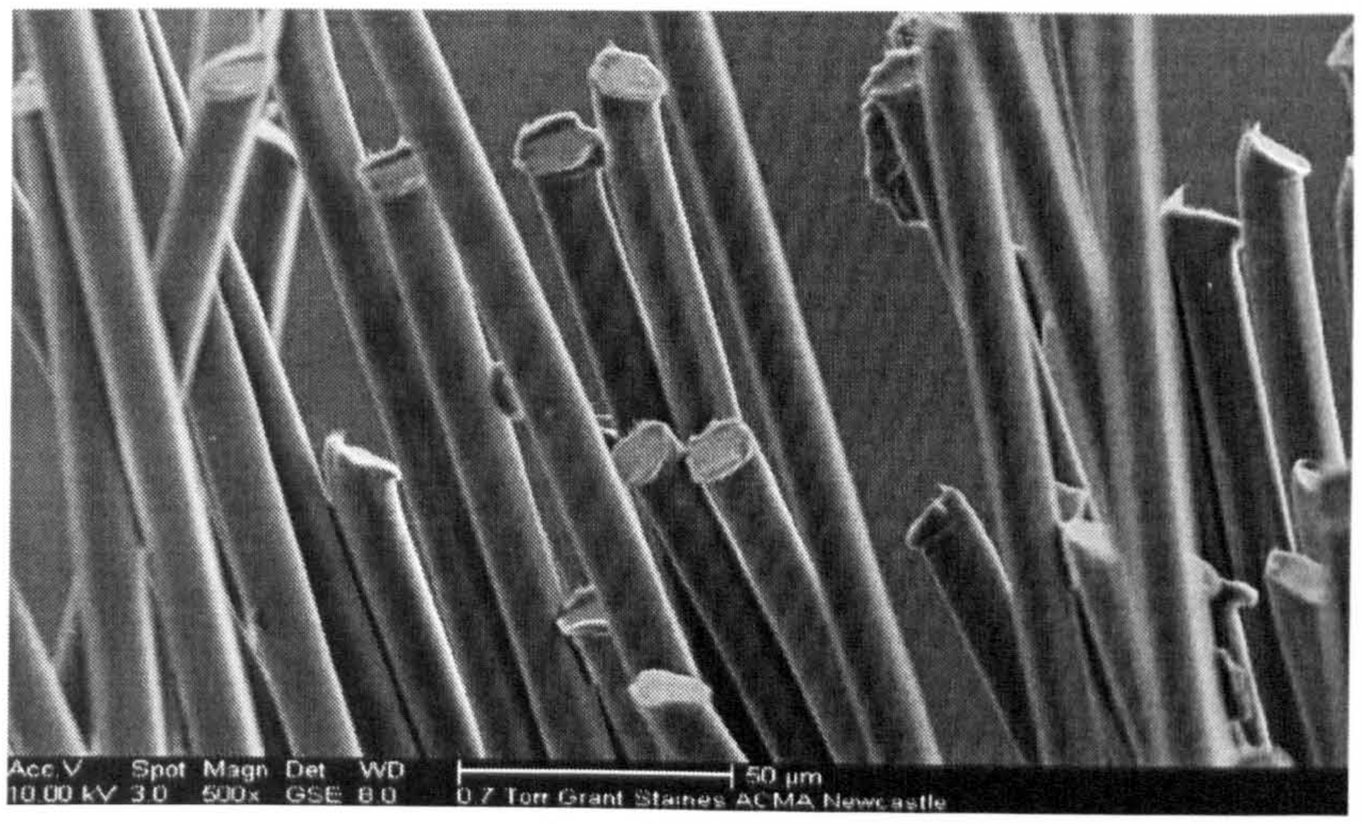

(a) 500X

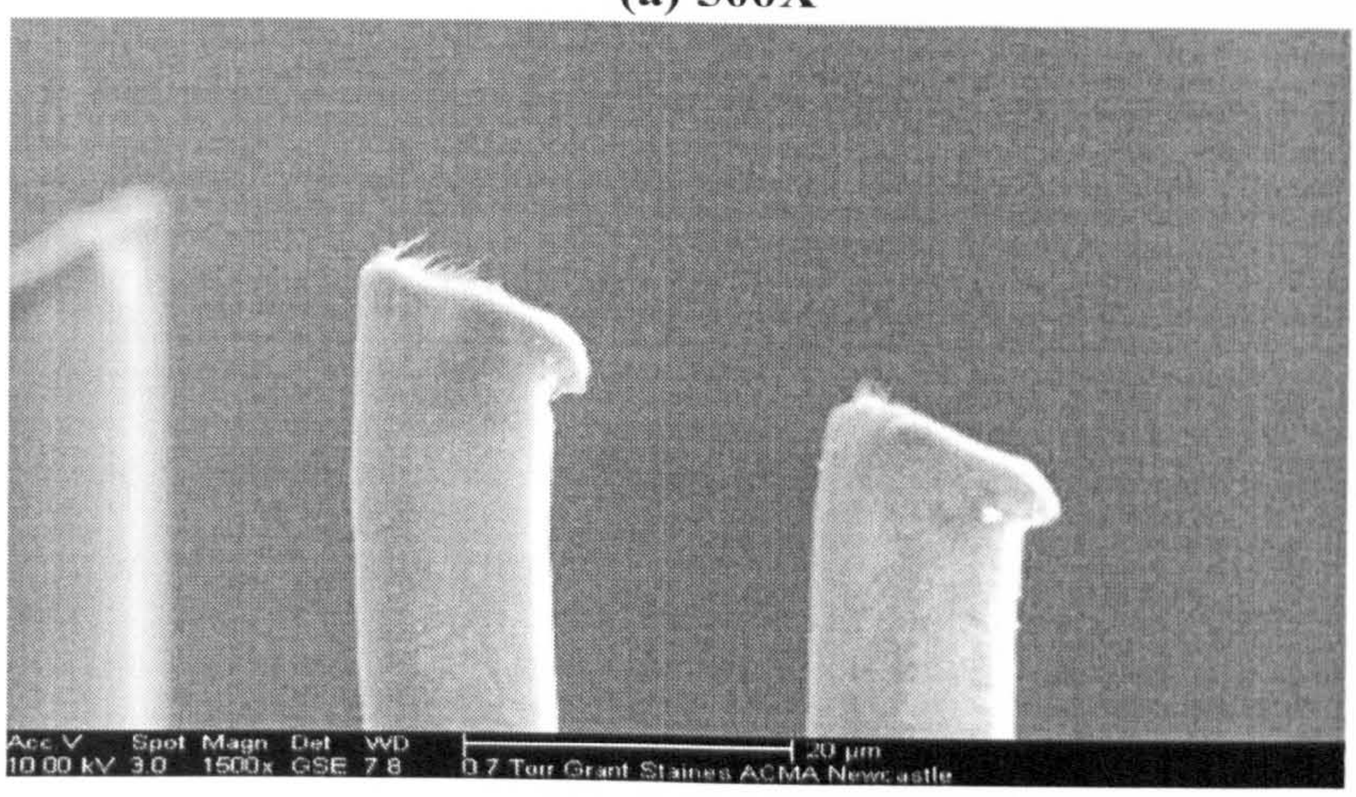

(b) 1500X

Figure 7.4 SEM photographs of cut fibre ends

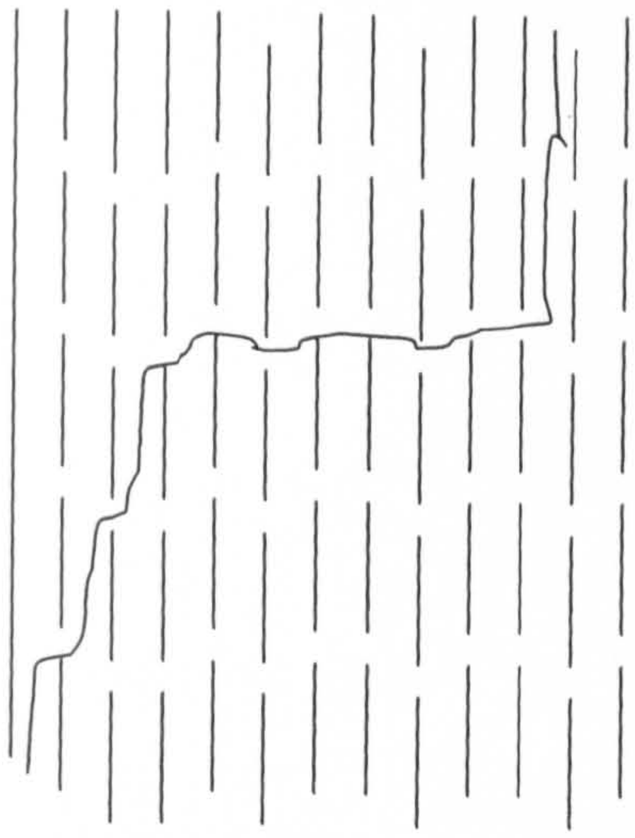

Figure 7.5 Schematic of the crack propagation path

7.3 Conclusions from SEM characterization

The splitting and fibrillating was the major characteristics of fracture morphology observed in the SEM analysis of the failed samples. This attributed to the low radial strength caused by the high drawing ratio employed in the manufacturing and/or internal cracks and defects in the fibre during the manufacturing process.

The following conclusions can be drawn from the SEM characterization conducted on the aramid fibres tested:

- Splitting and fibrillating are the major observed characteristics of the fractured aramid fibres.
- High manufacturing drawing ratios, internal cracks and defects in fibres, and/or the high anisotropic fibre structure are the main likely root causes for the splitting and fibrillating observed on the failed fibres.
- The physical failure model, which suggests that crystallites plastic flow in a direction parallel to the fibre's axis, is supported by the observed striation marks in the high SEM magnification photographs.

Chapter 8 Final Discussion and Conclusions

8.1 Final Discussion and Further Work

8.1.1 Stress Rupture Tests

An investigation of the creep rupture of Kevlar® 29 and Twaron® 1000 aramid fibre yarns was carried out in four different temperatures, namely 25°C, 65°C, 95°C, and 120°C in air and three other environments at 65°C (Saudi/Iranian crude oil, pure water, and low pH water) with the objective of characterising the long term failure behaviour of these fibres.

Three different predictive methods were used to model and interpret the results of the tests. These methods are: the standard $\log_{10}$-$\log_{10}$ ISO 9080 extrapolation procedure, the modified lin-$\log_{10}$ ISO 9080 extrapolation procedure, and the time temperature superposition method.

When tested in air, the different yarns produced values of the regression line slope, *G*, near to those values measured by the manufacturers of RTP pipes. This supports the idea of utilizing stress rupture tests conducted on the fibre yarns in the prediction of RTP behaviour, and hence reducing the need for the expensive long term tests on pipe samples. Additionally, the different yarns showed only small differences in results, confirming that they are effectively interchangeable.

There was some scatter in data compared to that noticed when testing RTP pipes. This is believed to be caused by statistical variations in strength along the fibres, and the fact that when a pipe is tested the behaviour of several hundred yarns is effectively averaged, which greatly reduces the scatter.

The results of the standard $\log_{10}$-$\log_{10}$ ISO 9080 and the modified lin-$\log_{10}$ methods correlated well. The standard $\log_{10}$-$\log_{10}$ form, however, gave slightly higher values for the

20 year mean stress and LPL. Its use is recommended because it is consistent with the model assumed in the regression of RTP.
There was no evidence of any 'knee' in the relationships after long periods or at high temperatures. This suggests that there is no change in failure mechanism, and lends confidence to both the long term use of aramid fibre in air and the recommended qualification procedures.

Crude oil immersion produced a small but significant reduction in performance as a result of plasticization effects. At 65°C a suitable crude oil reduction factor applied to the long term LPL would be 0.9. Pure water produced a marked reduction in strength after short periods at 65°C. Finally, water of low pH resulted in a large reduction in performance and considerable scatter with one fibre type. With the other, the effect appeared to be similar to that of pure water. Difference between the two fibres in the low pH water effect is attributed to either differences in the intensity of local regions of acid attack or differences in the chain end (or termination) chemical groups.

Further Work

Further work on the regression behaviour of aramid fibre both in air and other environments could address the following areas:

- The use of different interpretation methods such as Miner's Law and comparison of the results with those obtained using the methods in this thesis.
- An investigation into the mechanism of environmental degradation occurring in the fibres in the crude oil and water environments; in particular, studying the reversible hydrolysis effect
- Statistical study, using Weibull analysis, of the data scatter with the aim of developing a relationship between such scatter and the fibre's structural variability.
- Careful stress rupture analysis on single fibres rather than yarns in similar environments to those used in this study. This will provide an insight into the fibre's performance in the absence of twisting effect.
- Using the data generated in the verification of some of the predictive models.

8.1.2 Aramid Fibre Creep Behaviour and Failure Model

One of the structural views of aramid fibres is that they are unidirectional crystals containing imperfections corresponding to the ends of individual crystal sequences. While loaded, deformation involves sliding or plasticity around the defect region. Based on this understanding, and using the knowledge about the constituent laws that govern the failure behaviour, a model is proposed for relating stress to time to failure and estimating the strain to failure based on the material's properties.

Further Work

Further work on aramid fibre creep behaviour could include:

- Improving the failure model by taking into account the effects of molecular weight distribution, yarn twist and the length dependence of the strength of individual yarns.
- Comparing the different failure mode models with recommendations based on matching experimental results with the predictive models.
- Conducting creep tests for longer periods at different temperatures, and especially at the most useful design temperature of 65°C.
- Conducting creep tests in different environments similar to those where the fibres are expected to used.
- Developing a method that will eliminate the equipment limitations encountered here in capturing the exact profile of the initial creep curves.

8.1.3 SEM Failure Analysis

Splitting and fibrillating were the major characteristics of fracture morphology observed in the SEM analysis of the failed samples. The cause of such morphology is thought to be due to the low radial strength caused by the high drawing ratio employed in the manufacturing process and/or internal cracks and defects in the fibre.

Further Work

Further work on the SEM characterization of aramid fibres could include:

- Conducting SEM analysis to investigate the fractography of field samples from different environmental tests.

- Investigating the differences, if any, in the fractography of samples with different times to failure.

8.2 Final Conclusions

The objective of this work was to answer questions on the usability of long term stress rupture tests on aramid fibres as an alternative for the expensive tests usually conducted on RTP for qualification purposes. From the work presented in this thesis, it can be concluded that future qualification procedures could avoid the 10,000 hour regression test, replacing it with tests on the reinforcement fibres or a test for conformity of the regression line slope. The following are the main conclusions drawn from this study:

8.2.1 Air Stress Rupture Tests

- All three prediction methods gave similar predictions for the 20 year mean stress and the 20 year LPL stress.
- Due to the scatter in properties among individual fibre samples it was necessary to conduct a large number of tests in order to reduce the scatter effect under each test condition. This scatter is thought to be due to the fact that along the length of a fibre there is statistical variation in strength due to the distribution of flaws or weak points in its morphology.
- The $\log_{10}$-$\log_{10}$ plots, by their shape, give a more optimistic prediction of the long term behaviour of aramid fibres than the lin-$\log_{10}$ plots.
- The values of the regression line slope, *G*, for both fibres were near to the values measured by the manufacturers of RTP pipe. This is interesting, as it had been anticipated that the regression line slopes for the yarns by themselves might be a little flatter. This supports the idea of utilizing stress rupture tests conducted on the fibre yarns in the prediction of RTP behaviour, and hence reduces the need for expensive long term tests on pipe samples needed for qualification
- Considerable tensile strength reductions were observed over long testing periods at different temperatures.
- The tests results showed only small differences between the yarn types when tested in air, confirming that the products are, for most purposes, effectively interchangeable.

- The results suggest that there is unlikely to be a change in failure mechanism after long periods, which lends confidence to the use of aramid fibre in highly loaded long term tensile applications.
- Regardless of the loss of strength encountered as a result of long-term loading, aramid fibre performance is sufficiently high so that they can be used in many applications where high strength is required.

8.2.2 Environmental Stress Rupture Tests

- It is evident that exposure to crude oil and water resulted in a form of failure mechanism different from that in exposure to air.
- A crude oil immersion factor was calculated for each crude oil experimental point by dividing the failure stress in crude oil by the failure stress in air at the same time to failure, as predicted by the ISO 9080 model. The average values taken for all the experimental points were 0.93 and 0.91 for Kevlar and Twaron respectively.
- Due to the decay in stress as a result of exposure to crude oil and water compared to air, it is believed that different failure mechanisms are taking place as a result of changing the test environment, which therefore means that the principles of superposition no longer applies in the case of these environmental tests.
- Water immersion resulted in plasticization and chain scission in the form of hydrolysis.
- No significant difference between the effect of pure water and low pH water was noticed in the case of the fibres. It is believed that deterioration in strength when exposed to these environments is dominated by hydrolysis, and that the low pH has very little influence.
- The difference between the two fibres in the effect of low pH water is attributed to either differences in intensity of the local regions of acid attack or differences in the chain end (or termination) chemical group.
- Plasticization and chain scission in the form of hydrolysis are the forms of adverse environmental effect that have been produced as a result of immersion in both pure and low pH water.

8.2.3 Aramid Fibre Creep Behaviour and Failure Model

- Aramid yarns showed a short 'primary creep' period of deformation, lasting less than 0.1 hours, after which the creep rate fell to a slow steady value during the 'secondary' creep period that lasted throughout most of the test until the rupture of the yarn's fibres.
- There was a slight increase in creep rate prior to failure in some samples, while in others there was little or no indication of any increase in creep rate prior to failure.
- The small and limited gradual increase in the strain rate suggests that some internal molecular movement or readjustment is taking place similar to the annealing process in metals after which the molecular structure becomes locked and progressive failure from local weaknesses in the individual fibres reaches its limit and fracture occurs.
- Creep is generally linear with $\log_{10}$ time as well as with time on a linear scale.
- It has been thought that creep rate is independent of stress, but, as it has been demonstrated here, it seems that creep rate is in fact sensitive to applied stresses.

8.2.4 SEM Failure Analysis

- Splitting and fibrillating are the major observed characteristics of the fractured aramid fibres.
- High manufacturing drawing ratios, internal cracks and defects in fibres, and/or the high anisotropic fibre structure are the main likely root causes for the splitting and fibrillating observed in the failed fibres.
- The physical failure model which suggests that crystallites plastic flow in a direction parallel to the fibre's axis is supported by the striation marks observed in the high SEM magnification photographs.

References

1. Alwis, K. G. N. C. and Burgoyne, C. J.
Time-Temperature Superposition to determine the stress-rupture of aramid fibres;
Applied Composites Materials, Vol. 13, 2006, pp. 249 - 264.

2. Andersson, U.
Which factors control the lifetime of plastic pipes and how the lifetime can be extrapolated;
Plastics Pipes XI Conference, Munich Germany, 3rd – 6th September 2001, pp. 311 - 320.

3. Andrews, M. C., Lu, D. and Young, R. J.
Compressive properties of aramid fibres;
Polymer, Vol. 38 No. 10, 1997, pp. 2379 - 2388.

4. ASTM D2837-98a
Standard test method for obtaining hydrostatic design basis for thermoplastic pipe materials.

5. ASTM D2992-96
Standard practice for obtaining hydrostatic or pressure design basis for "Fibreglass" (Glass-Fibre-Reinforced Thermosetting-Resin) pipe and fittings;

6. Benham, P.P., Crawford, R.J., and Armstrong, C.G.
Mechanics of engineering materials;
2nd edition, 1996, Longman.

7. Bernstein, R., Derzon, D. K. and Gillen, K. T.
Kevlar degradation studies;
Polymer Preprints, Vol. 44, Section 2, 2003, p. 952.

8. Bernstein, R., Derzon, D. K. And Gillen, K. T.
Nylon degradation: Thermal-oxidation and oxygen consumption;
Polymer Preprints, Vol. 45, Section 1, 2004, pp. 976 - 977.

9. Bhuvanesh, Y. C. And Gupta, V. C.
Long-term predication of creep in textile fibres;
Polymer, Vol. 35, No. 10, 1994, pp. 2226 - 2228.

10. Billmeyer, F. W.,
Textbook of polymer science;
3rd edition, 1984, John Wiley & Sons.

11. Bourbigot, S. and Flambard, X.
Heat resistance and flammability of high performance fibres: A review;
Fire Materials, Vol. 26, 2002, pp. 155 - 168.

12. Brody, H.
Synthetic fibre materials;
1st edition, 1994, Longman Scientific & Technical.

13. Bunsell, A. R.
Fibre reinforcements for composite materials;
1st edition, 1988, Elsevier.

14. Bunsell, A. R.
The tensile and fatigue behaviour of Kevlar-49 (PRD-49) fibre;
Journal of Materials Science, Vol. 10, 1975, pp. 1300 - 1308.

15. Bunsell, A. R. and Hearle, W. S.
The fatigue of synthetic polymeric fibres;
Journal of Applied Polymer Science, Vol. 18, 1974, pp. 267 - 291.

16. Buschow, K. H. J.
Encyclopaedia of Materials: Science and Technology;
1st edition, 2001, Elsevier.

17. Cantrill, J. L.
Structural integrity of Reinforced Thermoplastic Pipes;
PhD Thesis, 2002, University of Newcastle upon Tyne.

18. Ciferri, A. and Ward, I. M.
Ultra-High Modulus Polymers;
1st edition, 1979, Applied Science Publishers.

19. Chapman, B.J., Evans, J. T., Frost, S. R. and Gibson, A. G.
The mechanical testing of continuous fibre reinforced thermoplastic pipes;
Proceeding of ICCM-11, Gold Coast, Australia, 1997.

20. Chailleux, E. and Davies, P.
Modelling the non-linear viscoelastic and viscoplastic behaviour of aramid fibre yarns;
Mechanics of Time Dependant Materials, Vol. 7, 2003, pp. 291-303.

21. Cook, J., Howard, A., Parratt, N. J., and Potter, K. D.
Creep and static fatigue of aromatic polyamide fibres;
Proceeding of the 3rd RISO International Symposium on Metallurgy and Materials Science, London, The UK, 1982.

22. Cox, H. L.
The elasticity and strength of paper and other fibrous materials;
British Journal of Applied Physics, Vol. 3, March 1952, pp. 72 - 79.

23. Deteresa, S. J., Allen, S. R., Farris, R. J. and Porter, R. S.
Compressive and torsional behaviour of Kevlar 49 fibre;
Journal of Materials Science, Vol. 19, 1984, pp. 57 - 72.

24. Dobb, M.G., Johnson, D.J., Majeed, A. and Saville, B.P.
Microvoids in aramid-type fibrous polymers;
Polymer, Vol. 20, 1979, pp. 1284 - 1288.

25. Dobb, M.G., Johnson, D.J. and Saville, B.P.
Direct observation of structure in high-modulus aromatic fibres;
Journal of Polymer Science: Polymer Symposium, Vol. 58, 1977, pp. 237 - 251.

26. Dobb, M.G. and Robson, R. M.
Structural characteristics of aramid fibre variants;
Journal of Materials Science, Vol. 25, 1990, pp. 459 - 464.

27. du Pont,
Properties and processing of du Pont Kevlar brand yarn for mechanical rubber goods;
du Pont, 2001.

28. Erickson, R.H.
Creep of aromatic polyamide fibres;
Polymer, Vol. 26, 1985, pp. 733 - 746.

29. Erickson, R.H.
Room temperature creep of Kevlar 49/epoxy composites;
Composites, July 1976, pp. 189 - 194.

30. Fallatah, G. M., Gibson, A. G., Dodds, N.
Behaviour of highly loaded aramid fibre as used in reinforced thermoplastic pipes;
Proceedings of NACE 11th Middle East Corrosion Conference, Kingdom of Bahrain, 2006.

31. Fallatah, G. M., Gibson, A. G., Dodds, N.
Long term creep and tress rupture of aramid fibre;
Proceedings of the 7th International Conference on Durability of Composite Systems, Blacksburg, Virginia, USA, Septembers 2006.

32. Frost, S. R.
The development of reinforced thermoplastic pipes for use on the oil industry;
Proceedings of Composite Materials for Offshore Operation -2 (CMOO-2), Houston TX 77060, USA, 1999.

33. Gibson, A. G.,
Creep and failure behaviour of aramid fibres;
Implementation of Reinforced Thermoplastic Pips (RTPs) in the Oil and Gas Industry
Joint Industry Program-Phase II Report,
University of Newcastle upon Tyne, 2005.

34. Gibson, A. G.,
Materials qualification for reinforced thermoplastic pipes;
Implementation of Reinforced Thermoplastic Pips (RTPs) in the Oil and Gas Industry
Joint Industry Program-Phase I Report,
University of Newcastle upon Tyne, 2002.

35. Gibson, A.G.
Qualification and design of reinforced thermoplastic Pipework;
Proceedings of NACE 10th Middle East Corrosion Conference, Kingdom of Bahrain, 2004

36. Gibson, A.G., Dodds, N., Frost, S.R., Stratfold, M. and Sheldrake T.
A novel approach to the qualification of nonmetallic pipe systems- as applied to reinforced thermoplastic pipe;
Plastic, Rubbers and Composites, Vol. 34, No. 7, 2005, pp 301 - 304.

37. Gol'dman A. Ya.
Prediction of the deformation properties of polymeric and composite materials;
1st edition, 1994, American Chemical Society.

38. Greenwood, J. H. and Rose, P. G.
Compressive behaviour of Kevlar 49 fibres and composites;
Journal of Materials Science, Vol. 9, 1974, pp. 1809 - 1814.

39. Guimaraes, G. B.
Parallel lay aramid ropes for use in structural engineering;
PhD Thesis, 1988, Imperial College London.

40. Holister, G. S. and Thomas, C.
Fibre-reinforced Materials;
1st edition, London, 1966, Elsevier.

41. Hongu, T. and Phillips, G. O.
New Fibres;
1st edition, 1990, Ellis Horwood.

42. ISO/TS 14692-1,
Petroleum and natural gas industries – glass reinforced (GRP) piping – Part 1-4

43. ISO 9080:2003,
Plastic pipe and ducting systems-Determination of the long-term hydrostatic strength of thermoplastics materials in pipe form by extrapolation.

44. Kelly A. and Macmillan, N. W.
Strong solids;
3rd edition, 1986, Oxford University Press.

45. Kerr, M., Chawla, N., and Chawla K. K.
The cyclic fatigue of high-performance fibres;
Journal of Materials, February 2005, pp.67 - 70.

46. Knoff, W. F.
Relationship between the tensile and shear strength of aramid fibres;
Journal of Materials Science Letters, Vol. 6, No. 12, 1987, pp. 1392 - 1394.

47. Konopasek, L. and Hearle, W. S.
The tensile fatigue behaviour of para-oriented aramid fibres and their fracture morphology;
Journal of Applied Polymer Science, Vol. 21, 1977, pp. 2791 - 2815.

48. Kostikov, V. I.
Fibre science and technology;
1st edition, 1995, Chapman & Hall Publisher.

49. Kroschwitz, J. I.
Concise encyclopaedia of polymer science and engineering;
1st edition, 1990, Wiley.

50. Kruijer, M. P., Warnet, L. L. and Akkerman, R.
Analysis of the mechanical properties of a Reinforced Thermoplastic Pipe (RTP);
Composites Part A: applied science and manufacturing, 2004.

51. Lafitte, M. H. and Bunsell, A. R.
The creep of Kevalr-29 fibres;
Polymer Engineering and Science, Vol. 25, No. 3, 1985, pp. 182 - 187.

52. Lafitte, M. H. and Bunsell, A. R.
The fatigue behaviour of Kevalr-29 fibres;
Journal of Materials Science, Vol. 17, 1982, pp. 2391 - 2397.

53. Lang, R. W., Pinter, G., and Stern, A.
Applicability and limitations of current lifetime predication models for thermoplastics pipes under internal pressure;
Proceedings of Plastics Pipes XI Conference, Munich Germany, 3rd – 6th September 2001.

54. Leijstrom, H. and Ifwarson, M.
Results and experiences obtained by Studsvik from long-term pressure tests on plastic pipes for validation of Miner's rule;
Proceedings of Plastic Pipes X Conference, Gotenborg, Sweden, 1998.

55. Magat, E. E.
Fibres from extended chain aromatic polyamides;
Philosophical Transaction of the Royal Society of London, A 294, 1980, pp. 463 - 472.

56. Maksimov, R. D. and Plume, E.
Long-term creep of hybrid aramid Glass-fibre-reinforced plastics;
Mechanics of Composite Materials, Vol. 37, No. 4, 2001, pp. 271 - 280.

57. McCrum, N.G., Read, B.E., and Williams, G.
Anelastic and Dielectric Effects in Polymeric Solids;
1st edition, 1977, John Wiley & Sons.

58. Minoshima, K, Maekawa, Y. and Komai, K.
The influence of vacuum on fracture and fatigue in a single aramid fibre;
International Journal of Fatigue, Vol. 22, 2000, pp. 757 - 756.

59. Morgan, R. J., Pruneda, C. O., Steele, W. J.
The relationship between the physical structure and the microscopic deformation and failure process of Poly(p-Phenylene Terephthalamide) fibres;
Journal of Polymer Science: Polymer Physics Edition, Vol. 21, 1983, pp. 1757 - 1783.

60. Northolt, M. G.
Tensile deformation of Poly(p-phenylene terephthalamid) fibres, and experimental and theoretical analysis;
Polymer, Vol. 21, 1980, pp. 1199 - 1204.

61. Northolt, M. G. and Van Aartesn, J. J.
Chain orientation distribution and elastic properties of Poly (p-Phenylene Terephthalamide), a "Rigid Rod" Polymer;
Journal of Polymer Science Part C : Polymer Symposia, Vol. 58, 1977, p. 283.

62. Olabisi, O.
Emerging composite materials technology in the exploration and production industry;
Saudi Aramco Journal of Technology, 2000, pp. 1 - 10.

63. Panar, M. Avakian, P. Blume, R. C. Gardner, K. H. Gierke, T. D. and Yang, H. H.
Morphology of Poly(p-Phenylene Terephthalamide) fibre;
Journal of Polymer Science, Polymer Physics Edition, Vol. 21, 1983, pp. 1955 - 1969.

64. Penn, L. and Larsen F.
Physicochemical properties of Kevlar 49 fibre;
Journal of Applied Polymer Science, Vol. 23, 1979, pp. 59 - 73.

65. Phoenix, S. L. and Tierney, L. J.
A statistical model for the time dependent failure of unidirectional composite materials under local elastic load-sharing among fibres;
Engineering Fracture Mechanics, Vol. 18, 1983, pp. 193 - 215.

66. Picken, S. J., van der Zwaag, S. and Northolt, M. G.
Molecular and macroscopic orientational order in aramid solution: a model to explain the influence of some spinning parameters on the modulus of aramid yarns;
Polymer, Vol. 33, No. 14, 1992, pp. 2998 - 3006.

67. Piggott, M. R.
Load-bearing fibre composites;
1st edition, 1980, Pergamon Press.

68. Pigliacampi, J. J.
Organic fibres;
Engineering Materials Handbook, Volume 1 Composites, 1995, ASM International.

69. Pottick, L. A., Allen, S. R. and Farris, R. J.
Force-temperature behaviour of rigid rod polymeric fibres;
Journal of Applied Polymer Science, Vol. 29, 1984, pp. 3925 - 3935.

70. Powell, P. C.
Engineering with fibre-polymer laminates;
1st edition, 1994, Chapman & Hall.

71. Preston, J.
High-strength/high-modulus organic fibres;
Polymer Engineering and Science, Vol. 15, Number 3, 1975, pp. 199 - 206.

72. Rogozinsky, A.K. and Bazhenov, S.L.
Effect of creep on Young's modulus of aramid fibres;
Polymer, Vol. 33, No. 7, 1992, pp. 1391-1398.

73. Sentler, L.
Reliability of high performance fibre composites;
Reliability Engineering and System Safety, Vol. 56, 1997, pp. 249 - 256.

74. Slattery, K. T.
Probabilistic micromechanical model of creep-rupture in filamentary composites;
Composites, Par B Vol. 27B, 1996, pp. 381 - 386.

75. Teijin,
Technora, high tenacity aramid fibre;
Teijin, 2001.

76. Twaron Technical Report QET 99023,
Temperature, chemical and UV resistance of Twaron p-aramid fibre;
Teijin, 2001.

77. Twaron Technical Report QET 96013,
Creep of Twaron aramid yarn;
Teijin, 2000.

78. Van Den Heuvel, C.J.M.
Time to failure of Twaron 1000 yarns;
Twaron Products Research Institute, 2000.

79. Wagner, H. D., Schwartz, P. and Phoenix, S. L.
Lifetime statistics for single Kevlar 49 filaments in creep-rupture;
Journal of Materials Science, Vol. 21, 1986, pp. 1868 - 1878.

80. Walton, P. L. and Majumdar, A. J.
Creep of Kevlar 49 fibre and a Kevlar 49-cement composite;
Journal of Materials Science, Vol. 18, 1983, pp. 2939 - 2946.

81. Wang, J. Z., Dillard, D. A. and Ward, T.C.
Temperature and stress effects in the creep of aramid fibres under transient moisture conditions and discussion on the mechanisms;
Journal of Polymer Science Part B: Polymer Physics, Vol. 30, No. 12, 1992, pp. 1391 - 1400.

82. Weast, R.
CRC handbook of chemistry and physics;
1st edition, 1988, CRC Press.

83. Wilfong, R. E. and Zimmerman, J.
Strength and durability characteristics of Kevlar aramid fibre;
Journal of Applied Polymer Science, Applied Polymer Symposium, Vol. 31, 1977, pp. 1 - 21.

84. Wu, H. F., Phoenix, S. L., and Schwartz, P.
Temperature dependence of lifetime statistics for single Kevlar filaments in creep-rupture;
Journal of Materials Science, Vol. 23, 1988, pp. 1851 - 1860.

85. Yang, H.H.
Kevlar aramid fibre;
1st edition, 1992, John Wiley & Sons.

86. Yeh, W. Y. and Young, R. J.
Molecular deformation processes in aromatic high modulus polymer fibres;
Polymer, Vol. 40, 1999, pp. 857 - 870.

87. Young, R. J., Lu, D., Day, R. J., Knoff, W. F., Davis, H. A.
Relationship between structure and mechanical properties for aramid fibres;
Journal of Materials Science, Vol. 27, 1992, pp. 5431 - 4550.

Appendix A - ISO 9080 4-Parameters Model Calculations

$$X=\begin{bmatrix} 1 & \frac{1}{T_1} & \log\sigma_1 & \frac{\log\sigma_1}{T_1} \\ \cdot & \cdot & \cdot & \cdot \\ \cdot & \cdot & \cdot & \cdot \\ 1 & \frac{1}{T_N} & \log\sigma_N & \frac{\log\sigma_N}{T_N} \end{bmatrix}; y=\begin{bmatrix} \log t_1 \\ \cdot \\ \cdot \\ \log t_N \end{bmatrix}; e=\begin{bmatrix} e_1 \\ \cdot \\ \cdot \\ e_N \end{bmatrix};$$

where, N is the total number of data point.

With $c=(c_1,c_2,c_3,c_4)^T$;

where T is the transposition operator. Hence, the 4-parameter model can be written as:

$$y=Xc+e$$

The least-squares estimates of the parameters are given by:

$$\hat{c}=\left(X^T X\right)^{-1} X^T y,$$

and the residual variance estimate is given by:

$$s^2=(y-X\hat{c})^T\frac{(y-X\hat{c})}{(N-q)};$$

where, q is the number of parameters in the model.

The predicted stress value corresponding to a given time to failure t and temperature T is given by:

$$\log\sigma=\frac{(\log t-c_1-c_2/T)}{(c_3+c_4/T)}$$

To calculate σ_{LPL}, corresponding to a given time to failure t and temperature T, the inversion operation in the following relation is carried out:

$$\log t=c_1+c_2/T+c_3\log\sigma+c_4\frac{(\log\sigma)}{T}-t_{St}s\left[1+x\left(X^T X\right)^{-1}x^T\right]^{1/2},$$

where, t_{St} is Student's t-value corresponding to a probability level of 0.975 with the number of degrees of freedom of $N-4$; x represents the vector $[1,1/T,\log\sigma,(\log\sigma)/T]$. The result is:

$$\log \sigma_{LPL} = \frac{-\beta - \sqrt{\beta^2 - 4\alpha\gamma}}{2\alpha},$$

where $\alpha = (c_{3+}\, c_4/T)^2 - t_{Si}{}^2 s^2 (K_{33} + 2K_{43}/T + K_{44}/T^2)$

$\beta = 2(c_1 + c_2/T - \log t)(c_{3+}\, c_4/T) - 2t_{Si}{}^2 s^2 [K_{31} + (K_{41} + K_{32})/T + K_{42}/T^2]$

$\gamma = (c_1 + c_2/T - \log t)^2 - t_{Si}{}^2 s^2 (K_{11} + 2K_{21}/T + K_{22}/T^2 + 1)$

K_{ij} is the element with subscripts i, j in the matrix $(X^T X)^{-1}$

The value of the σ_{LPL} can then be calculated from the following equation:

$$\sigma_{LPL} = 10 \exp(\log \sigma_{LPL})$$

Appendix B - ISO9080 4-Parameters VBA Model

```
Dim Counter, datapoints As Integer
Dim tbl, fillrange, sourcerange As Range
Dim Xarray, yarray
Dim N, param As Integer
Dim temperature, period, pressure
    Worksheets("multi regression").Activate
    Range("m6:q200").ClearContents  'clear the output cells
    Range("t:t").ClearContents
    Columns("T:T").Select           ' format the output cells
    Selection.NumberFormat = "0.000"
    Range("T4:T5").Select
    Selection.NumberFormat = "General"
    Range("t14").Select
    Selection.NumberFormat = "0.0"
    Range("c6").Select  'make active cell in data table then select the range
    Set tbl = ActiveCell.CurrentRegion
    tbl.Resize(tbl.Rows.Count - 1, _
    tbl.Columns.Count).Select
    N = tbl.Rows.Count - 1
    param = Range("f3").Value
    If Cells(3, 6) <> 3# Or 4# Then param = 4
    Range("t4").Value = N
    Range("t5").Value = param
'setup the transformed data for the arrays Xarray and Yarray 4 parameter model
    Range("m6").Select
    ActiveCell.Value = "1"
    Range("n6").Select
    ActiveCell.FormulaR1C1 = "=1/RC[-10]"
    Range("O6").Select
```

```
ActiveCell.FormulaR1C1 = "=LOG(RC[-10])"
Range("P6").Select
ActiveCell.FormulaR1C1 = "=LOG(RC[-11])/RC[-12]"
Range("Q6").Select
ActiveCell.FormulaR1C1 = "=LOG(RC[-11])"
Set sourcerange = Range("m6:q6")   ' Setup the autofill
Set fillrange = tbl.Offset(1, 10).Resize(tbl.Rows.Count - 1, tbl.Columns.Count + 1)
   sourcerange.AutoFill Destination:=fillrange, Type:=xlFillCopy
  ' name the arrays
   ActiveWorkbook.Names.Add name:="Xarray",
RefersTo:=fillrange.Resize(fillrange.Rows.Count, fillrange.Columns.Count - 1)
   ActiveWorkbook.Names.Add name:="yarray", RefersTo:=fillrange.Offset(0,
4).Resize(fillrange.Rows.Count, fillrange.Columns.Count - 4)
   ActiveWorkbook.Names.Add name:="N", RefersTo:=Range("t4")
   ActiveWorkbook.Names.Add name:="param", RefersTo:=Range("t5")
' calculate coefficients
   Range("t6:t9").Select
   Selection.FormulaArray =
"=MMULT(MINVERSE(MMULT(TRANSPOSE(Xarray),Xarray)),MMULT(TRANSPOSE(
Xarray),yarray))"
   ActiveWorkbook.Names.Add name:="coeffs", RefersTo:=Range("t6:t9")
' Residual variance
   Range("t11").Select
   Selection.FormulaArray = "=MMULT(TRANSPOSE((yarray-
MMULT(Xarray,coeffs))),(yarray-MMULT(Xarray,coeffs)))/(N-param)"
   ActiveWorkbook.Names.Add name:="variance", RefersTo:=Range("t11")
 ' LPL routine
   Range("t13").Select     'setup input vector
   ActiveCell.Value = "1"
   Range("n3").Select
   ActiveCell.Value = "1"
   Range("o3").Select
```

```
ActiveCell.Formula = "=1/(273+v1)"
Range("p3").Select
ActiveCell.Formula = "=LOG(t13)"
Range("q3").Select
ActiveCell.Formula = "=LOG(t13)/(273+v1)"
ActiveWorkbook.Names.Add name:="xlpl", RefersTo:=Range("n3:q3")
Range("t14").Select
   Selection.FormulaArray = "=10^(MMULT(transpose(coeffs),TRANSPOSE(xlpl))-
TINV(1-0.95,N-
4)*u11*(1+MMULT(MMULT(xlpl,minverse(MMULT(TRANSPOSE(Xarray),Xarray))),TRA
NSPOSE(xlpl)))^0.5)"
 ' solve with goal seek
   Range("T14").Select
   Range("T14").goalseek Goal:=Range("v2").Value, ChangingCell:=Range("T13")
   Range("T15").Select
End Sub
```